WASHINGTON UNIVERSITY

THE HENRY EDWIN SEVER GRADUATE SCHOOL

DEPARTMENT OF MECHANICAL & AEROSPACE ENGINEERING

ABSTRACT

NUMERICAL SIMULATION OF NATURAL CONVECTION HEAT TRANSFER IN NANOFLUIDS

By Mior Azman Meor Said

ADVISOR: Professor R.K. Agarwal

May 2005

Saint Louis, Missouri

The goal of this thesis is to model the behavior of the nanofluids so that their performances can be evaluated analytically and computationally. In this thesis, we consider analytical models that describe molecular viscosity μ, thermal conductivity k, density ρ, specific heat c_p and the coefficient of thermal expansion β for a nanofluid in terms of volume fraction ϕ of nanoparticles, size of the nanoparticles (e.g radius of the nanoparticle, r_p), size of the base fluid molecule (e.g. radius of the liquid molecule, r_f) and the temperature T. In order to validate these analytical models, we study numerically the natural convection heat transfer in a closed pipe using the commercially available CFD software FLUENT 6.0, since the experimental data is available for this configuration. In particular, we study the natural convection flow field in two configurations of L/D=0.5 and L/D=1.0, where L is the length of the pipe and D is the diameter. For nanofluids, we consider the suspensions of Al_2O_3 and CuO particles in water. Three cases with volume fraction $\phi = 0$, 1% and 4% for both Al_2O_3 and CuO are considered. It is assumed that the nanoparticles of Al_2O_3 or CuO are uniformly suspended in water; there is no aggregation of nanoparticles in the fluid medium. It is shown that the use of experimentally measured values of k, or the kinetic model of k, gives better correlation with experimental data for heat transfer compared to the Maxwell model.

To my family

Contents

Figures

Tables

Nomenclature

$\vec{A}$	Surface area vector
A_m	Surface area of fluid particle (molecule)
C_p	Specific heat of nanofluids
C_{pf}	Specific heat of the base fluid
C_{pp}	Specific heat of the nanoparticles material
D	Inner diameter of the cylindrical test cell
d_p	Diameter of nanoparticles
E_t	Total energy per unit volume
g	Acceleration due to gravity
h	Heat transfer coefficient
k_b	Boltzmann constant ($1.38 \times 10^{-23} J.K^{-1}$)
k_f	Thermal conductivity of the base fluid
k_m	Thermal conductivity of fluid particle (molecule)
k_n	Thermal conductivity of the nanofluids
k_p	Thermal conductivity of the nanoparticle
L	The length of the cylindrical model
n	Outward unit normal to the cell face
p	Pressure

(q_x, q_y, q_z)	Heat flux in (x, y, z) direction
Q	Input power
r_m	Radius of fluid particle (molecule)
r_p	Radius of nanoparticle
S_ϕ	Source term per unit volume
T	Nanofluids temperature
T_C	Temperature of the cold wall
T_H	Temperature of the hot wall
(u, v, w)	Velocity components in (x, y, z) directions
$\bar{u}_p$	Mean velocity of nanoparticle
V	Cell volume
α	Particle volume fraction
α_n	Thermal diffusivity of nanofluids
β	Thermal expansion coefficient
ϕ	Volume fraction of nanoparticles
ϕ_f	Value of scalar ϕ on face f
μ	Dynamic viscosity of nanofluid
μ_f	Dynamic viscosity of the base fluid
μ_o	Reference viscosity of water (0.001788 $kgm^{-1}s^{-1}$)
$\vec{v}$	Velocity vector

v_n	Kinematic viscosity of nanofluids
ρ_0	Density of nanofluids
ρ_f	Density of the base fluid
ρ_p	Density of the nanoparticles material
τ	Viscous stress tensor

Chapter 1: Introduction

1.1 Motivation

Nanotechnology is a branch of science covering many areas of study that deal with objects of size in the range of nanometer scale ("nano" means one billionth"). It is projected that nanotechnology – where materials at nanometer scale are being engineered for innovation - will be the next industrial revolution. This prediction is supported by the increasing number of applications of nanotechnology in the field of biology, physics, electronics, transportation and environment, among others.

In thermal fluid science, nanofluids are considered as a new form of solid-liquid materials where nanometer size metallic or non-metallic particles are suspended inside the base liquids. The presence of nanoparticles increases the thermal conductivity of the base fluid significantly. For example, when 1% of carbon nanotubes are suspended into oil, the thermal conductivity of the oil with nanoparticles increases 1.5 times compared to that of the oil alone [7]. This special property of the nanofluids has attracted a lot of attention recently since this can be used to improve performance in cooling and other applications in heat transfer systems. Conventional fluids such as water, oil and ethylene glycol have low thermal conductivity and therefore have limitations in enhancing the performance of a heat transfer system. Thus, the nanofluids are good candidates for improving the heat transfer characteristics in a variety of industrial applications.

The other significant property of the nanofluids when compared to conventional solid-liquid suspensions is that they do not aggregate (and therefore clog) easily and also no pressure drop occurs due to very minimal sedimentation of nanoparticles. Since the nanoparticles are smaller and lighter than the micro-sized particles, they suspend fairly uniformly in the base fluid and flow together with the motion of the base fluid. In the past, for solid-liquid suspensions with micro-sized particles, the problems of aggregation and sedimentation have been significant, which resulted in clogging, pressure drop, erosion of the wall, and the instability of the particle suspension. These problems minimally arise in nanofluids; the nanosized particles suspend almost uniformly inside the base fluid and therefore contribute minimally to sedimentation, coagulation and adhesion to the wall.

Due to the above described special features, nanofluids have high prospect for being used for super-cooling and lubricating processes in industrial applications. Thermal systems, such as radiators, engines and HVAC systems which depend on efficient cooling fluid, can benefit from nanofluids as a cooling agent due to their high thermal conductivity. For example, in case of radiators, their size could be reduced due to compensation gained by the use of high thermal conductivity fluid. The same can be true for a HVAC system, where the compressor can be made smaller without affecting the performance of the heat transfer system. High performance engines need super-cooling lubrication that is not only high in thermal conductivity, but also will not cause any erosion to the mechanical parts; nanofluids can be employed as a super-cooling lubricating agent.

The innovation of Micro-Electro-Mechanical-Systems (MEMS) has further demonstrated the need for high thermal conductivity fluids such as nanofluids in MEMS design, since they can be used as efficient cooling fluids in small passages and will not cause clogging, erosion and pressure drop along the micro-channel.

1.2 Objective

The objective of this study is to perform numerical simulations of natural convection heat transfer in nanofluids and to compare the results with experimental data.

1.3 Problem Statement

With efforts over the past three decades, Computational Fluid Dynamics (CFD) has now developed into an accurate, efficient and robust technology for the analysis and design of systems involving fluid flow, heat transfer and associated phenomena by means of computer-based simulations. The technology is very powerful and now spans a wide range of industrial applications because of its many advantages. With the use of CFD, the time needed to perform the analysis and design of a system can be reduced significantly. Furthermore, a large number of simulations can be easily performed by varying a number of design parameters for design optimization.

In contrast, an experimental study requires significant amount of time to design and construct the experimental set up and perform the experiment; it may also be limited in the range of parameters that can be varied. Thus, an experimental study is usually quite expensive and requires more time compared to numerical simulations. This is not to imply that the experimental data is not needed and one can solely rely on computations; the experimental data is very important for validation of numerical simulations. But once the CFD simulation has been validated against the experimental data, CFD software can be effectively utilized to analyze and evaluate a number of candidate configurations for a wide range of parameters thereby leading to design optimization as well as a better understanding of the flow properties. CFD technology can reduce the cost and time required in analysis and design significantly.

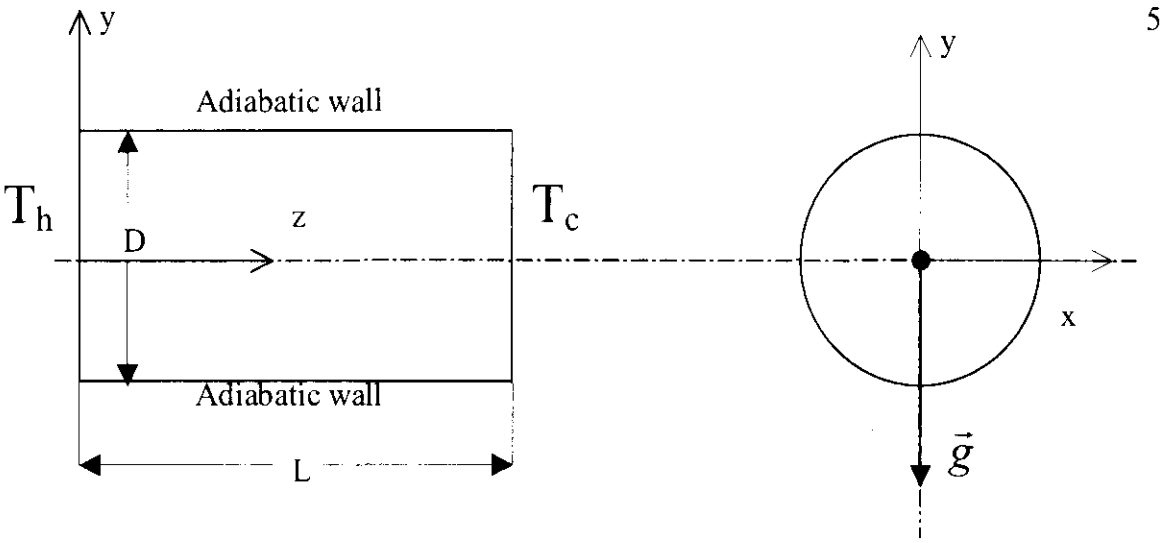

$\mathbf{T}_h$ = Hot Wall
$\mathbf{T}_c$ = Cold Wall
D = Diameter
L = Length
$\vec{g}$ = Force of Gravity

Figure 1-1: Plan View and Side View of the Cylinder

In this study, CFD software "FLUENT" is employed to study the behavior and characteristics of nanofluids in natural convection heat transfer. Nanofluids containing the Aluminum Oxide (Al_2O_3) and Copper Oxide (CuO) particles in water are studied. The CFD results are compared with the experimental data for validation. In the numerical simulations, the two geometries of the models employed are exactly the same as in the experiment, where two axi-symmetric enclosed cylinders of L/D = 0.5 and 1.0, containing nanofluids are bounded by a hot and a cold wall on the left and right end respectively and an adiabatic wall on the round surface of the cylinders as shown in Figure 1-1. The numerical results are presented in terms of non-dimensional parameters

(Nusselt number and Rayleigh number) in order to compare them with the available experimental results [16]. In the CFD solver Fluent 6.0, all the theoretical models describing the nanofluid properties (density, viscosity, thermal conductivity, coefficient of thermal expansion, and the specific heat) are input as User Defined Functions (UDF) [9]. The velocity, pressure and temperature fields are computed inside the cylinder for different volume fractions of Al_2O_3 and CuO nanoparticles in water. The variation in Nusselt number with volume fraction of nanoparticles ϕ is computed and compared with the experimental data.

1.4 Literature Review

1.4.1 The Synthesis of Nanofluids

There are currently two methods of synthesizing the nanofluids that are widely employed by researchers: These are designated as a "two-step process" and a "one-step process".

Two-Step Process of Synthesis

This involves two processes. The first stage involves vaporization of the source material (from which the nanoparticles are formed) inside a vacuum chamber and then the vapor is condensed into solid nanoparticles under cool, inert, reduced and controlled pressure environment [5]. Usually helium is used as the inert gas.

In the second stage, the nanoparticles are dispersed inside the fluid. Dispersion is done by adding the nanoparticles to the liquid base using a chemical measuring flask and then applying ultrasonic vibration to the solution. Stabilizers such as oleic acid or laurett salts are added to stop sedimentation and aggregation [4].

The advantage of this process is that the technique can be applied to mass production of nanofluids. The two-steps process provides better control of the environment and therefore, lowers the risk of manufacturing failure. This is not the case with one-step process described below, where the ambient conditions must be controlled strictly, since the dispersion and the evaporation occur simultaneously.

One-Step Process of Synthesis

It is also called the direct evaporation technique. Whereas in the two-step process the source material of nanoparticles is first evaporated and then condensed into solid nanoparticles before the dispersion into the liquid base, one-step process only involves the direct evaporation of the source material of nanoparticles into the base fluid. This process starts with the vaporization of source material under vacuum condition. The condensation of nanoparticles occurs when the vapor comes into contact with the liquid. Figure 1-2 shows a diagram of the one-step nanofluid production system employed by the Argonne National Laboratory [6].

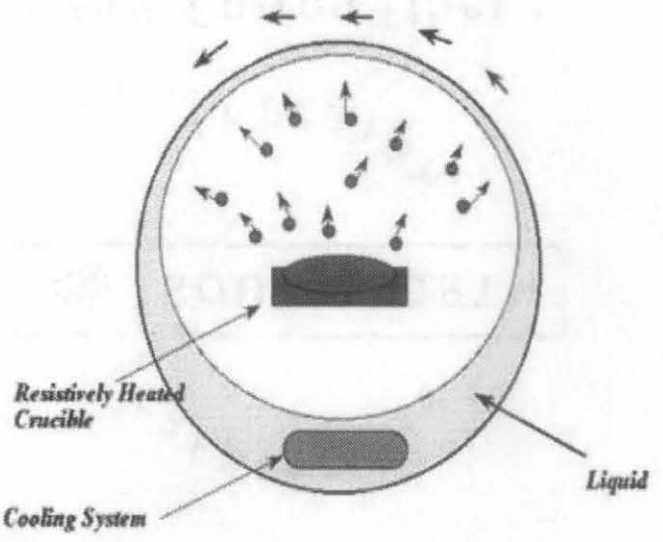

Figure 1-2 : Diagram of a One-Step Nanofluid Production System [6].

The nanofluid synthesizing system in Figure 1-2 displays the direct evaporation technique. The source material of nanoparticles is heated by a resistively-heated crucible whereby it evaporates into a thin layer of low vapor pressure liquid contained inside a rotating cylinder. The vapor condenses into nanoparticles on contact with the liquid. The rotating cylinder spreads the nanoparticles evenly to produce a uniform concentration of nanofluids. A cooling system maintains the low vapor pressure of the liquid; it is necessary because of the radiation heat transfer from the resistively-heated crucible.

1.4.2 Description of the Experimental Setup for the Study of Natural Convection Heat Transfer in Nanofluids

Since the goal of this thesis is to numerically simulate the flow field measured in the experimental study on natural convection heat transfer in nanofluids, performed by a team of researchers led by Putra [16], this section provides a brief description of the experimental setup and the data obtained. In the simulation, the geometry of the fluid container, the nanofluids composition and the thermal boundary conditions are the same as those in the experiment.

The schematic of the experimental setup is shown in Figure 1-3 and the details of the test section – a cylindrical tube with end plates containing the nanofluid, are shown in Figure 1-4. In the test section, the temperature of the two end-covers is controlled to provide the conditions of the hot wall and the cold wall at the two ends of the cylindrical tube. The heat for the hot wall is provided by the resistive heating element which controls the hot wall temperature. The temperature of the cold wall is controlled by cold water flowing near the cold wall. The curved boundary of the cylindrical tube is insulated throughout the experiment to minimize heat loss.

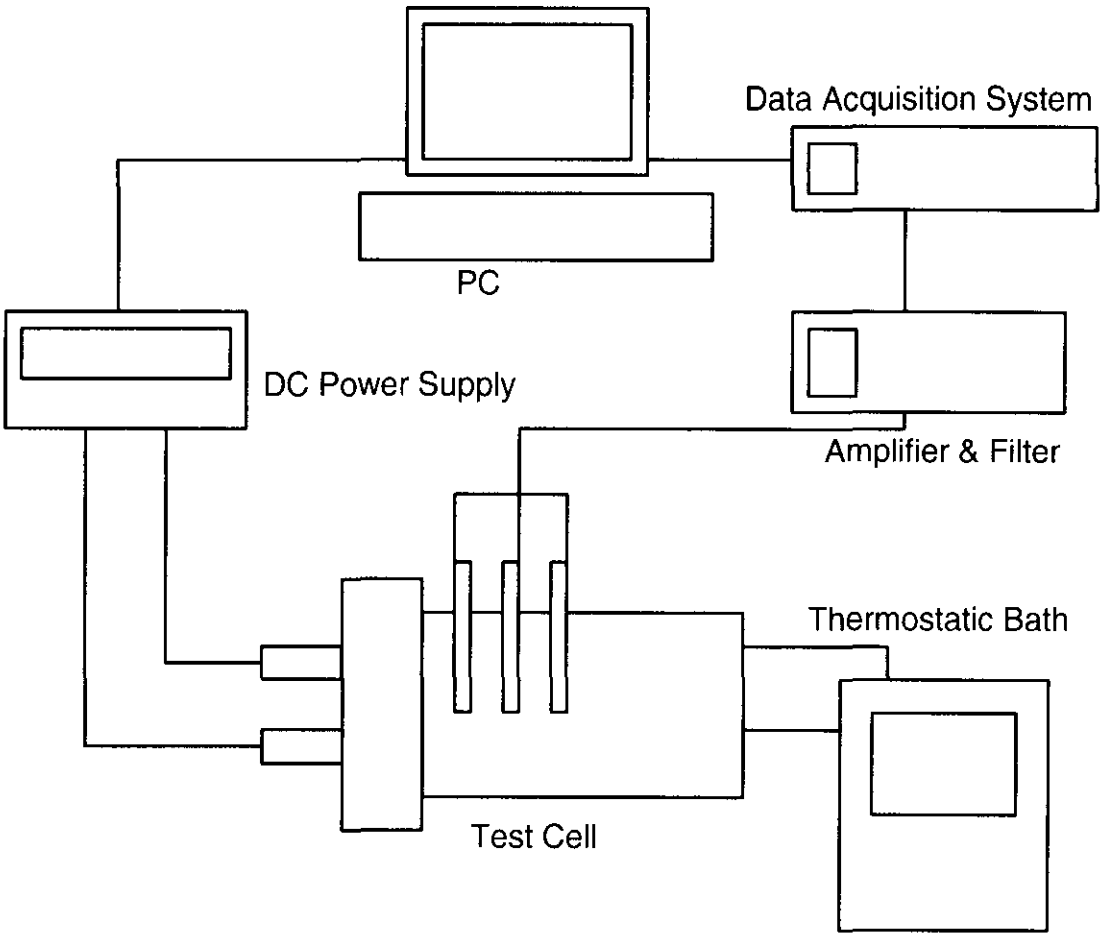

Figure 1-3: Schematic Diagram of the Experimental Setup [16]

The test cell is connected to a DC Power Supply for the power source to its resistive heating elements to provide heat to the end-cover (as hot wall), and is connected to the thermostatic bath to provide cooling to the end-cover (as cold wall). The water in thermostatic bath is supplied by a tube with an inlet and outlet as shown in Figure 1-4. The temperatures at the cold and hot wall are recorded by three K-type 0.1mm diameter thermocouples welded into each of the end-covers. These temperatures at the end-covers

are controlled to be isothermal by a software which runs on a PC and uses data from the data acquisition system. There are three other thermocouples with their tips at the center of the axis of the cylinder, which are located 10mm apart from each other as shown in Figure 1-4. These three thermocouples measure the temperature inside the cylinder containing the nanofluid at three different locations on the axis of the cylinder. Digital multi-meters are used to record the input voltage and current.

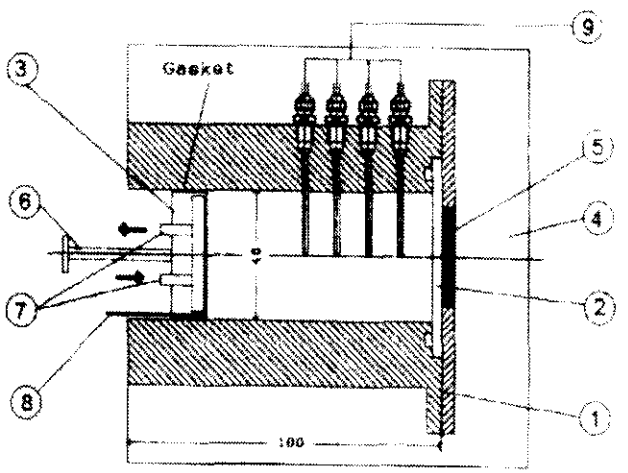

1. Cylindrical block
2. End cover as hot wall
3. End cover as cold wall
4. Cap
5. Resistive heating elements
6. The piston shaft
7. Cooling water inlet and outlet
8. Narrow tube
9. Thermocouple

Figure 1-4: Sketch of the Test Cell [16]

The non-dimensional parameters - Nusselt number (*Nu*) and Rayleigh number (*Ra*) are determined from the experimental data using the values of the temperatures of the end-covers and input power. *Nu* and *Ra* are defined as:

$$Nu = \frac{hL}{k_n} \tag{1-1}$$

$$Ra = \frac{g\beta_n \Delta T L^3}{\nu_n \alpha_n} \tag{1-2}$$

where L = Length of the cylindrical fluid container

h = Heat transfer coefficient

k_n = Thermal conductivity of the nanofluid

g = Acceleration due to gravity

ΔT = Temperature difference between the hot and the cold wall

ν_n = Kinematic viscosity of the nanofluid

α_n = Thermal diffusivity of the nanofluid

Heat transfer coefficient is obtained by the value of the input power:

$$h = \frac{4Q}{\pi d^2 (T_H - T_C)} \tag{1-3}$$

where Q = Input power

d = Inner diameter of the cylindrical test cell

T_H = Temperature of the hot wall

T_C = Temperature of the cold wall

The goal of the experiment was to find the effect of higher thermal conductivity of the nanofluid on natural convection heat transfer in the cylinder containing nanofluid. The hot wall temperature was controlled by adjusting the input power, supplied by the DC power supply. It was varied from 305 K to 345 K, while the cold wall temperature was kept constant at 285 K. The heat transfer coefficients were then calculated from equation (1-3) using the values of the input power and the temperature difference between the end walls. Nusselt number and Rayleigh number were then obtained from equations (1-1) and (1-2) respectively. Experimental plots of Nusselt number vs Rayleigh number were obtained for two nanofluids (Al_2O_3-water and CuO-water) by varying the volume-fraction ϕ of the nanoparticels (ϕ=0, 1% and 4%) for three different values of $\Delta T=(T_H - T_C)$ for the two aspect ratio of the cylinder (L/D = 0.5 and 1.0).

The results of the experiment show that the natural convection heat transfer deteriorates due to the presence of nanoparticles in the cases considered. According to the authors of the experiment study [16], this phenomenon is evident by the decrease in Nusselt number with increase in the volume-fraction of the nanoparticles. The degradation in heat transfer is greater in cylinder of aspect ratio L/D = 1.0 compared to

that in cylinder of L/D = 0.5. Also, the degradation of heat transfer is found to be larger in CuO-water nanofluid compared to that in Al_2O_3-water nanofluid with all other experimental conditions including the volume-fraction of nanoparticles being the same [16]. This result is contrary to that obtained for forced convection heat transfer where the higher thermal conductivity of the nanofluids helps in augmenting the heat transfer.

The authors of the experiment [16] suggest that the possible reason for degradation of heat transfer in natural convection flow can be attributed to the presence of slip between the nanoparticles and the fluid molecules, judging by the results where the higher density CuO-water nanofluids show greater deterioration in heat transfer compared to the lower density Al_2O_3-water nanofluids. In general, the deterioration of natural convection heat transfer in nanofluids, appears to be a function of three factors: nanoparticle material density and concentration, and aspect ratio of the cylinder [16]. However, the main reason behind the degradation in natural convection heat transfer remains unclear.

1.4.3 Review of Thermal Conductivity Theory of Nanofluids

In experimental measurements, nanofluids have been shown to have higher thermal conductivity than base liquid [16]. Therefore, in recent years, there have been several efforts towards modeling the thermal conductivity of nanofluids [5]. Majority of the models treat the nanofluid as a solid-liquid mixture with suspended particles. The first reported theoretical work on the thermal conductivity of a solid-liquid suspension is

due to Maxwell [14]. In the Maxwell model, the suspended particles are considered to be of uniform spherical shape. The effective thermal conductivity of the suspension containing spherical particles increases with the volume fraction of the solid particles. The equation for thermal conductivity of the solid-liquid suspension using the Maxwell model is given in Chapter 3.

Batchelor and O'Brien [1] obtained an expression for the effective thermal conductivity of a solid-liquid suspension that contains micro-sized metallic particles as follows:

$$k_{eff} = \left[4\ln(\frac{k_p}{k_f}) - 11 \right] k_f \qquad (1\text{-}4)$$

where k_p = Thermal conductivity of the metallic particle

k_f = Thermal conductivity of the base fluid

This model, however, is based on the hypothesis of a point-contact porous medium where effective thermal conductivity is independent of the conductivity ratio $(\frac{k_p}{k_f})$, if no contact occurs between the particles.

Hamilton and Crosser [7] modified the thermal conductivity model of Maxwell [14] by introducing the effect of increasing particle surface area and the shape of the

particles. In contrast to the Maxwell model, non-spherical shape of the particles is considered in their formulation. According to this model, the effective thermal conductivity of a solid-liquid suspension is given by:

$$k_{eff} = k_f \left[\frac{k_p + (n-1)k_f - (n-1)\alpha(k_f - k_p)}{k_p + (n-1)k_f + \alpha(k_f - k_p)} \right] \qquad (1\text{-}5)$$

where k_f = Thermal conductivity of the base fluid

k_p = Thermal conductivity of the solid particle

α = Particle volume fraction

$n = 3 / \Psi$

Ψ = Sphericity, ratio of surface area of a sphere that has volume equal to that of the particle, to the surface area of the particle

The model given by equation (1-5) predicts that the non-spherical shape of the particles increases the thermal conductivity.

Recently, a model based on the kinetic theory has been developed by Hemanth Kumar *et al.* [11]. In this model, the base liquid itself is considered as a cluster of particles in which the movement of nanoparticles is considered. The equation for thermal conductivity of the nanofluid is derived using the kinetic theory. There are two models that have been developed using this approach: the "Stationary Particle Model" and the "Moving Particle Model" [11]. In the stationary particle model, the nanoparticles are considered motionless in the suspension while in the moving particle model, the

Brownian motion of nanoparticles inside the liquid is considered. The stationary particle model predicts that the thermal conductivity increases by decreasing the particle size and increasing the particle concentration. The moving particle model relates not only to the particle size and concentration but also to the temperature as an additional factor that increases the thermal conductivity of the nanofluids [11]. As the mean particle velocity increases with the temperature, the thermal conductivity of the nanofluid increases, since the mean particle velocity is directly proportional to the temperature and is inversely proportional to the viscosity of the base fluid (which also decreases with increase in temperature). Equations describing the effective thermal conductivity of a nanofluid, based on these two kinetic models, are given in Chapter 3.

Chapter 2: Grid Generation

2.1 Overview of Grid Generation

Grid generation is a process of representing the physical domain by a group of elements (or control volumes) on which the governing equations of fluid flow can be solved to desired accuracy by applying a stable and robust numerical algorithm. Each element is described by a set of points, which determine the nature of the cells or the control volumes (e.g. in 2D, the element could be a triangle with three vertices or a quadrilateral with four vertices). Grid generation is not unique for a given problem; the choice of grid topology, the type of grid, the grid clustering etc. depend upon the user who must consider several criteria (described in section 2.2) in designing a suitable mesh for a given problem in order to obtain a solution of desired accuracy.

The suitable grid topology is generally determined by the geometry and the physics of the problem. We will not go into details of this issue in this thesis; the interested reader can refer to the book by Farrashkhalvat [8]. There are generally two types of grids employed in discretizing a computational domain, which are called "structured" and "unstructured" grids. Structured grid is a mesh generation that has the same number of connections to the vertices of all its elements and has the same number of neighboring elements (except at the boundaries).

The mesh that has different number of connections to the vertices of its elements and also has different number of neighboring elements is called an unstructured grid. Figure 2-1 shows a sketch of a structured and an unstructured mesh inside a 2D rectangular computational domain. The grid should also be appropriately clustered in regions of the computational domain where flow gradients are high in order to resolve the shear layers, boundary layers, wakes etc. Furthermore, too-coarse a grid can also impair the solution accuracy because of excessive numerical diffusion in generally employed second-order schemes as described in section 2.2.1.

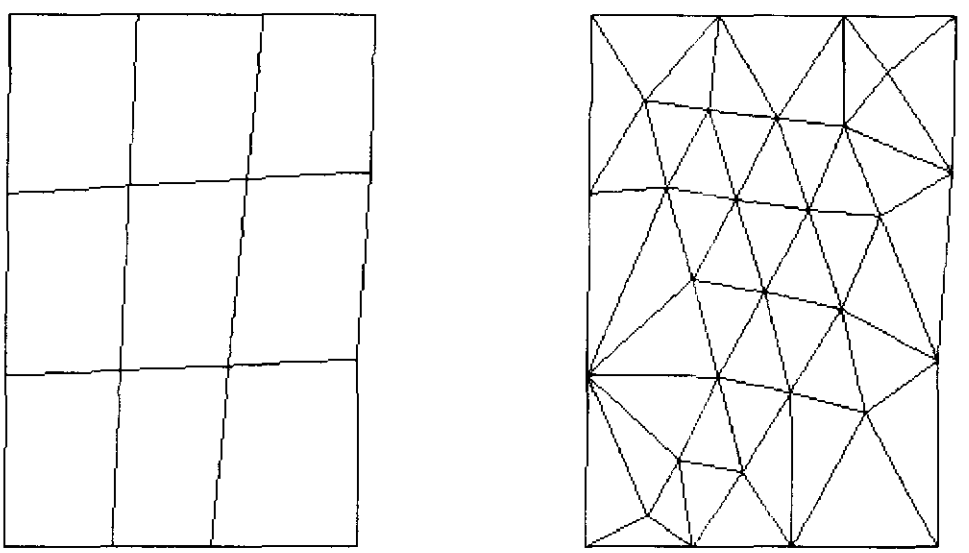

Structured Mesh Unstructured Mesh

Figure 2-1: Structured and Unstructured Meshes [8]

2.2 Selection Criteria for Grid Generation

In this numerical study, GAMBIT 2.0 software is employed for grid generation. GAMBIT 2.0 can generate triangular and quadrilateral mesh in two-dimensions and tetrahedral, hexahedral, pyramid and wedge type mesh in three dimensions. However, as mentioned in section 2.1, several factors must be considered in choosing an appropriate mesh for a given geometry and physical problem to be solved. One must consider numerical diffusion, solution accuracy and efficiency, and geometric complexity in deciding upon an appropriate mesh.

2.2.1 Numerical diffusion

Numerical diffusion contaminates the accuracy of the solution due to truncation errors in the numerical schemes that represent the governing partial differential equations in discrete form on a given mesh. Numerical diffusion is a major source of error in multi-dimensional simulations of fluid flow. It contributes to a "false diffusion" in the flow field and adds to the real diffusion due to viscosity. Thus, numerical diffusion must be minimized to obtain accurate solutions.

There are several ways to reduce the numerical diffusion. One of them is to use a higher-order scheme. Higher-order schemes have smaller truncation error compared to a low-order scheme (e.g. first-order scheme) on the same mesh and therefore less numerical diffusion. Higher-order schemes require more computing time compared to low-order schemes and also contribute to instability near the boundaries.

Another way to reduce the numerical diffusion is to refine the mesh. Smaller mesh width decreases the truncation error and thus reduces the numerical diffusion. In high flow gradient regions, where the changes in flow variables are rapid, the need to reduce the mesh spacing becomes crucial for obtaining accurate solutions.

Numerical diffusion can also be reduced by aligning the mesh with the dominant flow direction. It should be noted that with triangular and tetrahedral mesh, the grid can never be aligned with the flow [8]. Only with the use of the quadrilateral or hexahedral mesh, it is possible to align the mesh with the flow direction, although it is quite difficult for flow past (or in) a complex geometry. In many cases, a combination of structured and unstructured grid (hybrid grid) is employed to align the grid with the flow over (or in) a complex geometry.

2.2.2 Solution Accuracy and Efficiency

Unstructured mesh of triangular (in 2D) and tetrahedral (3D) cells is more suitable for flow over (or in) a complex geometry, because the triangular (in 2D) and tetrahedral mesh (3D) can be made to fit the shape in selected regions of the flow domain more easily than the quadrilateral (in 2D) or hexahedral (in 3D) cells of a structured mesh. The geometric corners are a good example of such region. Thus, an unstructured mesh may be more accurate and efficient for flow field calculations. However, an unstructured mesh is not very accurate in computing viscous boundary layers. Triangular (in 2D) or tetrahedral (in 3D) cells with very high aspect ratio cells near the boundary introduce significant

errors in flux calculations [17]. On the other hand, a structured mesh can give accurate solutions on cells of high aspect ratio. Thus, in many viscous flow problems, a hybrid mesh may be the most suitable; structured mesh with high aspect ratio cells near the solid walls to resolve the viscous boundary layer and an unstructured mesh in region away from the boundary.

2.3 Mesh Generation Inside a Circular Tube with End Walls

As mentioned in chapter 1, the geometric configuration employed in this study as well as in the experiment [16] is a circular tube with end plates. Two tubes, each of diameter D = 40mm, but of two different lengths of L = 20mm and L = 40mm are employed in both the experiment [16] and the simulations performed in this thesis. Thus, the mesh is generated in two circular tubes of L/D = 0.5 and 1.0.

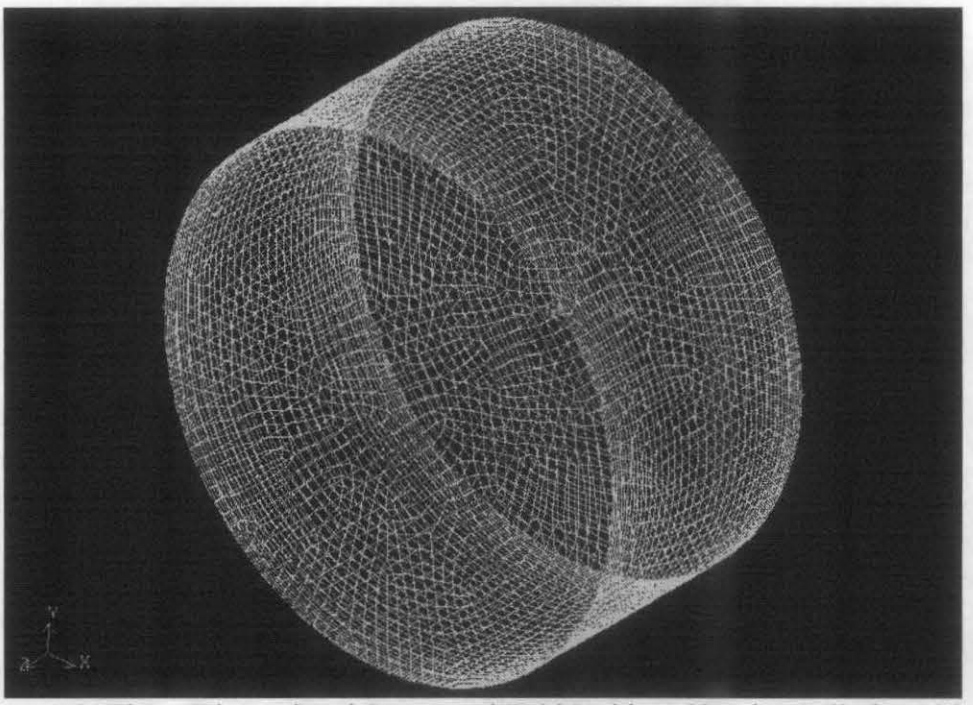

Figure 2-2: Three-Dimensional Structured Grid Inside a Circular Cylinder with End-Walls, L/D =0.5

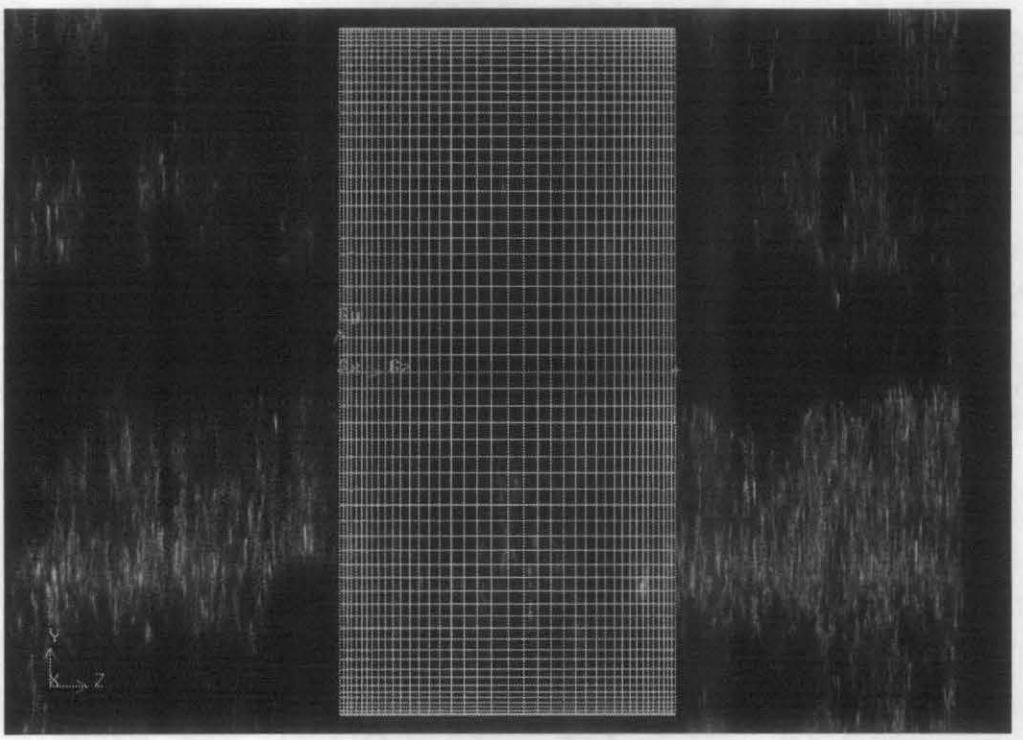

Figure 2-3: Side View of the Grid for the Circular Cylinder with End-Walls, L/D=0.5

Figure 2-2 shows the 3D structured grid for a cylinder of aspect ratio L/D=0.5. The mesh is generated using the GAMBIT software with the option of meshing the volume with hexahedral elements option (Table 2-1). This type of element is chosen because of the simplicity of the geometry of the model. As mentioned in section 2.1.1, for simple geometry, structured elements are preferred since they more accurately resolve the viscous layers near the walls (see Figure 2-3) and also save time in grid generation. The design of the mesh is exactly the same for a cylinder of aspect ratio L/D = 1.0 (Figure 2-4 and Figure 2-5) except that the length of the cylinder is two times that of the cylinder shown in Figure 2-2 and Figure 2-3.

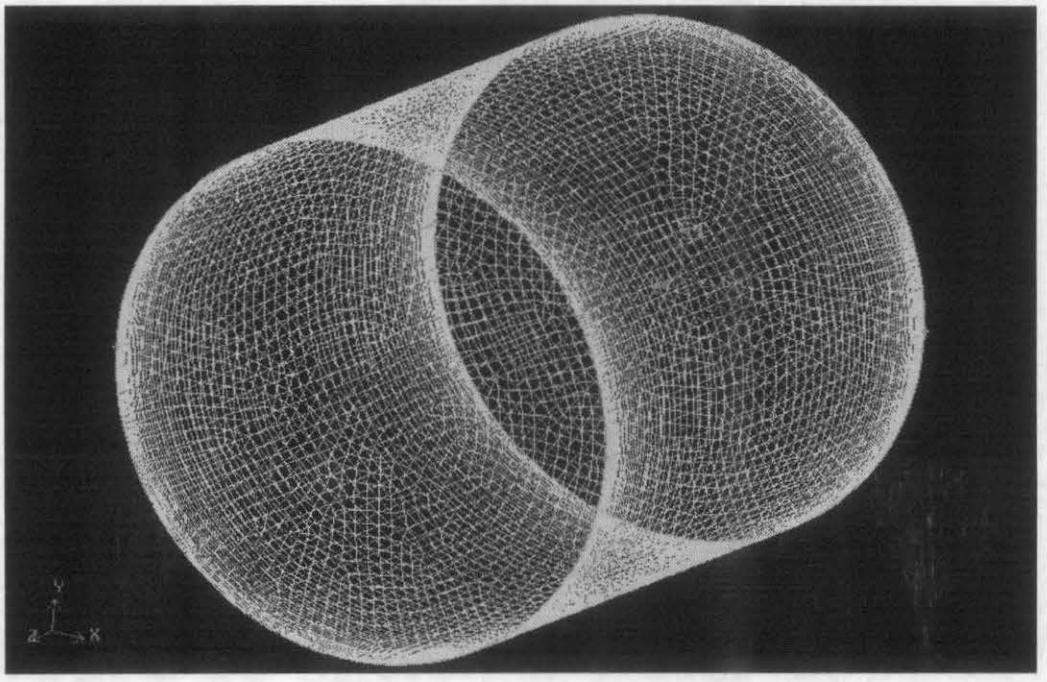

Figure 2-4: Three-Dimensional Structured Grid Inside a Circular Cylinder with End-Walls, L/D =1.0

As mentioned above, there are boundary layers near the solid walls. Therefore mesh is refined near the cold and hot end-walls, as well as near the boundary of the curved wall as shown in Figure 2-3 and Figure 2-5. This refinement is needed to accurately compute the large temperature gradients between the walls and the fluid inside the cylinder.

The mesh interval size is 0.5 and the refinement ratio is 1.08 on either side of the hot and cold wall for cylinder of aspect ratio L/D = 0.5. For cylinder of aspect ratio L/D = 1.0, the mesh interval size is again 0.5 but the refinement ratio is 1.07.

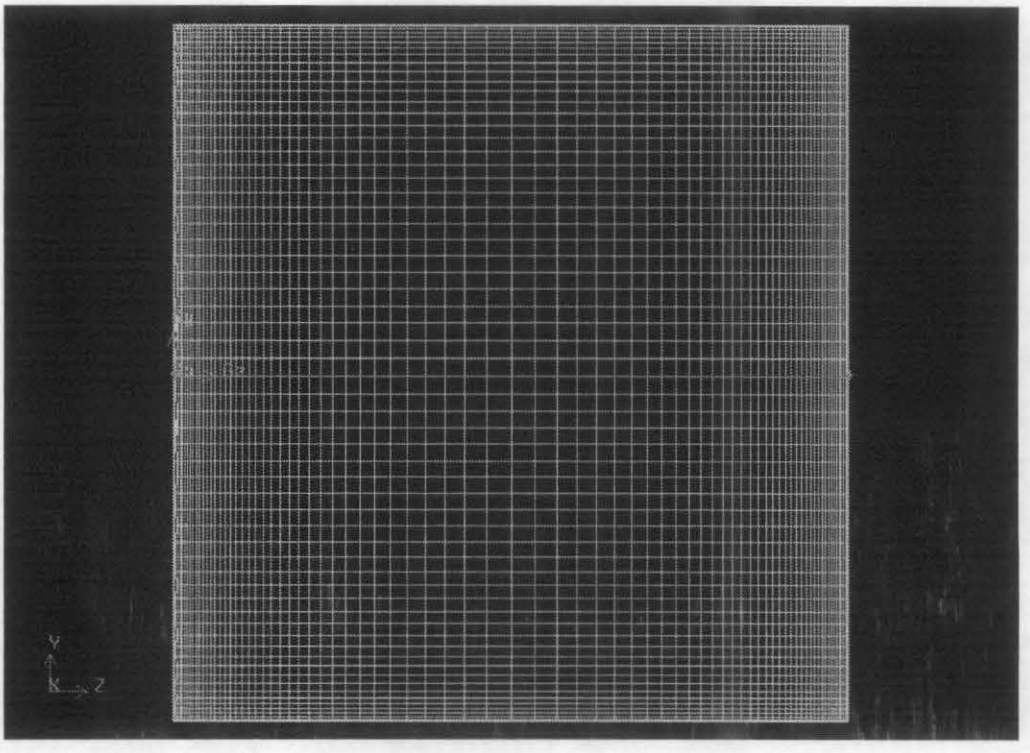

Figure 2-5: Side View of the Grid for the Circular Cylinder with End-Walls, L/D=1.0

For generating the mesh, Cooper option inside the GAMBIT is chosen in which the meshes on the hot wall and the cold wall are swept across the cylinder (see Table 2-2). Cooper option represents a meshing algorithm and the arrangement of mesh elements inside the model such that the meshes on the hot and cold wall are generated first as the source faces. Then, the meshes on source faces are projected throughout the volume of the cylinder. This is the most suitable scheme for generating the mesh in the cylinder model, since it can refine the mesh to accommodate the boundary layers near the hot and cold wall with structured elements.

Table 2-1: Table of Volume Meshing Options in GAMBIT [9]

Mesh Option	Function
Hexagon	Generates hexahedral mesh elements
Hexagon and Wedge	Generates mesh that is composed primarily of hexahedral mesh elements. Wedge elements are employed at locations that require better accuracy than that would be obtained with hexahedral elements
Tetrahedral and Hybrid	Generates mesh that consists primarily of tetrahedral mesh elements. Hexahedral, pyramidal, and wedge elements are applied where necessary

Table 2-2: Table of Various Schemes of Generating Mesh in GAMBIT [9]

Scheme Option	Function
Map	Produces a regular, structured grid consisting of hexahedral mesh elements
Submap	Separates unmappable volume into mappable regions and produces a structured grid of hexahedral mesh elements in each region
Tetrahedral Primitive	Splits four hexahedral regions from a four-sided volume and generates a mapped mesh in each region
Cooper	Creates sweeping mesh node patterns that are derived from source faces throughout the volume
Tetrahedral and Hybrid	Creates mesh consisting of majority tetrahedral elements. Hexahedral, pyramidal, and wedge elements are applied where suitable
Stairstep	Produces a hexahedral mesh in a faceted volume that approximates the structure of the original volume

2.4 Boundary Conditions

The boundary conditions applied to the numerical model are the same as those in the experiment [16]. No slip velocity boundary condition along with isothermal temperature boundary condition are applied at the hot and cold end-walls. At the curved surface of the cylinder, the no-slip velocity boundary conditions along with the adiabatic condition for the wall temperature are employed. The flow field is initialized by assuming zero velocity field inside the cylinder and a linear interpolation of the temperature field from hot to cold end-wall. The cold wall is kept at a constant temperature of 285 K, while the temperature of the hot wall is changed to 310 K, 329 K and 345 K. Two nanofluids, Al_2O_3-water and CuO-water at volume fraction of 0%, 1% and 4% of nanoparticles are considered. The flow field is three-dimensional due to the effect of gravity.

Chapter 3: Material Properties

3.1 Overview of Material Properties

The physical properties of a liquid (viscosity, thermal conductivity, density, specific heat, coefficient of thermal expansion etc.) are altered when nanoparticles are suspended in it. Due to their very small size (one billionth of a meter), the random motion of suspended nanoparticles behaves similar to the Brownian motion of the fluid particles; thus the nanofluids could be considered as a mixture of two fluids. Hence, there are two ways to describe the material properties of nanofluids. One method to characterize is to assume the nanofluids as single-phase fluids and the other approach is to treat the nanofluids as multiphase consisting of the base liquid and the dispersed nanoparticles [21]. In this study, the former description is chosen because of its simplicity.

3.2 Thermal Conductivity

Even a small volume fraction of nanoparticles inside a base fluid can effectively increase its thermal conductivity, and as a consequence, its heat transfer characteristics. The reason behind this increase in thermal conductivity has been attributed to large surface-area to volume ratio of nanoparticles, thermal conductivity of the solid nanoparticles, existence of interface layers between the liquid and the nanoparticles, and the ballistic movement of nanoparticles [2].

Since the heat transfer occurs at the surface of the particles, increasing the surface-area to volume ratio increases the thermal conductivity and therefore, the heat transfer rate. Thus, theoretically, the smaller is the size of the particles, the higher is the thermal conductivity. Since even a small volume fraction of nanoparticles has a large surface area, therefore nanofluids have a strong potential in increasing the heat transfer.

The low thermal conductivity of conventional heat transfer liquids such as water, ethylene glycol and engine oil can be increased by addition of higher thermal conductivity of nanoparticles. As shown in Table 3-1, the thermal conductivity of most solids whether metallic or nonmetallic, is larger than fluids. For example, the thermal conductivity of aluminum is about 940 times higher than that for ethylene glycol and the thermal conductivity of a carbon nanotube is about 4900 times greater than that of water. In nanofluids, these solid nanoparticles suspend almost uniformly inside the fluid and thus contribute towards enhancing their heat transfer capability.

As the nanoparticles are extremely small (of the order of a few hundred nanometers), inside a nanofluid, they are subjected to ballistic movement and therefore thermal dispersion occurs due to heat conduction and diffusion of solid particles [2]. Ballistic conduction is related to the large phonon mean-free path of the nanoparticles.

In regions close to the surface of the solid nanoparticles, fluid molecules behave more like solids. This is due to the fact that the molecules of the base fluid form a layered structure close to the surface of the nanoparticles which has thermal conductivity higher than that of the base fluid and thus facilitates the heat transfer caused by ballistic conduction and diffusivity of the nanoparticles. This phenomenon is analogous to heat transfer process that occurs from a solid wall to the adjacent fluid. The structured solid-like layer acts as the main transporter of heat from the wall to the fluid [5].

Table 3-1: Thermal Conductivity of Selected Materials [5]

Material		**Thermal Conductivity (W/m-K)** (at 298 K)
Nonmetallic fluids	Water	0.613
	Ethylene glycol	0.253
	Engine oil	0.145
Metallic Solid	Silver	429
	Copper	401
	Aluminum	237
Nonmetallic solid	Diamond	3300
	Carbon nanotubes	3000
	Silicon	148
	Alumina (Al_2O_3)	40

All theoretical models of thermal conductivity for both liquids and solid particles have their origin in the Fourier's Law of heat conduction. In the simulations presented in this thesis, we employ two theoretical models of thermal conductivity,: Maxwell model and the kinetic model.

3.2.1 Maxwell Model

This model was developed for solid-liquid suspensions containing micro-sized particles. Maxwell model predicts that the effective thermal conductivity of suspensions containing spherical particles increases with an increase in volume fraction of the solid particles. This model assumes that all the particles are of uniform spherical shape [14].

The formula for thermal conductivity is given as [14]:

$$k = \left[1 + \frac{3(\alpha - 1)\phi}{(\alpha + 2) - (\alpha - 1)\phi}\right] k_f \qquad (3\text{-}1)$$

where $\alpha = k_p / k_f$

k_p = Thermal conductivity of the nanoparticles

k_f = Thermal conductivity of the fluid

ϕ = Volume fraction of nanoparticles

3.2.2 Kinetic Model

Recently, there are two types of kinetic models that have been proposed in the literature [5]: one assumes that the nanoparticles in the fluid are stationary and the other assumes the movement of the particles inside the base fluids. In the present study, "stationary particle model" is employed in the simulations.

Stationary Particle Model

In the stationary particle model, heat flows along two similar paths through the suspension, that is through the liquid molecules and through the nanoparticles. The heat transfer rate can be represented by the formula [11]:

$$q = -k_m A_m \left(\frac{dT}{dx}\right)\left[1 + \frac{k_p \phi r_m}{k_m (1-\phi) r_p}\right] = -k_{eff} A_m \left(\frac{dT}{dx}\right) \qquad (3\text{-}2)$$

Based on this heat transfer rate equation, "Stationary Particle Model" of thermal conductivity can be deduced. The formula for effective thermal conductivity is shown below [11]:

$$k_{eff} = k_m \left[1 + \frac{k_p \phi r_m}{k_m (1-\phi) r_p}\right] \qquad (3\text{-}3)$$

where k_m = Thermal conductivity of the fluid particle

k_p = Thermal conductivity of the nanoparticle

A_m = Surface area of the fluid particle (molecule)

ϕ = Volume fraction of nanoparticles

r_p = Radius of nanoparticle

r_m = Radius of fluid particle

This effective thermal conductivity given by equation (3-3) is used in the numerical simulations reported in this thesis. The radius of fluid particles (water) used in this study is 3.2×10^{-10}m and the radius of nanoparticles (for both Al_2O_3 an CuO nanoparticles) is assumed to be 1×10^{-9}m.

Moving Particle Model

In this model, the effective thermal conductivity of the nanofluids also depends on the mean particle velocity of the nanoparticles. As mean particle velocity increases with the temperature, this model therefore takes into account the temperature of the fluid and its viscosity in determination of the effective thermal conductivity. The effective thermal conductivity of the nanofluid is given as [11]:

$$k_{eff} = \left[c.\bar{u}_p \frac{\phi r_m}{k_m (1-\phi) r_p} + 1 \right] k_m \qquad (3\text{-}4)$$

where c = Constant

k_m = Thermal conductivity of fluid particle

k_p = Thermal conductivity of nanoparticle

ϕ = Volume fraction of nanoparticles

r_p = Radius of fluid particle

r_m = Radius of nanoparticle

$\bar{u}_p$ = Mean velocity of nanoparticle

The mean velocity of a nanoparticle is related to the temperature by the Stokes-Einstein formula [11]:

$$\bar{u}_p = \frac{2k_b T}{(\pi \mu d_p^2)} \tag{3-5}$$

where k_b = Boltzmann constant ($1.38 \times 10^{-23} J.K^{-1}$)

T = Nanofluids Temperature

μ = Dynamic viscosity of base fluid

d_p = Diameter of Nanoparticles

Moving Particle Model of thermal conductivity is not employed in the numerical study reported in this thesis, since its effect on thermal conductivity of the nanofluid is determined to be negligibly small for cases of natural convection heat transfer in nanofluids considered in this thesis. This can be seen by performing the simple analysis as follows:

Substituting equation (3-5) into (3-4) yields:

$$k_{eff} = \left[c.\frac{2k_b \phi r_m}{k_m (\pi \mu d_p^2 (1-\phi) r_p)} T + 1 \right] k_m = \left[c.\frac{2k_b \phi r_m}{(\pi \mu d_p^2 (1-\phi) r_p)} T + k_m \right] \tag{3-6}$$

Equation (3-6) can be written as :

$$k_{eff} = b \cdot T + k_m \qquad \text{where} \qquad b = \frac{2ck_b\phi r_m}{(\pi\mu d_p^2(1-\phi)r_p} \tag{3-7}$$

Calculations of b have been performed for volume fraction ϕ of 0%, 1% and 4% for nanoparticles of diameter 1 nanometer in water at temperature 310 K; the values of b obtained are extremely small as shown in the Table 3-2. Thus, only the "Stationary Particle Model" is considered in our numerical computations.

Table 3-2: Calculation of Expression b of Equation (3-7)

Volume fraction ϕ	b
0	0
0.01	5.310923371495660E-08
0.04	2.190755890741960E-07

3.3 Density

The density of a nanofluid can be expressed in terms of the density of the base fluid, the density of the solid particles, and the volume-fraction of nanoparticles [5] as:

$$\rho_0 = (1-\phi)\rho_f + \phi\rho_p \tag{3-8}$$

where ρ_f is the density of the base fluid, ρ_p is the density of the nanoparticles material and ϕ is the volume fraction of nanoparticles inside the base fluid. Equation (3-8) shows that the density of nanofluids increases with the inclusion of nanoparticles. According to this model, the density of a nanofluid will increase about 5% by including about 1% volume-fraction of nanoparticles.

3.4 Specific Heat

Specific heat C_p is the only property of nanofluids that decreases by increasing the concentration. Equation (3-9) gives an expression for the specific heat of a nanofluid in terms of the volume fraction of nanoparticles ϕ, the density of the base fluid ρ_f, the density of the nanoparticles material ρ_p, the specific heat of base fluid C_{pf}, and the specific heat of the nanoparticles material C_{pp}.

$$C_p = \frac{(1-\phi)\rho_f C_{pf} + \phi\rho_p C_{pp}}{\rho} \qquad (3\text{-}9)$$

Equation (3-9) predicts only a very small decrease in the specific heat of the nanofluid compared to the base fluid. Experiments have also shown that for a small volume-fraction of less than 5% of nanoparticles inside water, the specific heat is almost the same as the base fluid [5].

3.5 Viscosity

In general, the viscosity of nanofluids increases with increase in the nanoparticles concentration. For nanofluids containing a low volume-fraction of nanoparticles, Einstein's model can be used to predict the viscosity of the nanofluid [5], [20]:

$$\mu = (1 + 2.5\phi)\mu_f \tag{3-10}$$

and

$$\mu_f = \mu_o \left[e^{-1.704 - 5.306\left(\frac{T_{ref}}{T}\right) + 7.003\left(\frac{T_{ref}}{T}\right)^2} \right] \tag{3-11}$$

where μ_f = Viscosity of the base fluid (water)

T = Temperature

T_{ref} = Reference temperature (293K)

ϕ = Volume fraction

μ_o = Reference viscosity of water (0.001788 $kgm^{-1}s^{-1}$)

Equation (3-11) shows the dependence of the viscosity of base fluid (water) on temperature. Einstein's equation (3-10) is valid only for small volume-fraction of nanoparticles, $\phi < 0.05$. It is applicable for the numerical simulations performed in this thesis, since the largest volume-fraction employed is 0.04. For higher concentration of nanoparticles ($\phi > 0.05$), Brinkman model can be applied. The Brinkman model of viscosity gives [21]:

$$\mu = \mu_f \left(\frac{1}{(1-\phi)^{2.5}} \right) \tag{3-12}$$

3.6 Thermal Expansion Coefficient

The coefficient of thermal expansion β is considered independent of the effect of the volume-fraction of nanoparticles. It is considered dependent only on the temperature of the base fluid. In the present study, the values of the coefficient of thermal expansion are considered to change with respect to the average temperature between the hot wall and the cold wall across the cylinder. The values of the coefficient of thermal expansion for water used in this study are shown in Table 3-3:

Table 3-3: Values of Thermal Expansion Coefficient of Water Used in Computation [10]

Average Temperature (K)	Thermal Expansion Coefficient, β ($1/K$)
298.15	0.0002
307.55	0.0003
315.55	0.0004

Chapter 4: Governing Equations

The governing equations describing the natural convection heat transfer are the equations of conservation of mass, momentum and energy in the presence of gravity as a body force. In our computations, we consider the nanofluid as a single phase fluid with material properties as given in Chapter 3. The fluid is considered incompressible with change in density due to body force (gravity) described by the Boussinesq approximation. The flow field is considered steady. Under these assumptions, the governing equations in differential form in Cartesian coordinate system are given below. These equations are solved in "FLUENT" using an appropriate numerical scheme on a suitable computational grid spanning the computational domain with appropriate boundary conditions. Various ymbols used in these equations are described in "Nomenclature".

4.1 Continuity Equation

The continuity equation is simply a mathematical expression of the principle of conservation of mass. In Cartesian coordinate system, for steady flow, the continuity equation can be written as:

$$\frac{\partial}{\partial x}(\rho u)+\frac{\partial}{\partial y}(\rho v)+\frac{\partial}{\partial y}(\rho w)=0 \qquad (4\text{-}1)$$

4.2 Momentum Equation

The momentum equation is a statement of the Newton's Second Law; it states that the sum of the forces acting on an element of fluid is equal to the rate of change of its momentum. In Cartesian coordinate system, the momentum equations in the three coordinate directions can be written as:

x-axis:

$$\frac{\partial}{\partial x}\left(\rho u^2 + p - \tau_{xx}\right) + \frac{\partial}{\partial y}\left(\rho uv - \tau_{xy}\right) + \frac{\partial}{\partial z}\left(\rho uv - \tau_{xv}\right) = 0 \qquad (4\text{-}2)$$

y-axis:

$$\frac{\partial}{\partial x}\left(\rho uv - \tau_{xy}\right) + \frac{\partial}{\partial y}\left(\rho v^2 + p - \tau_{yy}\right) + \frac{\partial}{\partial z}\left(\rho vw - \tau_{yz}\right) = -\rho g \qquad (4\text{-}3)$$

z-axis:

$$\frac{\partial}{\partial x}\left(\rho uw - \tau_{xz}\right) + \frac{\partial}{\partial y}\left(\rho vw - \tau_{yz}\right) + \frac{\partial}{\partial z}\left(\rho w^2 + p - \tau_{zz}\right) = 0 \qquad (4\text{-}4)$$

Note that in equation (4-3), ρg represents the body force term due to gravity acting on the fluid in the negative y-direction.

4.3 Energy Equation

The energy equation mathematically describes that the rate of change of total energy (internal energy plus the kinetic energy) of a fluid element is equal to the work done by various forces (pressure, viscous and body) and heat addition or subtraction. The equation describing the conservation of energy can be written as:

$$-\rho g v+\frac{\partial}{\partial x}\left(E_t u+pu-u\tau_{xx}-v\tau_{xy}-w\tau_{xz}+q_x\right)+\frac{\partial}{\partial y}\left(E_t v+pv-u\tau_{yx}-v\tau_{yy}-w\tau_{yz}+q_y\right)$$

$$+\frac{\partial}{\partial z}\left(E_t w+pw-u\tau_{xz}-v\tau_{yz}-w\tau_{zz}+q_z\right)=0 \qquad (4\text{-}5)$$

4.4 Boussinesq Approximation for Density

In natural convection heat transfer, the effect of buoyancy due to gravity is modeled as a body force in the vertical direction as shown by R.H.S term in equation (4-3). While the density can be considered constant in low speed flow in all the equations (4-1)-(4-5), its variation with temperature in the ρg term in equation (4-3) must be accounted. The relationship of density with temperature in ρg term in equation (4-3) is given by:

$$\rho=\rho_0\left(1-\beta\Delta T\right) \qquad (4\text{-}6)$$

Everywhere else in equations (4-1)-(4-5), the density is taken as constant, $\rho=\rho_0$.

Chapter 5: Numerical Solution Procedure

5.1 Overview of the Numerical Solution Procedure

The governing equations of fluid flow, equations (4-1) to (4-5), are numerically solved on a structured mesh described in Chapter 2 using the 3-D segregated steady state solver in FLUENT 6.0. The material properties of the nanofluids described in Chapter 3 are "input" in FLUENT as Used Defined Functions (UDF). In segregated solver, the steady state partial differential equations are discretized using finite-volume method described in section 5.2. The difference equations are solved using the Gauss-Siedal relaxation in conjunction with an algebraic multigrid method. Gauss-Siedal and multigrid iteration are performed until the convergence is achieved to a specified level of reduction in residuals ($1x10^{-6}$ in our case). Table 5-1 gives the values of under-relaxation factors employed in the numerical computations.

Table 5-1: Solution Controls (Under-relaxation Factors) Employed in the Computations

Under-relaxation factors		Discretized Equation	Algorithm
Pressure	0.3	Pressure	Standard Central Difference
Density	0.9	Pressure-velocity Coupling (Continuity)	SIMPLE [9]
Body Force	0.9	Momentum	First-order Upwind
Momentum	0.7	Energy	First-order Upwind
Energy	0.9		

5.2 Segregated Solver

In the steady state segregated solver in FLUENT 6.0, the nonlinear governing equations (mass, momentum and energy equations) of fluid flow are solved sequentially and thus are segregated from one to another. The numerical solution process goes through many iterations until the convergence criterion is met. In this study, the convergence criterion is set at $1x10^{-6}$, which implies that the difference in the solution of a flow variable between two successive iterations is 10^{-6}. Each iteration in the solution process is divided into several stages, which correspond to the solution of various conservation equations as shown in Figure 5-1.

The iteration process starts with initialization of the fluid properties, such as temperature, pressure and velocity, which are provided as "input" to FLUENT by the user. The momentum equations are first solved to obtain the velocity components u, v and w, utilizing the initial values of the flow variables. A pressure correction equation is introduced into the computation (derived from the continuity equation in SIMPLE algorithm [9]) and is solved if the velocity components u, v and w obtained from the momentum equations do not satisfy the continuity equation. This pressure correction equation (which is a Poisson equation) is derived from the linearized momentum equations and continuity equation. The computed pressure correction gives the correction required for the velocity components u, v, and w to satisfy the continuity equation. Thus this pressure correction adjusts not only the values of the velocity components but also the pressure and the face mass flux so that the conservation of mass is attained. After the continuity condition is met, the energy equation is solved for calculating the temperature distribution, utilizing updated flow variable values computed from the previous two steps as shown in Figure 5-1 [9]. At this stage, a convergence evaluation is performed for all the flow variables. If the convergence criterion is met, the iteration process is stopped, otherwise all the previous steps are repeated and the iteration process is continued until convergence is achieved.

In the segregated steady state solver, the discretized form of each of the governing equations is represented as a system of linear equations. This scalar system of linear equations is solved using a Gauss-Siedal linear equation solver together with the Algebraic Multigrid method (AMG) [9]. For example, in order to solve for w-velocity component at all cells in the computational domain, the z-momentum equation is linearized into system of algebraic equations where w-velocity components at different cell locations are the unknowns. Gauss-Siedal linear algebraic equations solver and the algebraic multigrid (AMG) method are applied to obtain the updated algebraic w-velocity components at all cell location in the computational domain. Thus, all the w-velocity components are obtained simultaneously. This process is repeated for other equations.

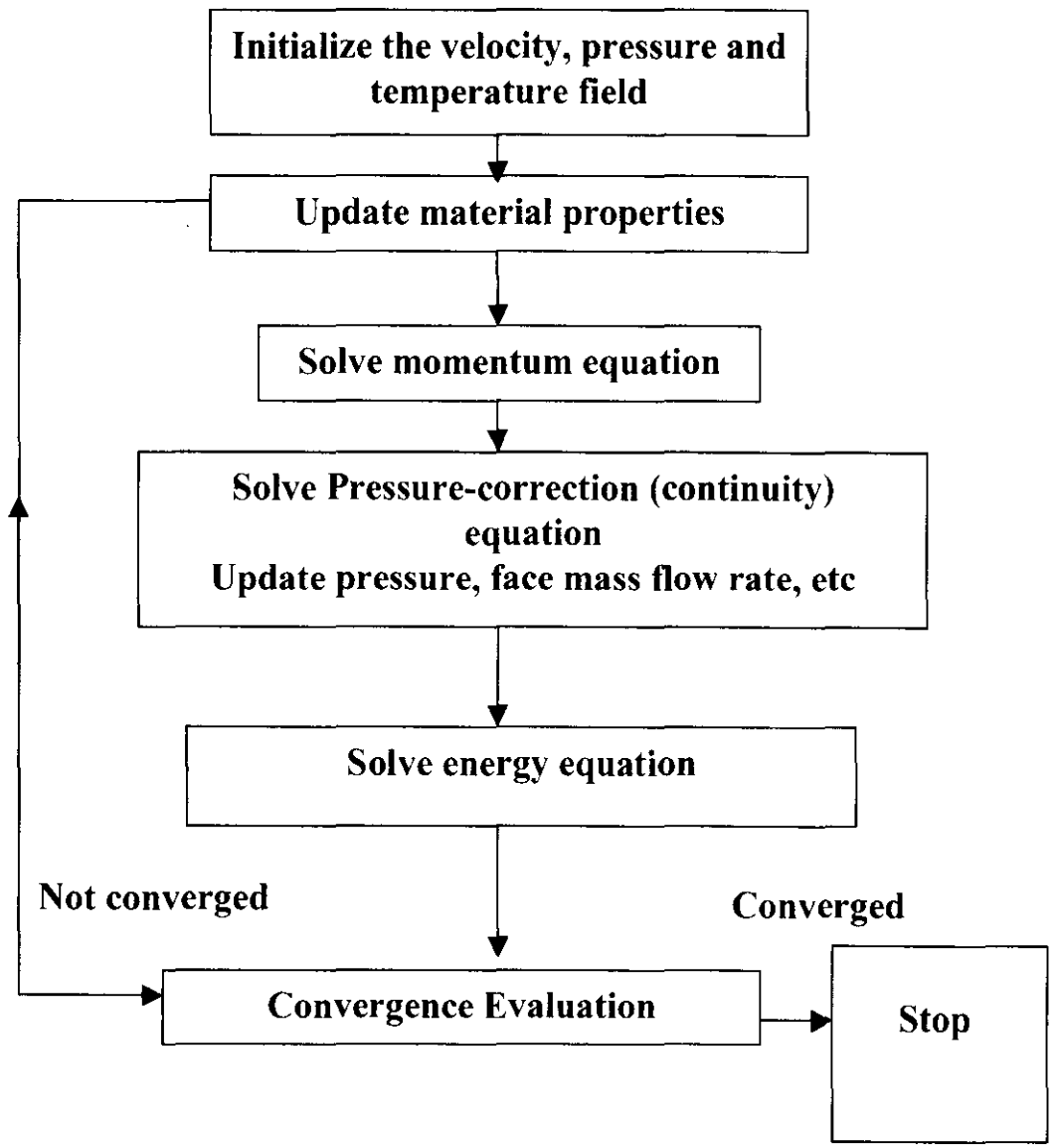

Figure 5-1: Overview of the Segregated Solution Method [9]

5.3 Discretization

In FLUENT, the governing partial differential equations of fluid flow are solved using the control-volume approach, wherein each element of the computational grid is treated as a control volume. The governing equations are converted into algebraic equations by integrating them on these control volumes created by the computational mesh. The set of algebraic equations (corresponding to a partial differential equation) is then arranged in a scalar system of linear equations which is solved by the Gauss-Siedal linear equation solver in conjuction with the Algebraic Multigrid method (AMG). The application of the control volume technique to a generic governing equation is given below [9]. The partial differential equation is integrated over a control volume (grid element) of volume V and surface area A to yield:

$$\oint_A \rho\phi\vec{v}\cdot d\vec{A} = \oint_A \Gamma_\phi \nabla\phi \cdot d\vec{A} + \int_V S_\phi dV \qquad (5\text{-}1)$$

where ρ = Density

ϕ = Scalar flow variable

$\vec{v}$ = Velocity vector

$\vec{A}$ = Surface area vector

Γ_ϕ = Diffusion coefficient

S_ϕ = Source term per unit volume.

For a cell with N faces, equation (5-1) can be written as:

$$\sum_{f=1}^{N_{faces}} \rho_f \vec{v}_f \phi_f \cdot \vec{A}_f = \sum_{f=1}^{N_{faces}} \Gamma_\phi (\nabla \phi)_n \cdot \vec{A}_f + S_\phi V \qquad (5\text{-}2)$$

N_{faces} = Number of faces enclosing a cell

ϕ_f = Value of scalar ϕ on face f

$\rho_f \vec{v}_f \cdot \vec{A}_f$ = Mass flux though cell face f

$\vec{A}_f$ = Vector area of cell face f

n = Outward unit normal to the cell face

V = Cell volume V

Equation (5-2) can be written for all cells in the computational domain. A set of equations of the type (5-2) for all cells in the computational domain gives a set of algebraic equations which are linearized and then solved by a linear algebraic equations solver as described before in section 5.2

Linear interpolation is used to obtain the face values from the cell center values. The face values are obtained from the cell upstream in the direction of the normal velocity v_n in equation (5-2). In FLUENT, there are several options of upwind schemes, namely the first-order upwind, second-order upwind, power law and QUICK schemes [9]. Central difference scheme is always applied to the diffusion terms in equation (5-2) and is always second order accurate. In this study, first-order upwind scheme is used in discretizing the convective terms in momentum and energy equations (Table 5-1).

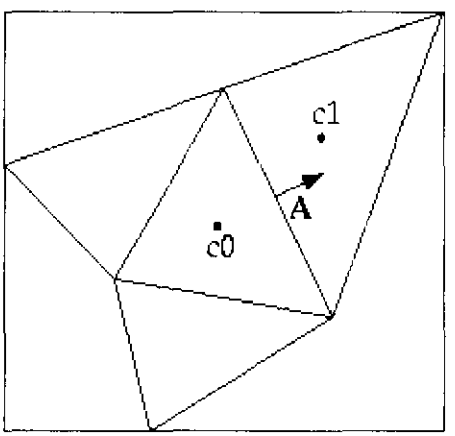

Figure 5-2 : Diagram of a Control Volume Displaying the Discretization of a Scalar Transport Equation [9]

The discrete values of material properties such as thermal conductivity, viscosity, etc. along with the discrete values of the other scalars such as pressure and temperature are stored at the cell centers.

5.3.1 Pressure Interpolation Scheme

In FLUENT, the values of pressure are stored at the center of the cells ($c0$ and $c1$ in Figure 5-1). However, in order to execute the discretized momentum equations, the pressure values at the cell faces must be obtained, and this is achieved through interpolation of the values of the pressure from the cell centers to the cell faces.

For the pressure interpolation, standard scheme option in FLUENT is chosen. Standard scheme interpolates the pressure values from cell centers to the cell faces using the momentum equations. This is considered a good approximation as long as the pressure variation between the cell centers is not too large. Standard pressure interpolation scheme is not suitable for flows that have large body forces, such as strongly swirling flows and very high Rayleigh number flows.

In the present study, the change in pressure and change in density are due to the buoyancy effect, and furthermore because of the small size of the geometry of test cylinder (40mm in diameter), standard scheme is reasonable.

5.3.2 Pressure-Velocity Coupling

In incompressible flow, continuity equation contains only the velocity components and is independent of pressure, while the momentum equations contain both the velocity components and the pressure. Thus, in order to determine a pressure and velocity field that satisfy both the equations, a method is needed that can couple the two equations strongly. Such a technique has been termed as "Pressure Velocity Coupling" procedure in the literature. In this procedure, a guessed pressure field is applied to the momentum equations which are then solved for the velocity field. In general, this velocity field does not satisfy the continuity equation. A small correction for the pressure and velocity field is then assumed which is then substituted into the continuity equation to derive a pressure-correction equation, which is a Poisson equation. It is solved to obtain the pressure correction which is then used to correct (or update) the velocity field. This procedure is repeated until both the computed pressure and velocity fields satisfy both the continuity and momentum equations as shown in Figure 5-1. There are three algorithms for pressure-velocity coupling in the segregated solver in FLUENT. These are called SIMPLE, SIMPLEC and PISO.

SIMPLE stands for Semi-Implicit Method for Pressure-Linked Equations. In this algorithm, a pressure correction equation is derived using the procedure described above [17]. SIMPLEC is an acronym for Semi-Implicit Method for Pressure-Linked Equations-Consistent or SIMPLE-Consistent. This algorithm is basically the same as SIMPLE

except that the initial pressure field is calculated from the assumed velocity field by solving a Poisson equation [8], rest of the algorithm is same as SIMPLE. PISO is defined as Pressure Implicit with Splitting of Operators. This algorithm was originally developed for non-iterative computation of unsteady compressible flow but was later modified for iterative computation of incompressible steady state problems. The basic philosophy behind PISO is the same as that of SIMPLE, however it is much more complex. It is a two-step predictor-corrector type of algorithm in which each step has its own pressure-correction equation. As a result, PISO requires additional computational effort but attains faster convergence especially for transient problems [17].

For majority of the steady state problems in relatively simple geometries, SIMPLEC is recommended for faster convergence, since it provides a more consistent treatment of pressure-velocity coupling compared to SIMPLE [17]. In this algorihm, relaxation factor for the pressure-correction equation is generally set to 1.0 to enhance convergence. However, for many complex problems, relaxation factor of 1.0 can lead to instability and divergence. In these situations, there may not be much difference in the convergence characteristics of SIMPLEC and SIMPLE algorithms. PISO algorithm is especially useful for transient flow calculations, since it allows for computations with large time step. It is also recommended for steady state calculations on highly distorted and skewed meshes [8]. In present study, SIMPLE algorithm is employed since the flow is laminar and the geometry is simple. The computational instabilility in SIMPLE can be easily controlled by selecting appropriate under-relaxation factors as shown in Table 5-1.

5.4 Under-Relaxation Factors

Under-relaxation factors are employed to prevent divergence of the solution in the iteration process; they do not affect the accuracy of the results. Because of the nonlinearity of the equations, it is sometimes necessary to control the change in the values of the computed variables from one iteration to the next. Under-relaxation factors that are applied in this computation are set to be as close to 1 as possible for faster convergence to the exact solution satisfying a convergence criterion. Under-realxation factors used in this study are shown in Table 5-1.

5.5 Computational Parameters and Data

In this study, as mentioned in Chapter 1, the goal is to simulate the natural convection heat transfer in nanofluids and compare the results of calculations with the experimental data. For a given geometry of the cylinder, first a mesh is generated using "GAMBIT" as described in Chapter 2. This mesh is then linked to the segregated solver in FLUENT. All the inputs (material properties of nanolfuids, initial values of the flow variables, under-relaxation factors etc) are provided to run FLUENT. A convergence criterion of 10^{-6} for reduction in residuals of the flow variables is set. The converged flow field data is then reduced in proper form to compare with the experimental results.

For each case, heat transfer rate Q from hot wall is computed by a FLUENT command that calculates the total value of the heat transfer rates of a surface. Using the value of the heat transfer rate, heat transfer coefficient is calculated using equation (1-3). Nusselt Number and Rayleigh Number are then computed from equations (1-1) and (1-2) respectively using the values of the material properties of the nanofluid. Plots of Nusselt Number vs Rayleigh Number are then obtained for two nanofluids (Al_2O_3-water and CuO-water) with 0%, 1% and 4% volume-fraction for two cylinders of aspect ratio of L/D=0.5 and L/D=1.0.

Chapter 6: Results and Discussions

In this chapter, the numerical solutions of natural convection heat transfer inside a cylinder containing nanofluid, bounded by a hot isothermal wall and a cold isothermal wall and an adiabatic wall on the curved surface, are presented. Computations are performed for two nanofuids: Al_2O_3-water and CuO-water with volume fraction of nanoparticles of Al_2O_3 and CuO in water of 0%, 1% and 4%. Two cylinder geometries of aspect ratio L/D=0.5 and 1.0 are considered. Three values of temperature difference $\Delta T = (T_H - T_C)$ between the hot wall and cold wall are considered. These cases correspond to those in the experiment [16]. The computed values of heat transfer rate using FLUENT 6.0 software are presented in terms of Nusselt Number. Graphs of Nusselt Number vs Rayleigh Number are plotted and compared with the experimental results. The computed results are in reasonable agreement with the experimental results for all the cases considered as discussed below. The results show that the Nusselt Number increases with the Rayleigh Number but it decreases with increase in nanoparticles concentration from 0% to 4%.

6.1 Numerical Solutions for Pure Water (ϕ=0%)

These calculations do not require models for material properties of the nanofluids as given in Chapter 3. Hence they are used to validate the numerical solutions against the experimental data. Figure 6-1 and Figure 6-14 show the variation in Nusselt Number with Rayleigh Number for volume-fraction of 0% nanoparticles in pure water for two

cylinders of aspect ratio (L/D) 0.5 and 1.0 respectively. Nusselt Number is computed for three Rayleigh Numbers corresponding to hot wall temperatures of 310 K, 329 K and 345 K and the cold wall temperature of 285 K. The computed results are in good agreement with the experimental data. Both the computations and the experimental data show an increase in Nusselt Number with increasing Rayleigh Number, as expected.

It should be noted here that the Rayleigh Number in the computations and the experiment is not exactly the same; there is a very small difference between the two values. It is due to differences in the values of the material properties (μ , k, β, C_p) used in the computations and those are in the experiment. The values of material properties in the experiment cannot be ascertained and are not given in the paper [16]. The material properties used in the simulations of pure water are gathered from the available FLUENT database [9] except for the viscosity and the thermal expansion coefficient. The viscosity of pure water, which changes with temperature, is obtained from the fluid dynamics textbook [20], and the value of thermal expansion coefficient is obtained through internet source [10]. The value of thermal expansion coefficient at a given temperature is obtained by linearly interpolating between its values of 0.0002 K^{-1} and 0.0004 K^{-1} at temperature of 20°C and 40°C respectively. All material properties that are "input" into FLUENT are obtained at the average temperature between the cold wall and the hot wall.

6.2 Numerical Solutions for 1% Volume Fraction of Nanoparticles

When nanoparticles of Al_2O_3 and CuO are added to the pure water to make up 1% of volume fraction, the numerical solutions show that the Nusselt Number decreases compared to that for the pure water. The numerical results exhibit the same trend as the experimental data although their accuracy is now dependent upon the theoretical models employed for the thermal conductivity of the nanofluid. Numerical solutions obtained using the experimental values of viscosity and thermal conductivity from [16] are closest to the experimental data for both cylinders of aspect ratio L/D=0.5 and L/D=1.0, as shown in Figures 6-6 and 6-19 for Al_2O_3-water nanofluid.

When theoretical models of thermal conductivity (Maxwell model and Kinetic model given in chapter 3) are employed, the discrepancy between the calculations and the experimental data is somewhat greater as shown in Figures 6-7 and 6-20 for cylinders of aspect ratio L/D = 0.5 and 1.0 respectively. Both the Maxwell model and Kinetic model predict the correct trend that the Nusselt Number increases with the Rayleigh Number, however the results obtained with the Kinetic model have better agreement with the data than those obtained with the Maxwell model. This is because the thermal conductivity formula in the kinetic model takes into account the size of the nanoparticles as well as the volume fraction of the nanoparticles in the nanofluid whereas the Maxwell model only accounts for the volume fraction. Also, the thermal conductivity calculated by the kinetic model is higher than that obtained from Maxwell model. In the kinetic model, the size of

nanoparticles is assumed to be 1nm for both Al_2O_3 and CuO nanoparticles. In the numerical calculation, the nanoparticles are assumed to be uniformly suspended in water, although in reality, some degree of agglomeration does occur even at low concentration of nanoparticles in the liquid [7]. This agglomeration affects the thermal conductivity and this effect also contributes to the difference between the numerical results and the experimental data.

In Figures 6-21, 6-22 and 6-23, the graphs of computed temperature distribution along the axis of the cylindrical are plotted for 1% Al_2O_3-water nanofluids for a cylinder of aspect ratio L/D=1.0 with hot wall temperature of 310 K, 329 K and 345 K respectively, the cold wall is kept at a constant temperature of 285 K. The numerical results display an almost constant temperature pattern in the center region of the cylinder, which is in agreement with the experimental findings. The temperature distribution along the axis of the cylinder is nearly constant due to the presence of thermal stratification in the vertical direction caused by the convective flow near the hot and cold wall [16].

When CuO nanoparticles with 1% volume fraction are suspended, the numerical solutions again show the same behavior as in the case of 1% Al_2O_3-water nanofluid as shown in Figures 6-30 and 6-31. At a given Rayleigh Number, the Nusselt Number is lower due to the presence of nanoparticles in the nanofluid compared to that for the pure water. Again, the numerical results obtained using the experimental values of thermal conductivity and viscosity are in closer agreement with the experimental data (Figure 6-30) than those obtained with the theoretical models of thermal conductivity. This

discrepancy can be attributed to the fact that the experimental value of viscosity was taken to be the same as that of Al_2O_3-water nanofluid and this contributes to the larger error. The numerical solutions with two thermal conductivity models (Figure 6.31) produce curves similar to those obtained for Al_2O_3-water nanofluid (Figure 6-20). Again the kinetic model shows a better agreement with the experiment than the Maxwell model. Again, similar to results of Al_2O_3-water nanofluid simulations, the Maxwell and kinetic model simulations for CuO-water nanofluid predict a higher Nusselt Number than the experimental data.

6.3 Numerical Solutions for 4% Volume Fraction of Nanoparticles

When the volume fraction of nanoparticles is increased to 4%, the numerical solutions exhibit the same trend in the graphs of Nusselt number vs Rayleigh number as observed in the experimental results. The higher the concentration of nanoparticles, lower is the Nusselt number for both Al_2O_3 and CuO nanoparticles. This trend becomes clear by comparing the results for nanofluids with 4% volume fraction of nanoparticles against those for nanofluids with 1% volume fraction of nanoparticles. This phenomenon is rather paradoxical as pointed out in Ref. [16], since it does not occur in forced convection heat transfer. The conventional wisdom is that the increase in volume fraction of nanoparticles in a nanofluid increases the thermal conductivity and therefore the heat transfer should increase. However, both the present computations and the experiment [16] show degradation in heat transfer in natural convection. In [16], one of the reasons

for this degradation in heat transfer has been attributed to the presence of slip between the nanoparticles and fluid particles which significantly disturbs the suspension of the nanoparticles inside the liquid especially in very low velocity natural convection flow.

CuO nanoparticles, with higher material density compared to Al_2O_3 nanoparticles, exhibit higher deterioration because of greater slip between the higher density nanoparticles and the fluid. In general, computations of heat transfer (Nusselt number) at different Rayleigh number for nanofluids with 4% volume fraction of nanoparticles give trends similar to those for nanofluids with 1% of volume fraction of nanoparticles.

Numerical results obtained by utilizing the experimental values of viscosity and thermal conductivity again show a better agreement with the experimental data (Figures 6-8, 6-24 and 6-32) than those obtained with the Maxwell and Kinetic models (Figures 6-9, 6-25 and 6-33). Again the results obtained with the Kinetic model are closer to the experimental data compared to those obtained with the Maxwell model.

It should be noted that as the volume fraction of nanoparticles in a nanofluid increases the error between the computations and the experimental data also appears to increase. This increase in discrepancy can be attributed to the fact that at higher concentration of nanoparticles, the suspension may not be uniform in the experiment. Additionally, the theoretical models also need further refinement.

Figures 6-2 and 6-3 show the temperature contours in x-y plane and y-z plane that cut through the center of the cylinder of aspect ratio L/D = 0.5 for pure water. Figures 6-10 and 6-11 show the temperature contours in x-y plane and y-z plane that cut through the center of the cylinder of aspect ratio L/D = 0.5 for Al_2O_3-water nanofluid with 4% volume fraction of nanoparticles. Figures 6-15 and 6-16 show the temperature contours in x-y plane and y-z plane that cut through the center of the cylinder of aspect ratio L/D = 1.0 for pure water. Figures 6-26 and 6-27 show the temperature contours in x-y plane and y-z plane that cut through the center of the cylinder of aspect ratio L/D = 1.0 for Al_2O_3-water nanofluids with 4% volume fraction of nanoparticles. It is evident that there is thermal stratification in the y-direction (direction of gravity), which was also noted in the experiment [16]; the temperature is almost constant along the horizontal axis of the cylinder but changes in the vertical direction [16]. The hot fluid occupies the top region of the cylinder, while the colder fluid settles at the bottom of the cylinder, as expected. With the inclusion of nanoparticles, the temperature distribution pattern essentially remains unchanged except that it results in a slight increase in the hot flow region.

Figures 6-4 and 6-5 show the velocity vectors in x-y plane and y-z plane that cut through the center of the cylinder of aspect ratio L/D = 0.5 for pure water. Figures 6-12 and 6-13 show the velocity vectors in x-y plane and y-z plane that cut through the center of the cylinder of aspect ratio L/D = 0.5 for Al_2O_3-water nanofluid with 4% volume fraction of nanoparticles. Figures 6-17 and 6-18 show the velocity vectors in x-y plane and y-z plane that cut through the center of the cylinder of aspect ratio L/D = 1.0 for pure water. Figures 6-28 and 6-29 show the velocity vectors in x-y plane and y-z plane that cut

through the center of the cylinder of aspect ratio L/D = 0.5 for Al_2O_3-water nanofluid with 4% volume fraction of nanoparticles. A circulation pattern in the velocity field can be seen, as expected. The velocity magnitudes are very small with the highest velocity being 0.0049m/s for pure water and 0.00556m/s for 4% Al_2O_3-water nanofluid in a cylinder of aspect ratio L/D = 0.5. The maximum velocity is 0.00463m/s for pure water and 0.00423m/s for 4% Al_2O_3-water nanofluid in a cylinder of aspect ratio L/D=1.0. This circulatory flow exists due to the thermal stratification resulting from the buoyancy effect. It should also be noted that the increase in concentration of nanoparticles does not affect the flowfield in any appreciable way; this is expected since our nanofluids model treats them as single phase fluid assuming that the nanoparticles are suspended in the base liquid uniformly.

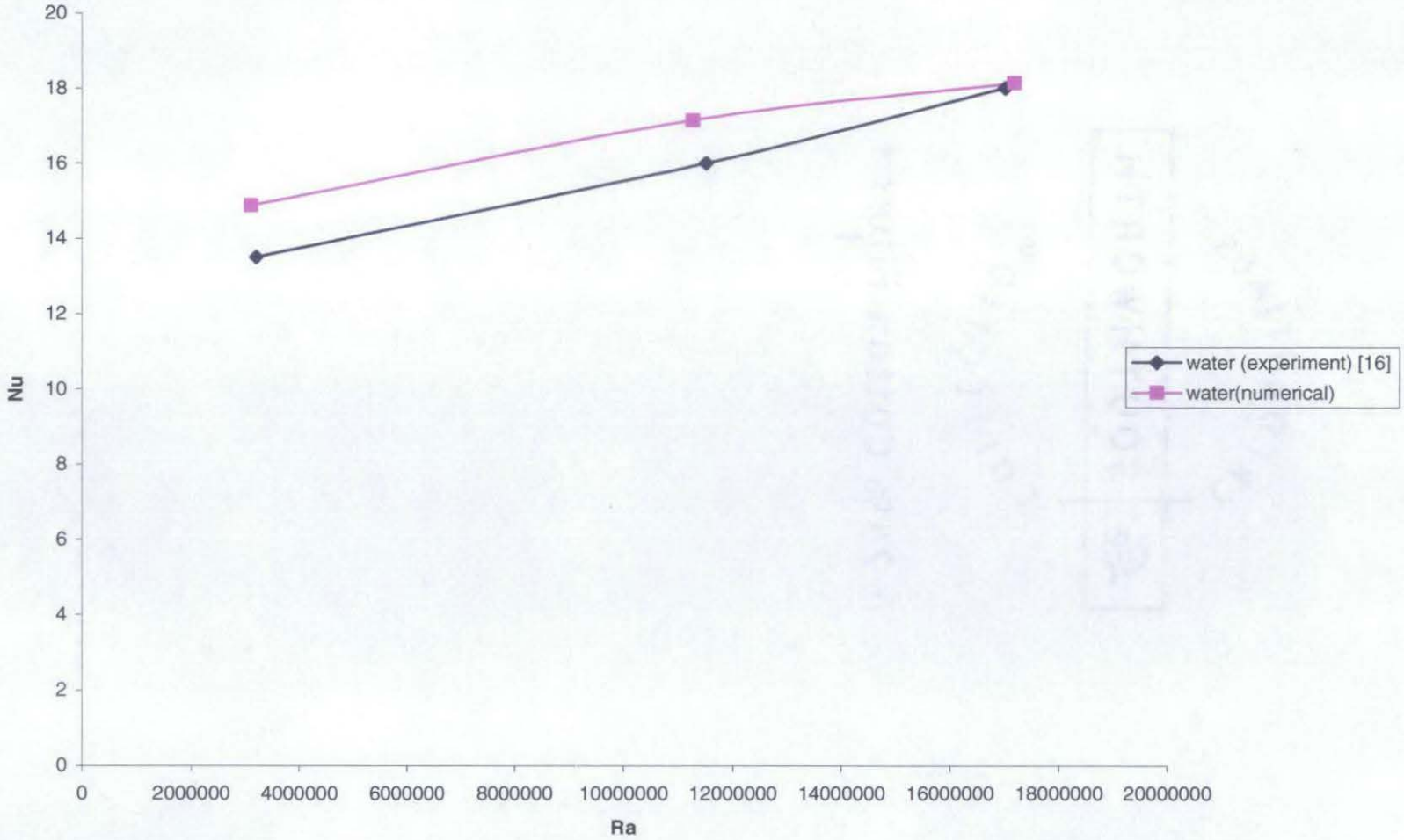

Fig 6-1: Graph of Nusselt Number vs Rayleigh Number for L/D=0.5 and $\phi = 0\%$ (Pure Water)

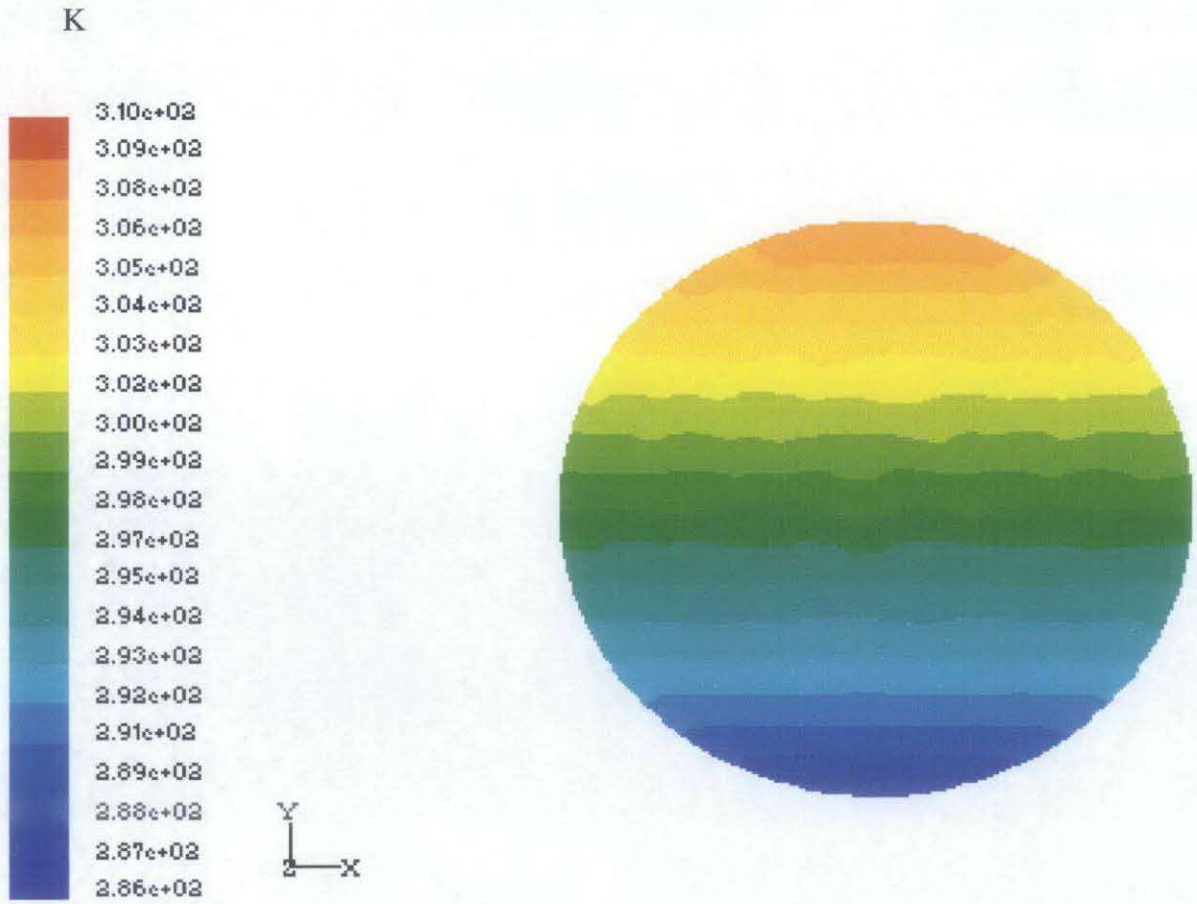

Fig. 6-2: Temperature Contours in x-y Plane at z=0.01m (the center of the cylinder), L/D=0.5, ϕ = 0% (pure water), T_h=310K, T_c=298K

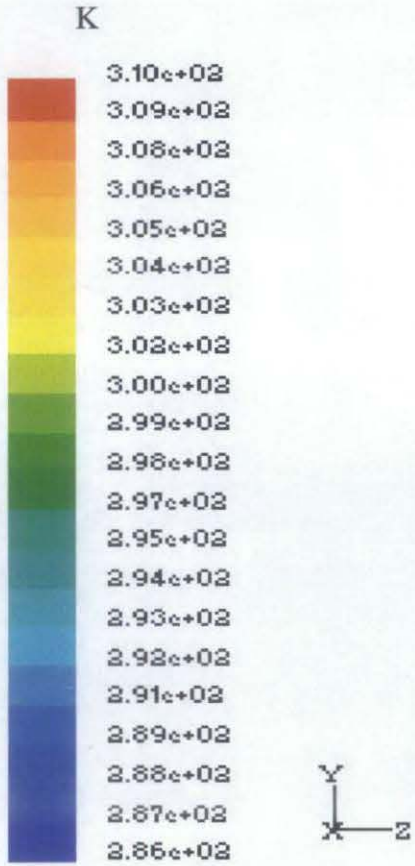

Fig. 6-3: Temperature Contours in y-z Plane at x=0 (the center of the cylinder), L/D=0.5, ϕ = 0% (pure water), T_h=310K, T_c=298K

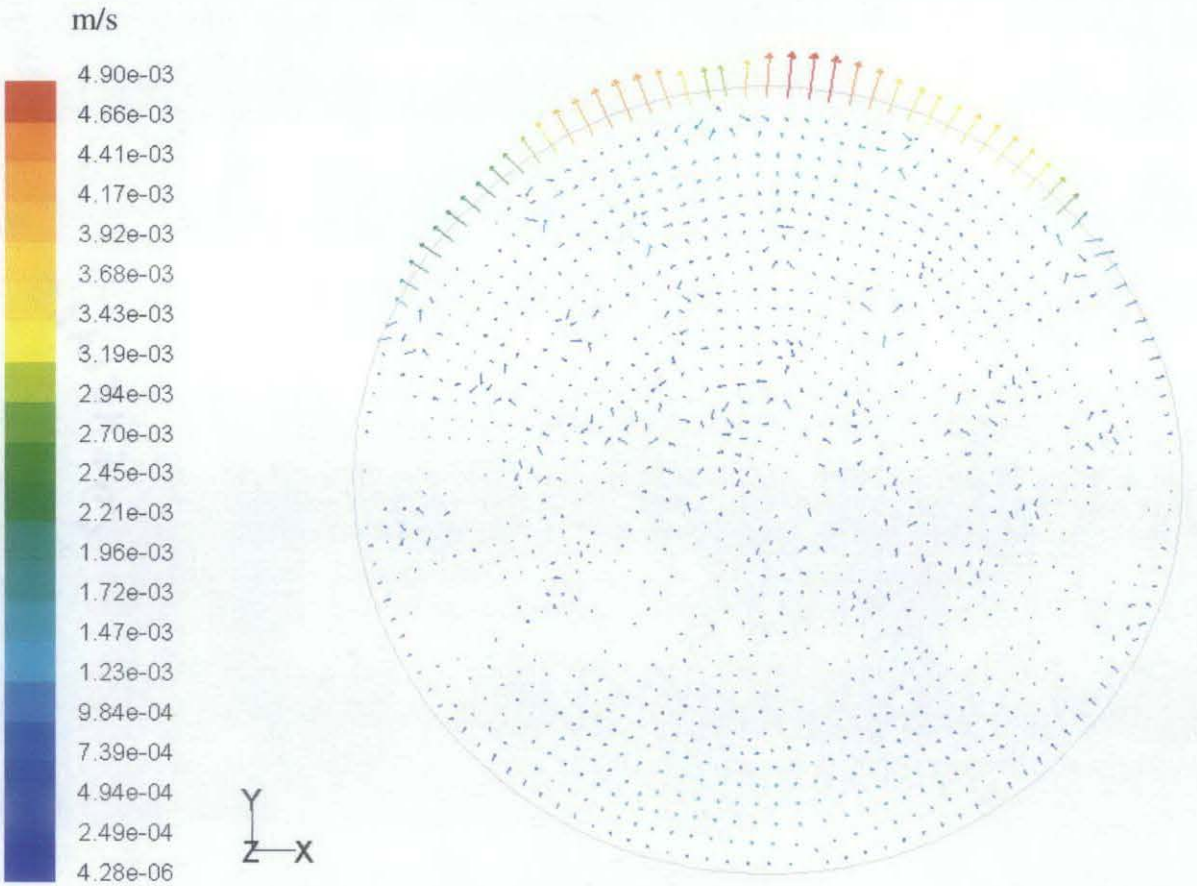

Fig. 6-4: Velocity Vectors in x-y Plane at z=0.01m (the center of the cylinder), L/D=0.5, ϕ = 0% (pure water), T_h=310K, T_c=298K

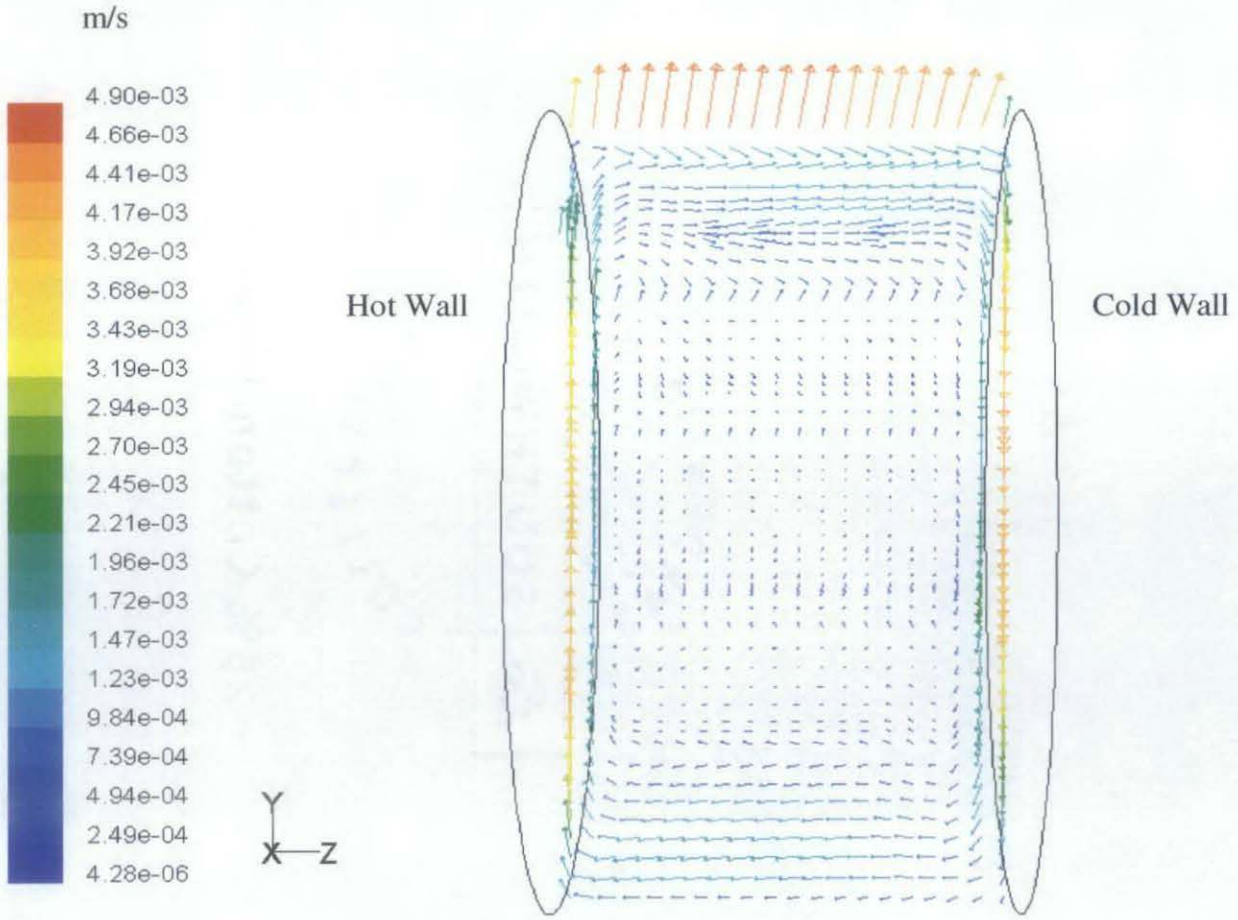

Fig. 6-5: Velocity Vectors in y-z Plane at x=0 (the center of the cylinder), L/D=0.5, ϕ = 0% (pure water), T_h=310K, T_c=298K

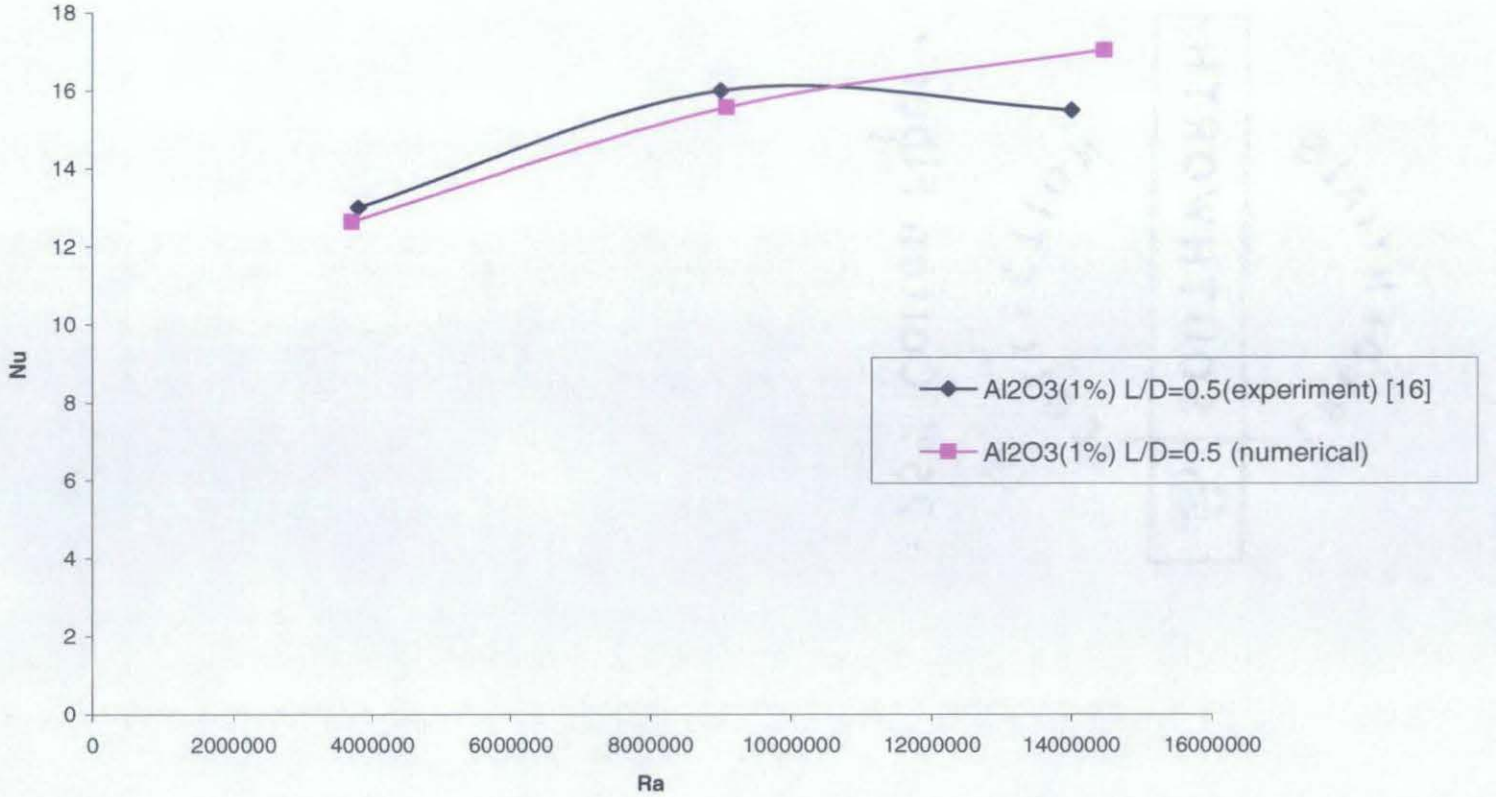

Fig 6-6: Graph of Nusselt No. vs Rayleigh No. for L/D=0.5 with Al_2O_3 Nanoparticles ($\phi = 1\%$) in Water. Experimental Values of μ and k are Employed.

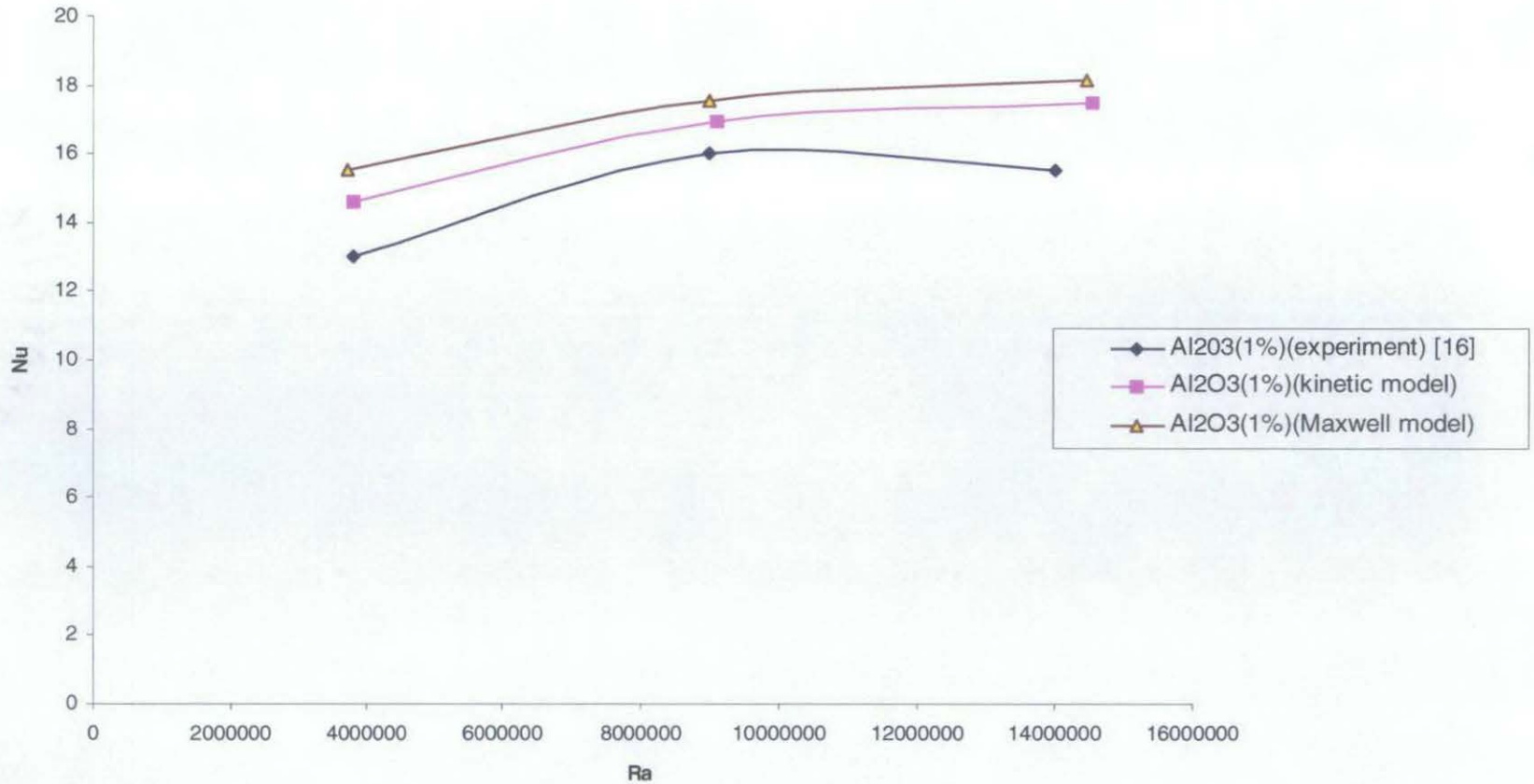

Fig 6-7: Graph of Nusselt No. vs Rayleigh No. for L/D=0.5 with Al_2O_3 Nanoparticles (ϕ=1%) in Water. Theoretical Models of Thermal Conductivity are Employed.

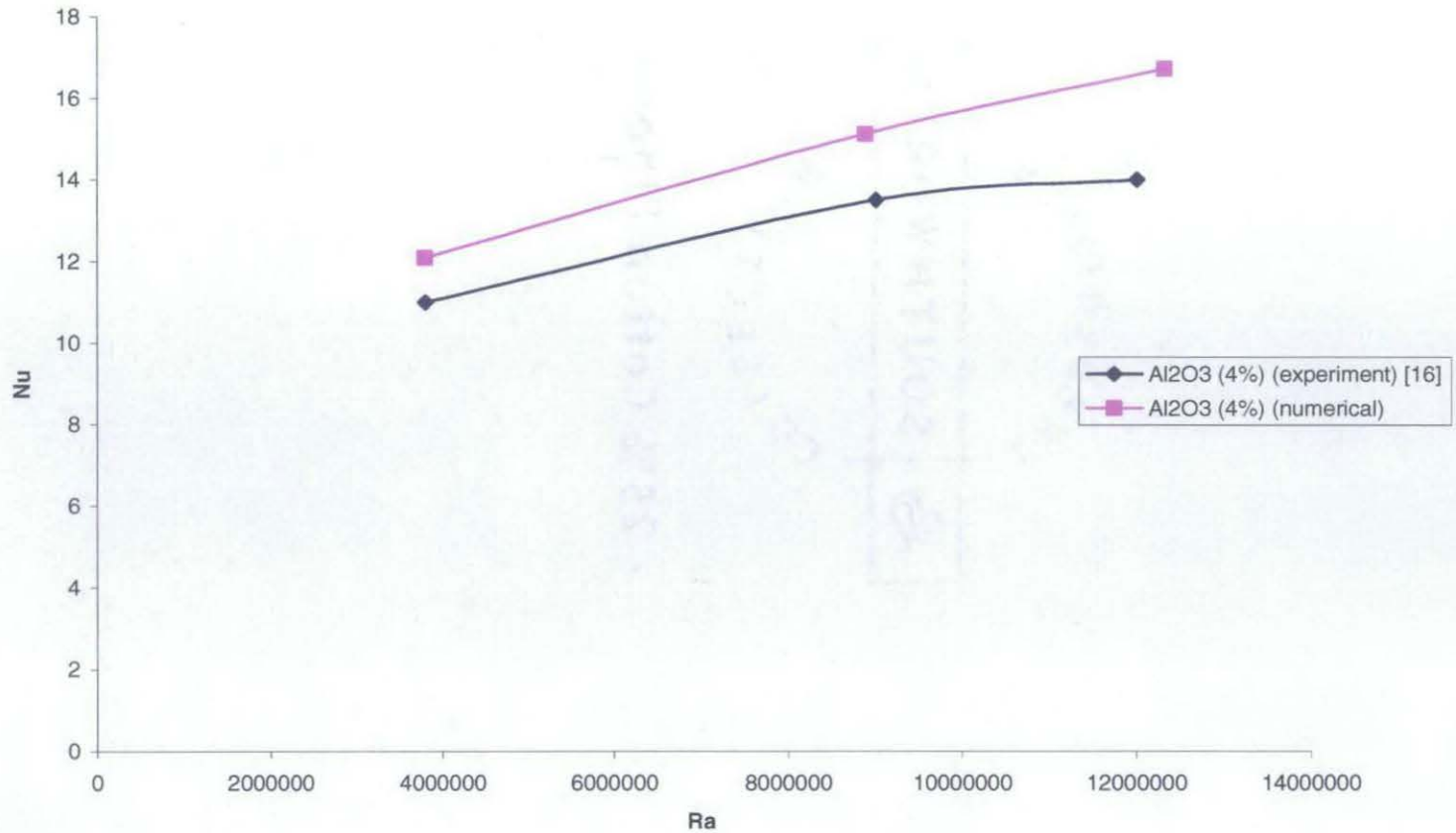

Fig 6-8: Graph of Nusselt No. vs Rayleigh No. for L/D=0.5 with Al_2O_3 Nanoparticles (ϕ=4%) in Water. Experimental Values of μ and k are Employed.

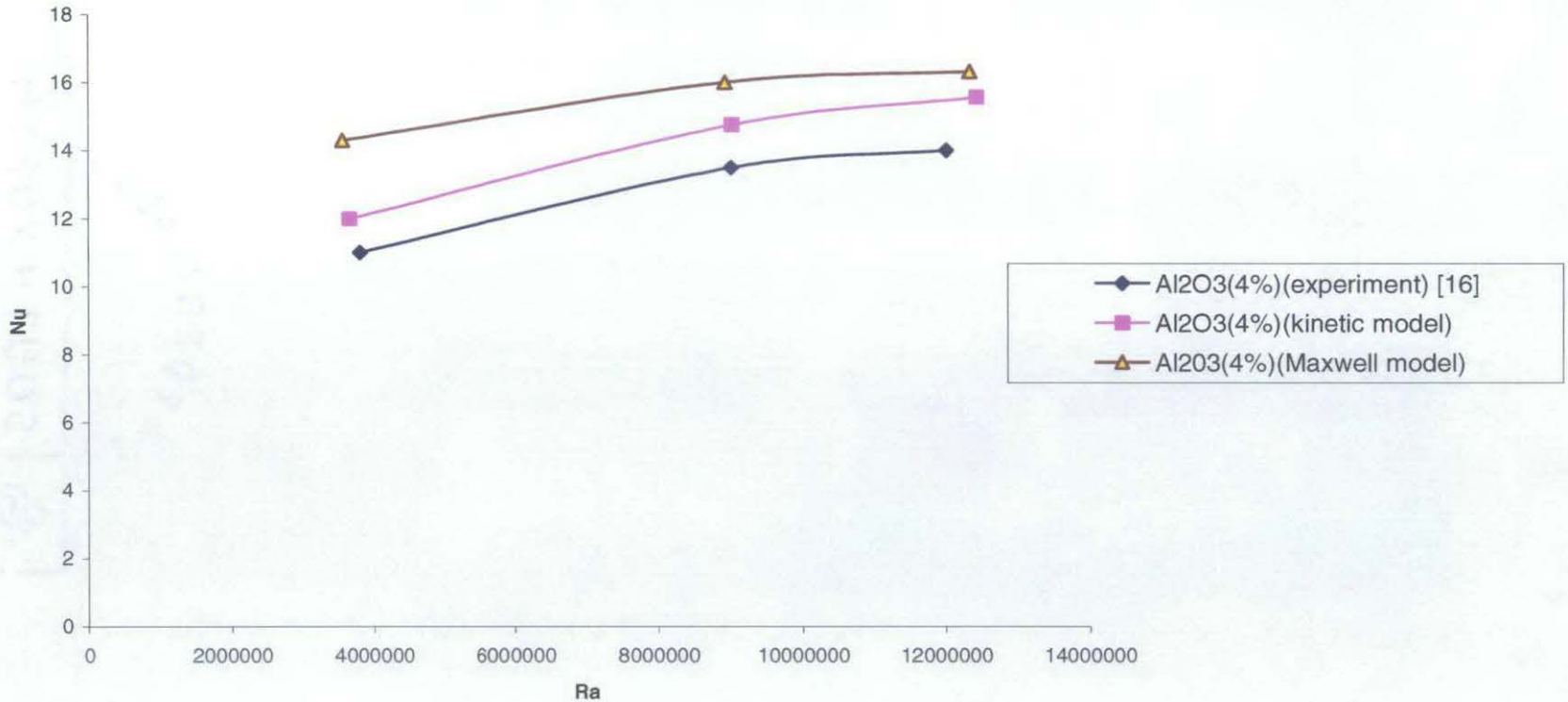

Fig. 6-9: Graph of Nusselt No. vs Rayleigh No. for L/D=0.5 with Al_2O_3 Nanoparticles (ϕ=4%) in Water. Theoretical Models of Thermal Conductivity are Employed.

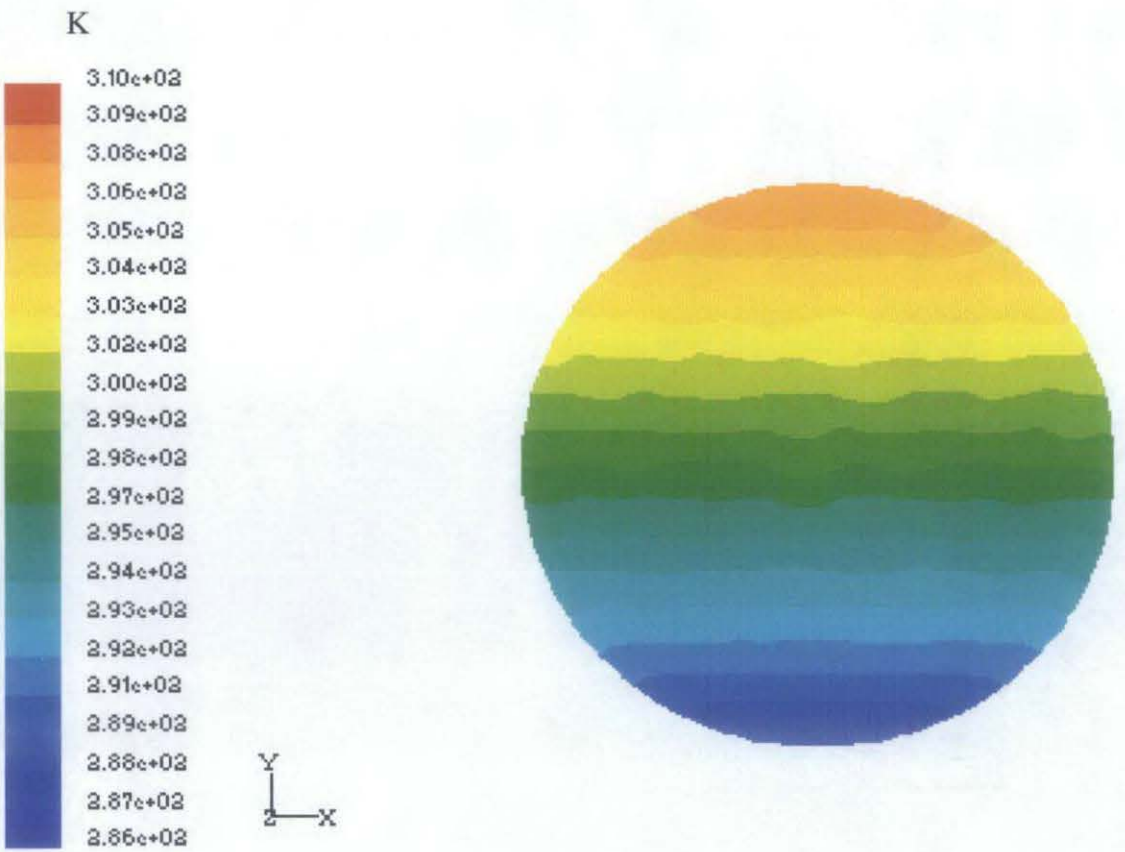

Fig 6-10: Temperature Contours in x-y Plane at z=0.01m (the center of the cylinder), L/D=0.5, Al_2O_3 Nanoparticles (ϕ = 4%) in water , T_h=310K, T_c=298K

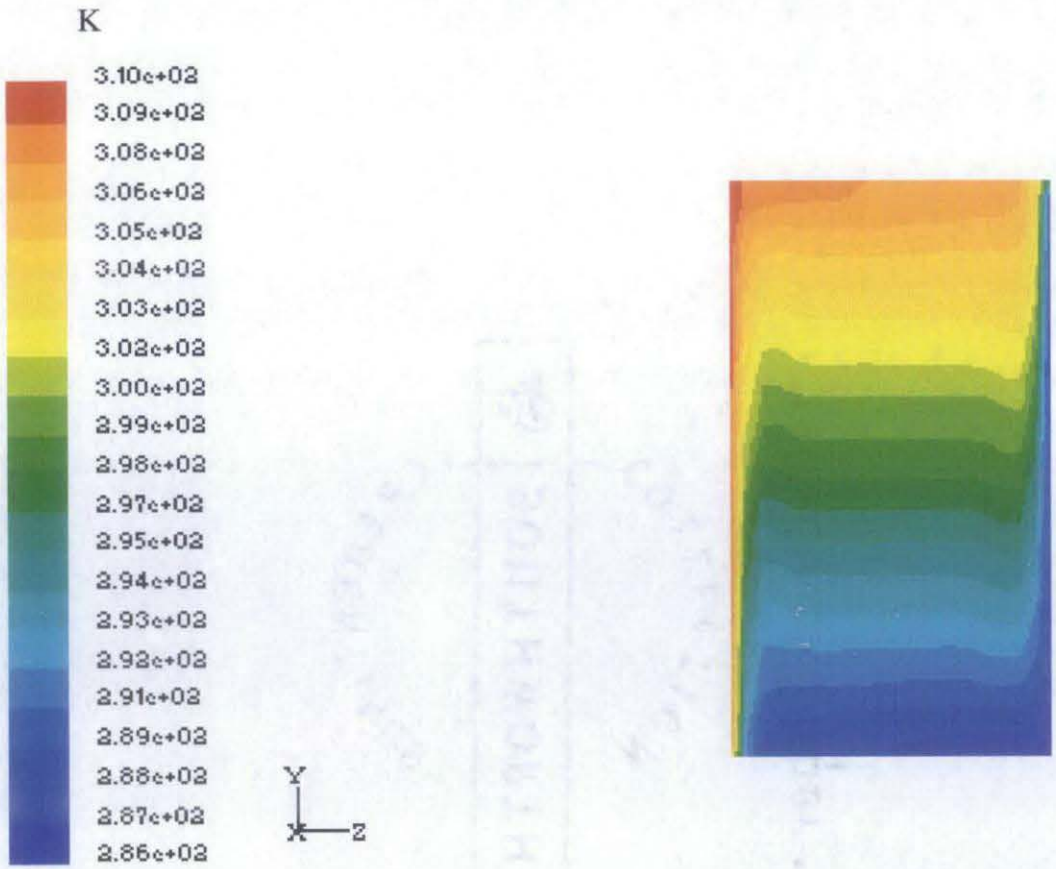

Fig. 6-11: Temperature Contours in y-z Plane at x=0 (the center of the cylinder), L/D=0.5, Al_2O_3 Nanoparticles (ϕ = 4%) in Water , T_h=310K, T_c=298K

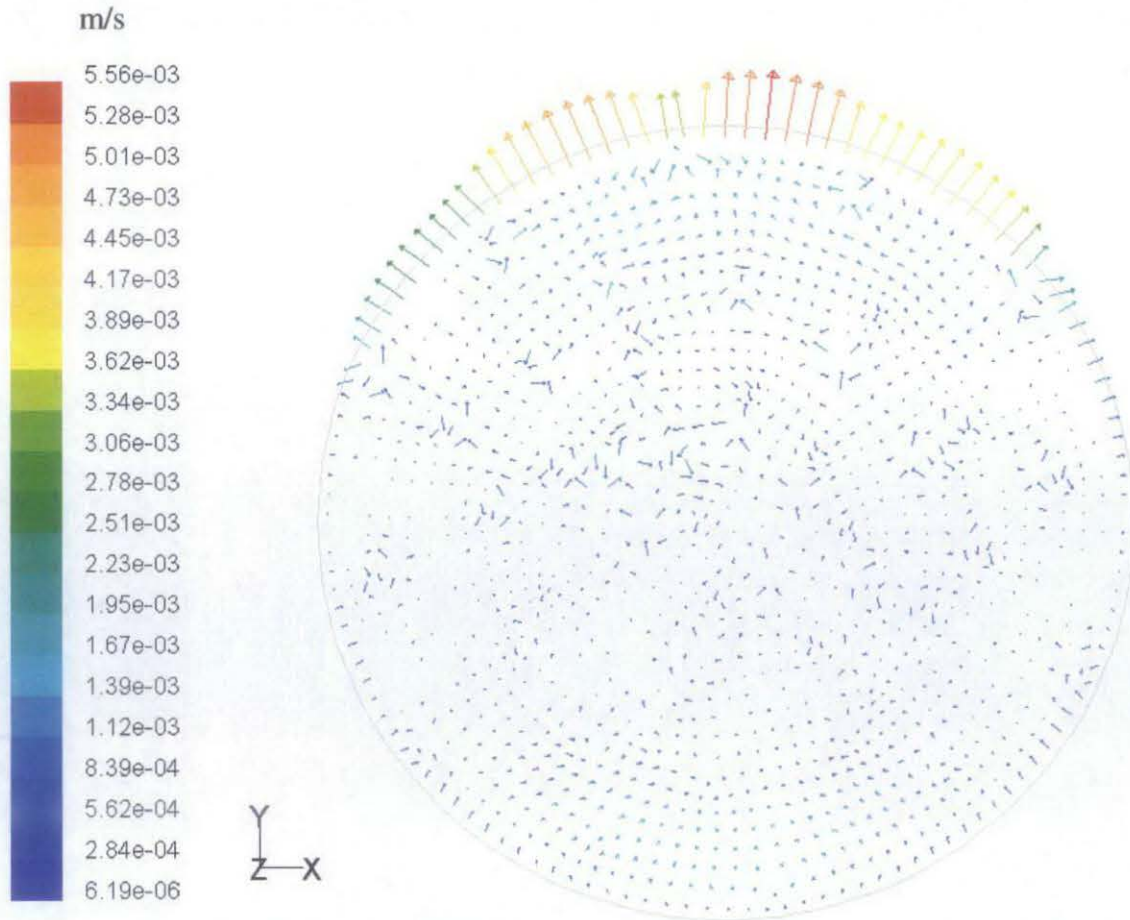

Fig. 6-12: Velocity Vectors in x-y Plane at z=0.01m (the center of the cylinder), L/D=0.5, Al_2O_3 Nanoparticles (ϕ = 4%) in Water, T_h=310K, T_c=298K

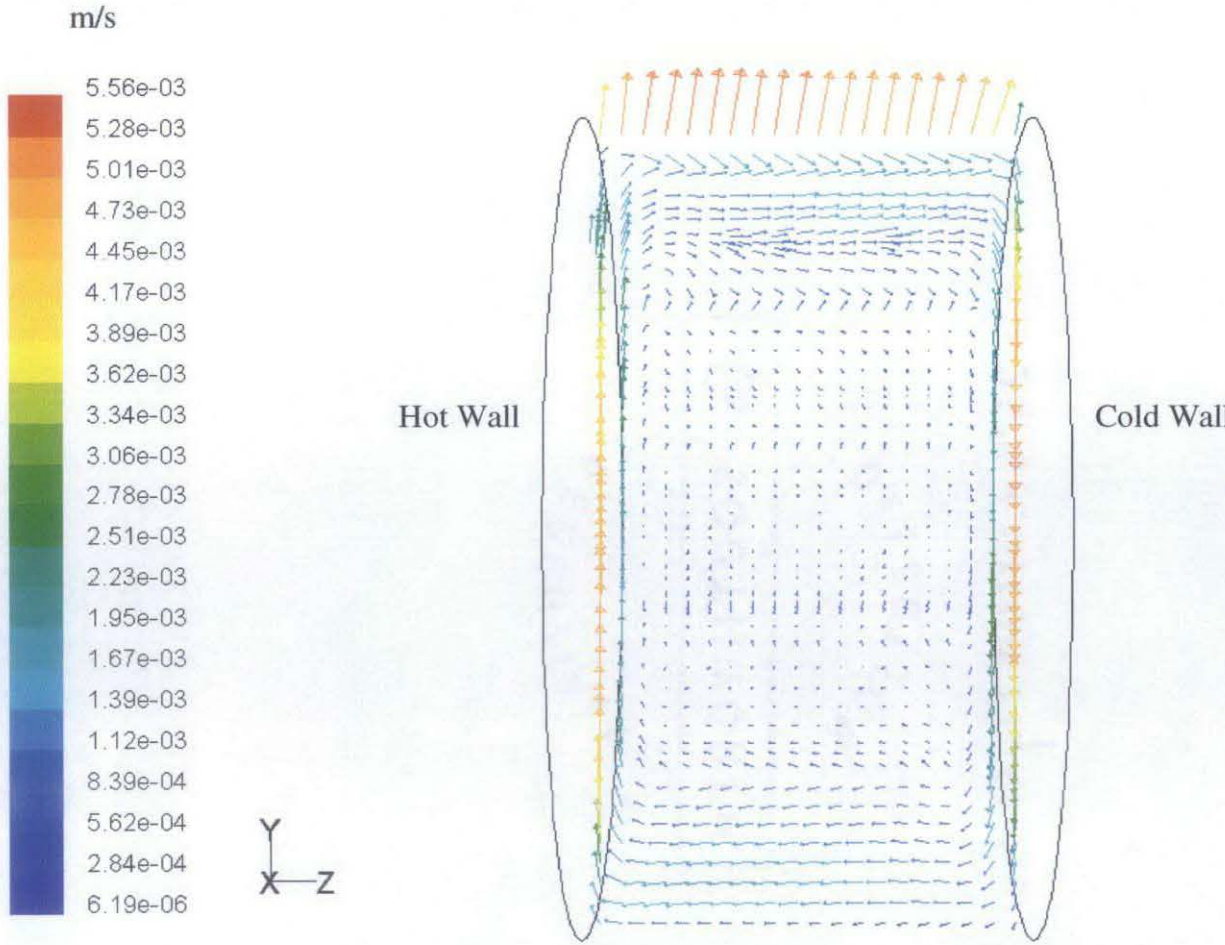

Fig. 6-13: Velocity Vectors in y-z Plane at x=0 (the center of the cylinder), L/D=0.5, Al_2O_3 Nanoparticles ($\phi = 4\%$) in Water, T_h=310K, T_c=298K

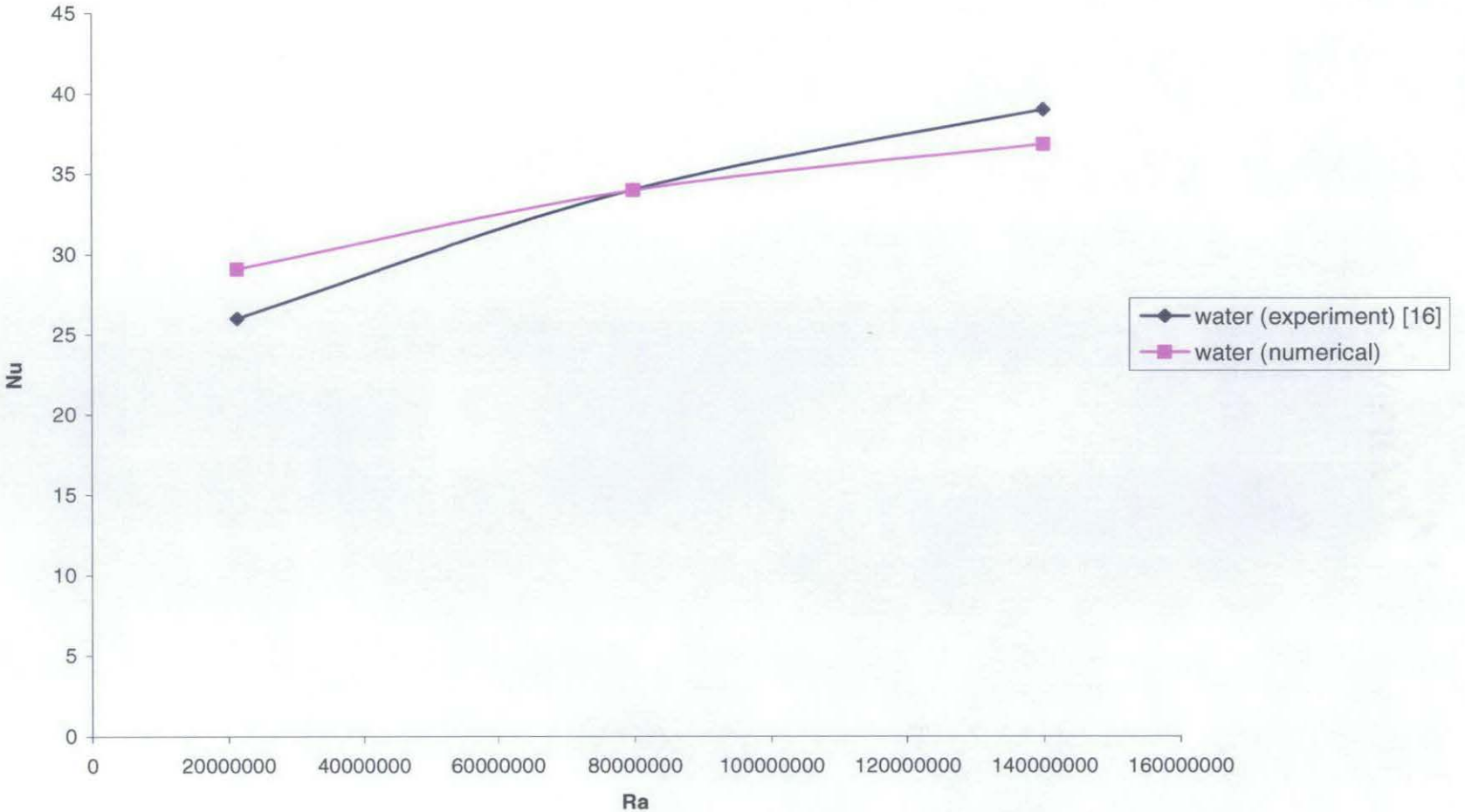

Fig 6-14: Graph of Nusselt Number vs Rayleigh Number for L/D=1.0 and $\phi = 0\%$ (Pure Water)

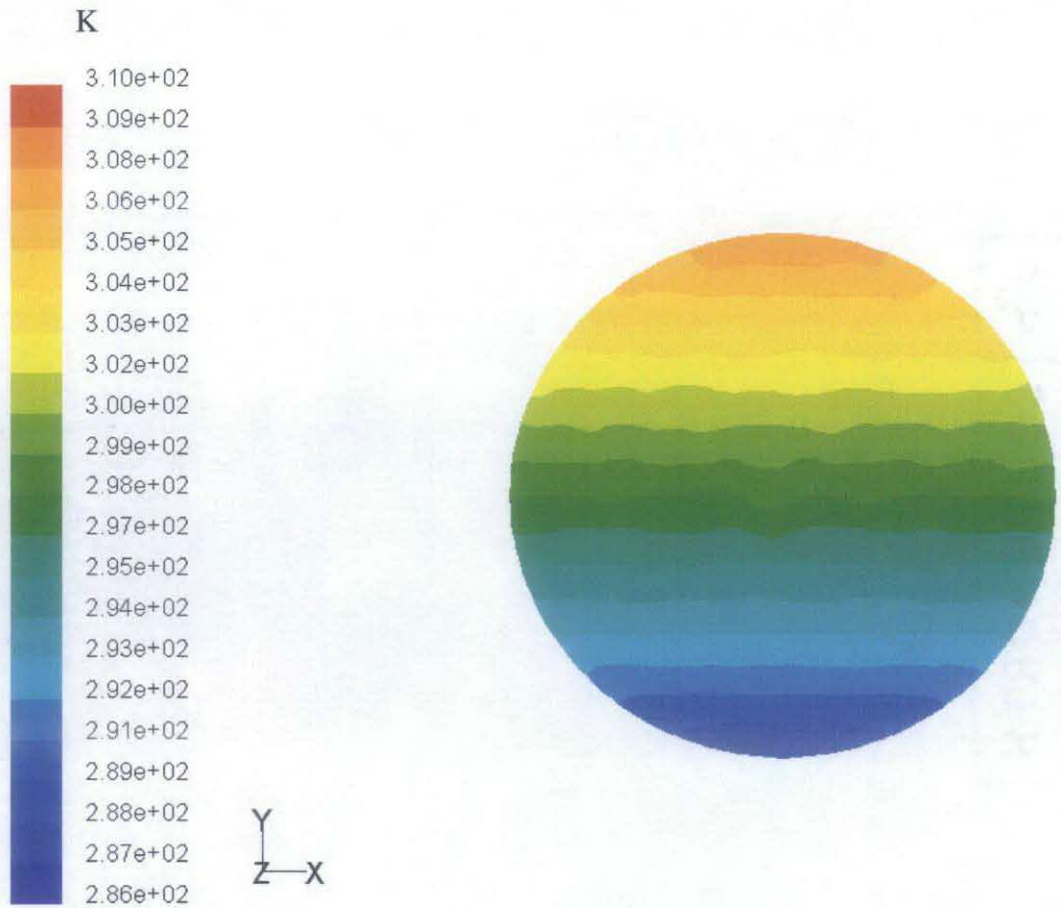

Fig. 6-15: Temperature Contours in x-y Plane at z=0.02m (the center of the cylinder), L/D=.1.0, ϕ = 0% (pure water), T_h=310K, T_c=298K

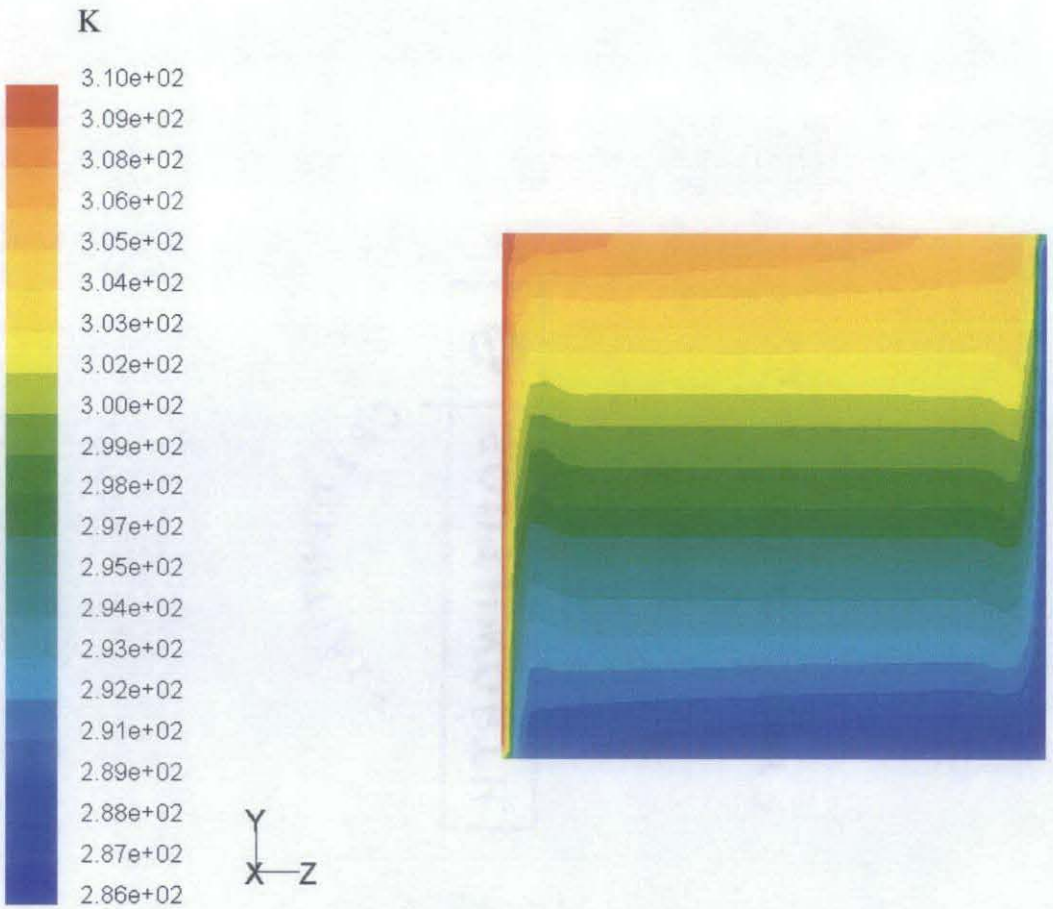

Fig. 6-16: Temperature Contours in y-z Plane at x=0 (the center of the cylinder), L/D=1.0, ϕ = 0% (pure water), T_h=310K, T_c=298K

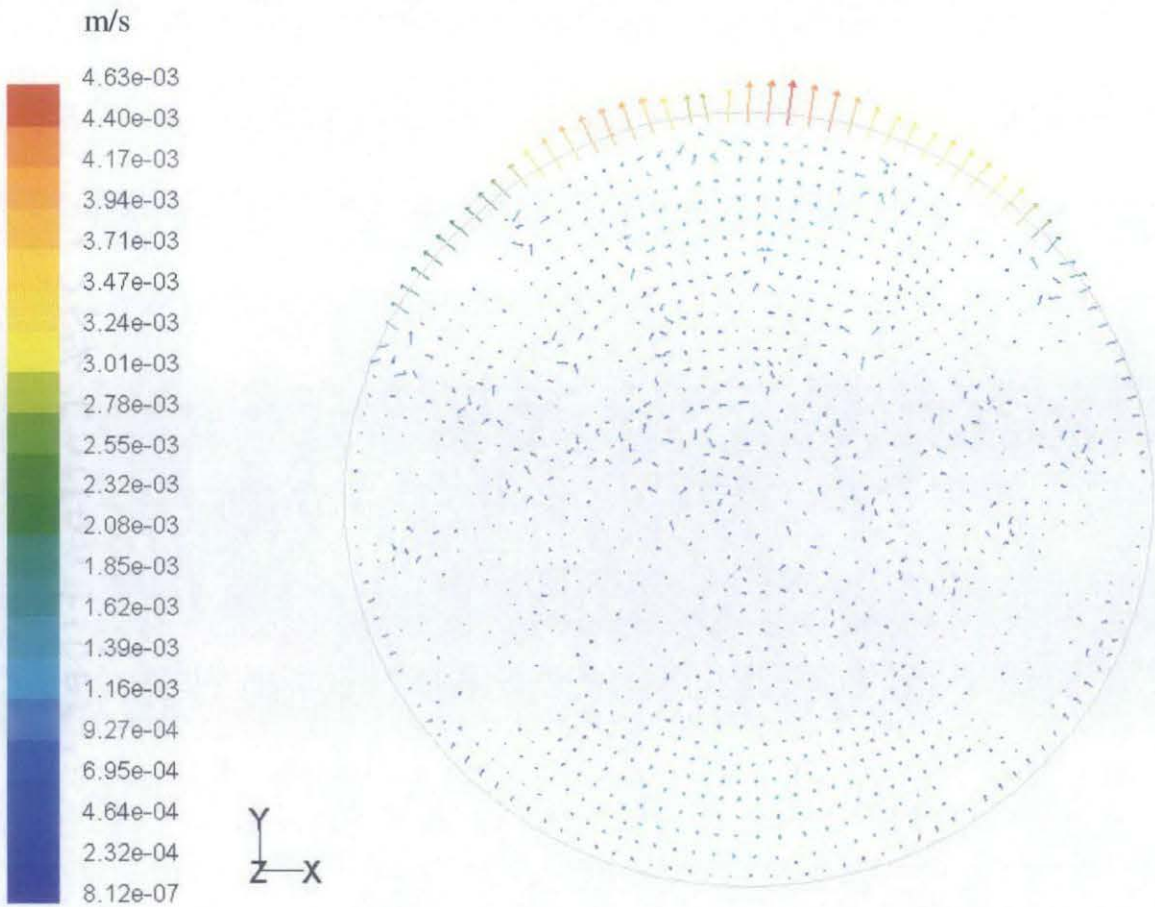

Fig. 6-17: Velocity Vectors in x-y Plane at z=0.02m (the center of the cylinder), L/D=1.0, ϕ = 0% (pure water), T_h=310K, T_c=298K

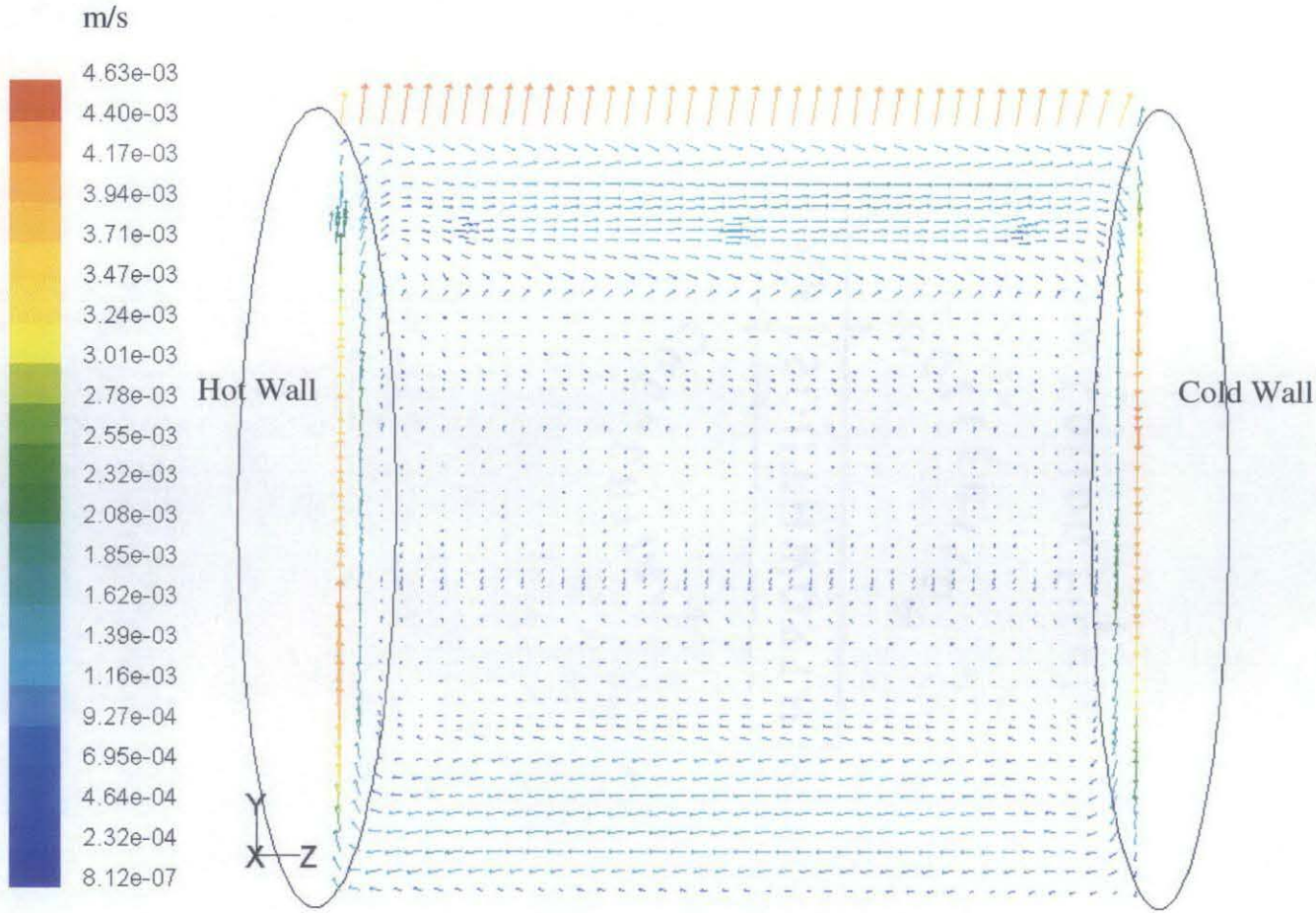

Fig. 6-18: Velocity Vectors in y-z Plane at x=0 (the center of the cylinder), L/D=1.0, ϕ = 0% (pure water), T_h=310K, T_c=298K

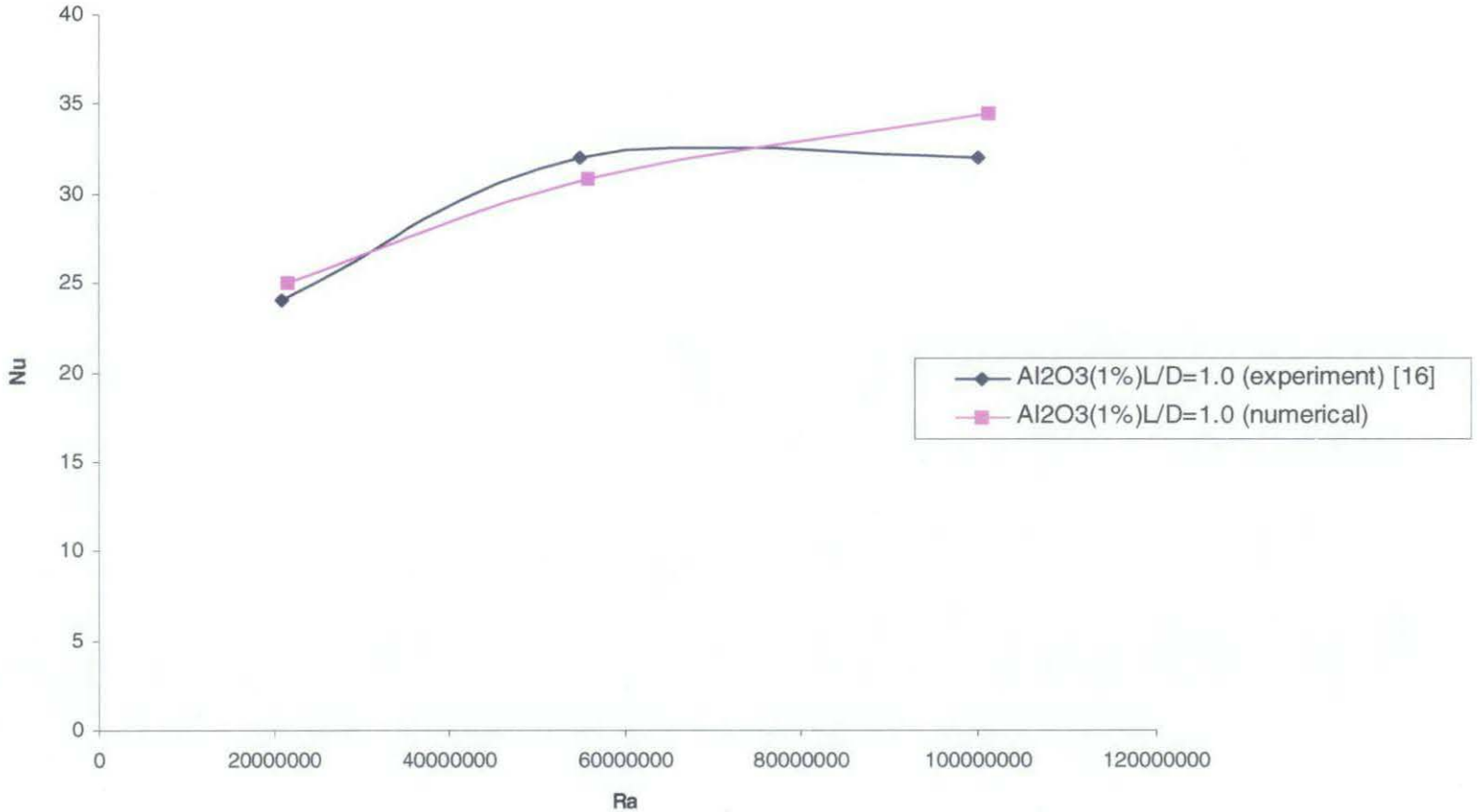

Fig 6-19: Graph of Nusselt No. vs Rayleigh No. for L/D=1.0 with Al_2O_3 Nanoparticles (ϕ=1%) in Water. Experimental Values of μ and k are Employed.

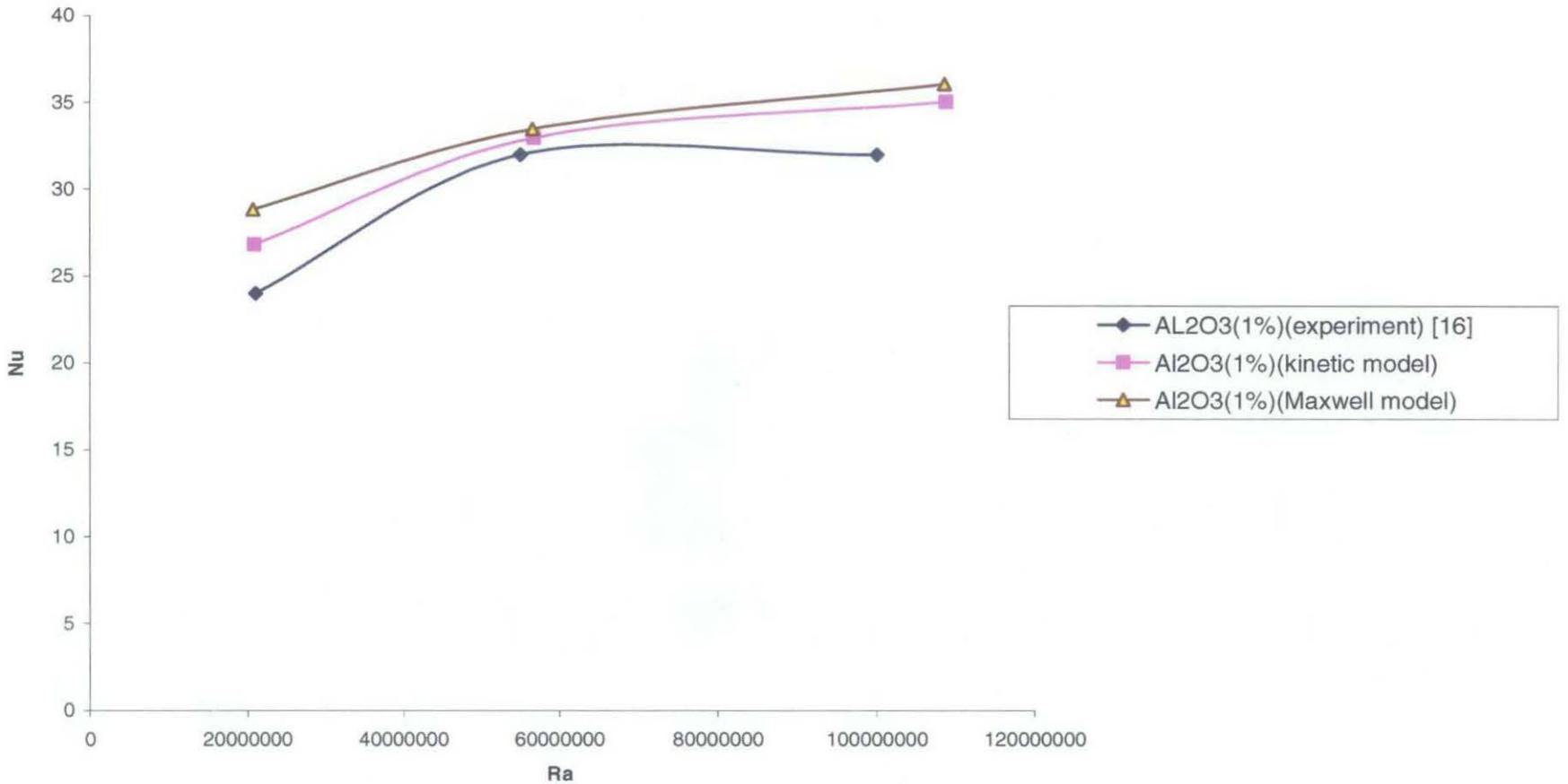

Fig 6-20: Graph of Nusselt No. vs Rayleigh No. for L/D=1.0 with Al_2O_3 Nanoparticles (ϕ=1%) in Water. Theoretical Models of Thermal Conductivity are Employed.

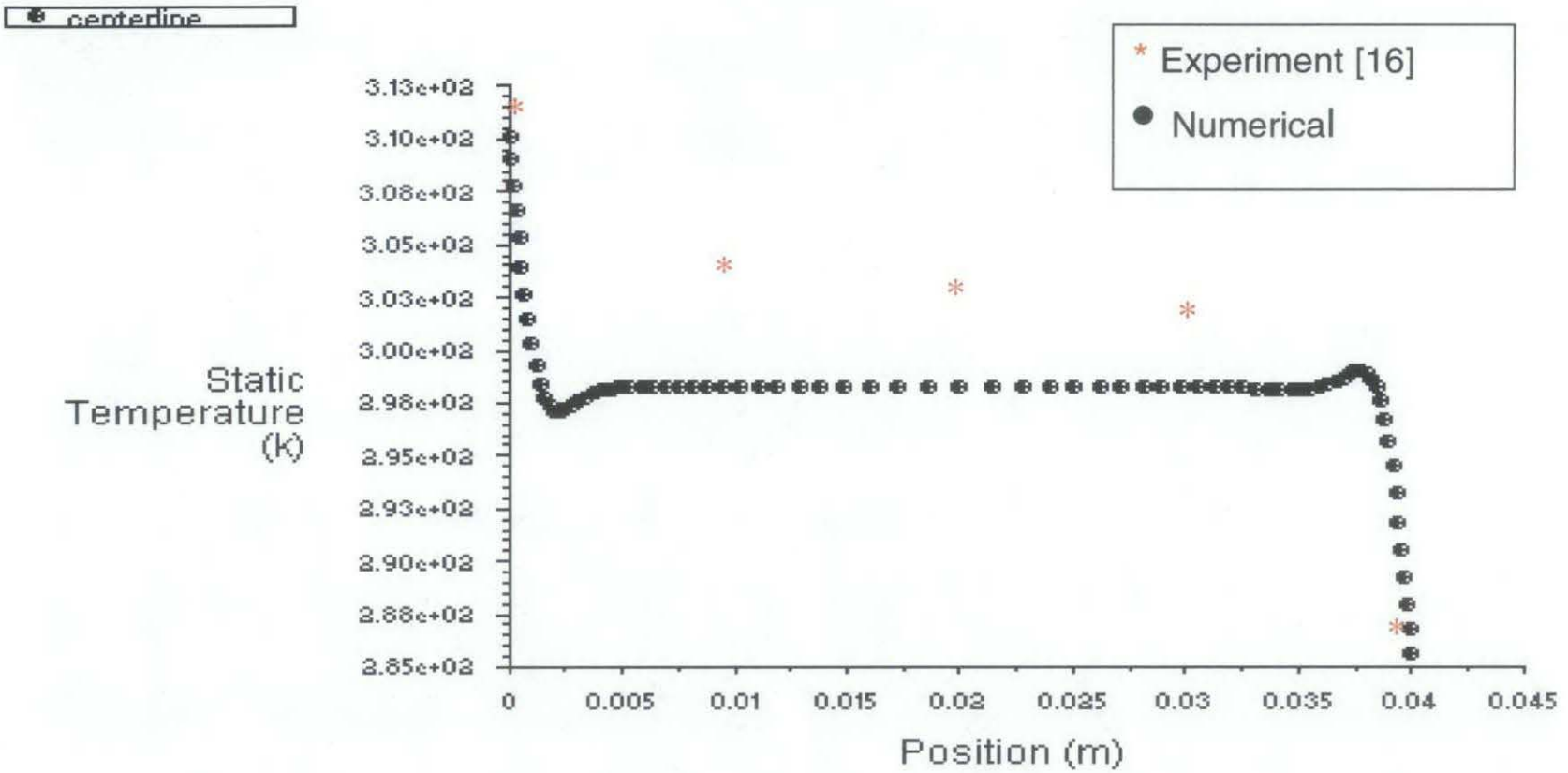

Fig. 6-21: Temperature Distribution Along the Centerline of the Cylinder with Al_2O_3-water (ϕ =1%), L/D=1.0, T_h=310K, Tc=285K

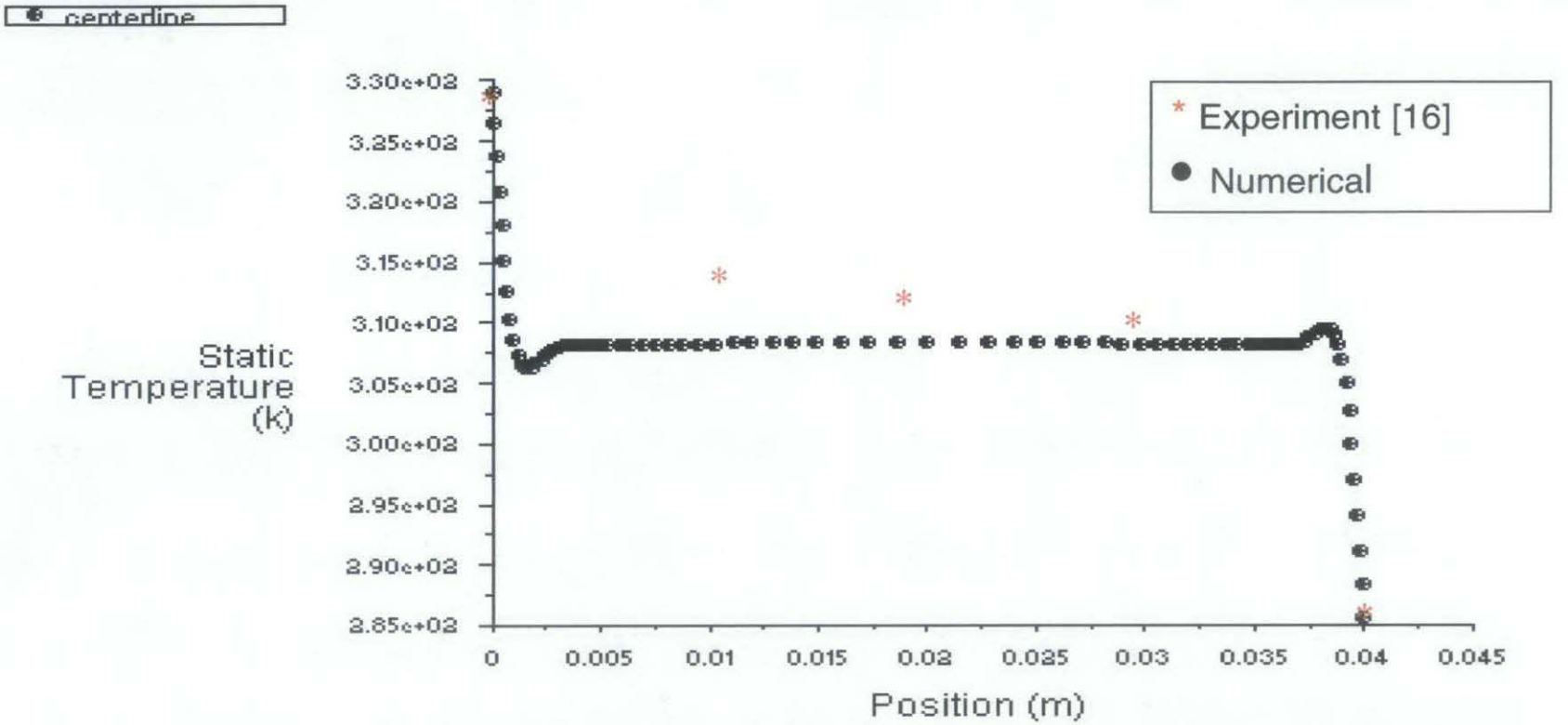

Fig. 6-22: Temperature Distribution Along the Centerline of the Cylinder with Al_2O_3-water (ϕ=1%), L/D=1.0, T_h=329K, Tc=285K

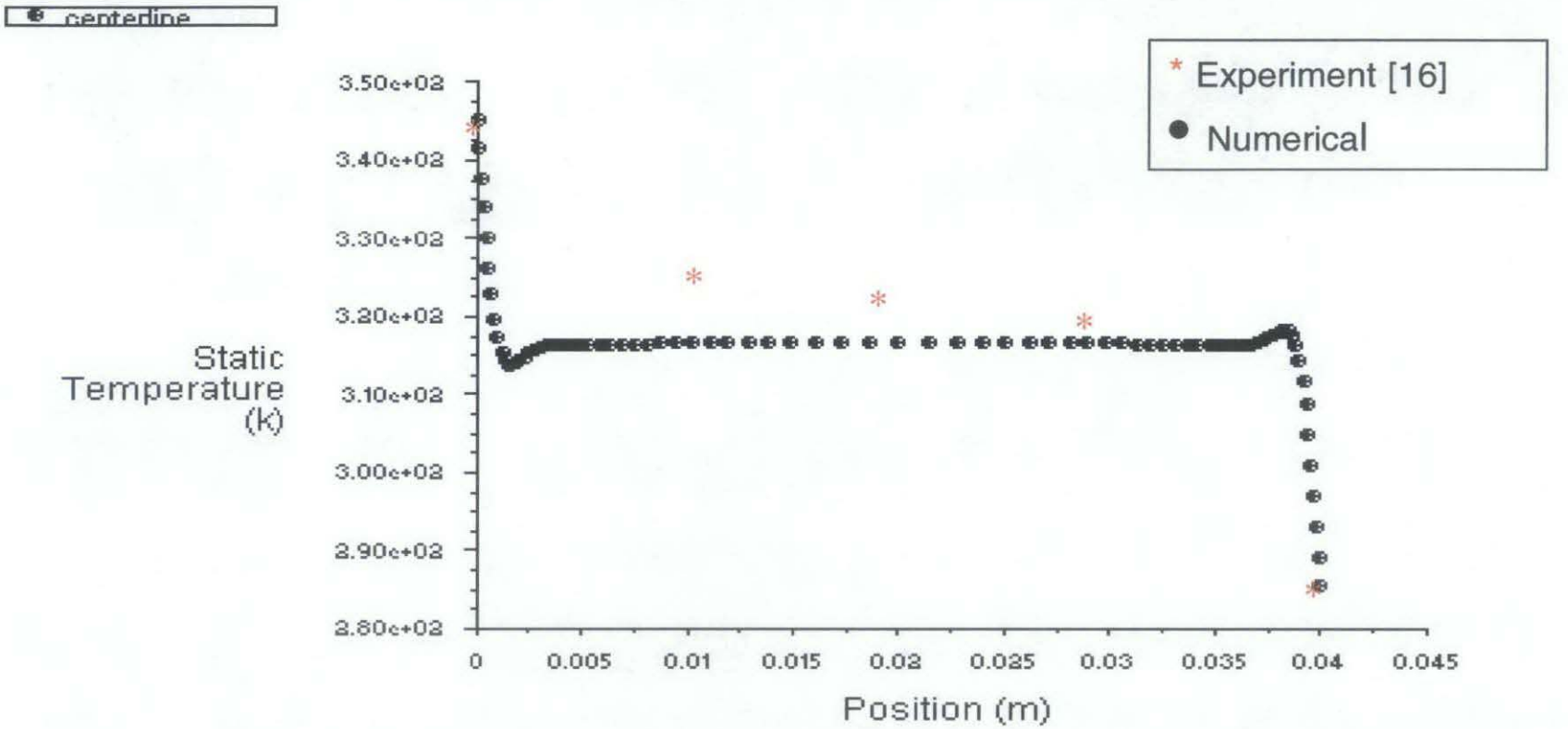

Figure 6-23:Temperature Distribution Along the Centerline of the Cylinder with Al_2O_3-water (ϕ =1%), L/D=1.0, T_h=345K, Tc=285K

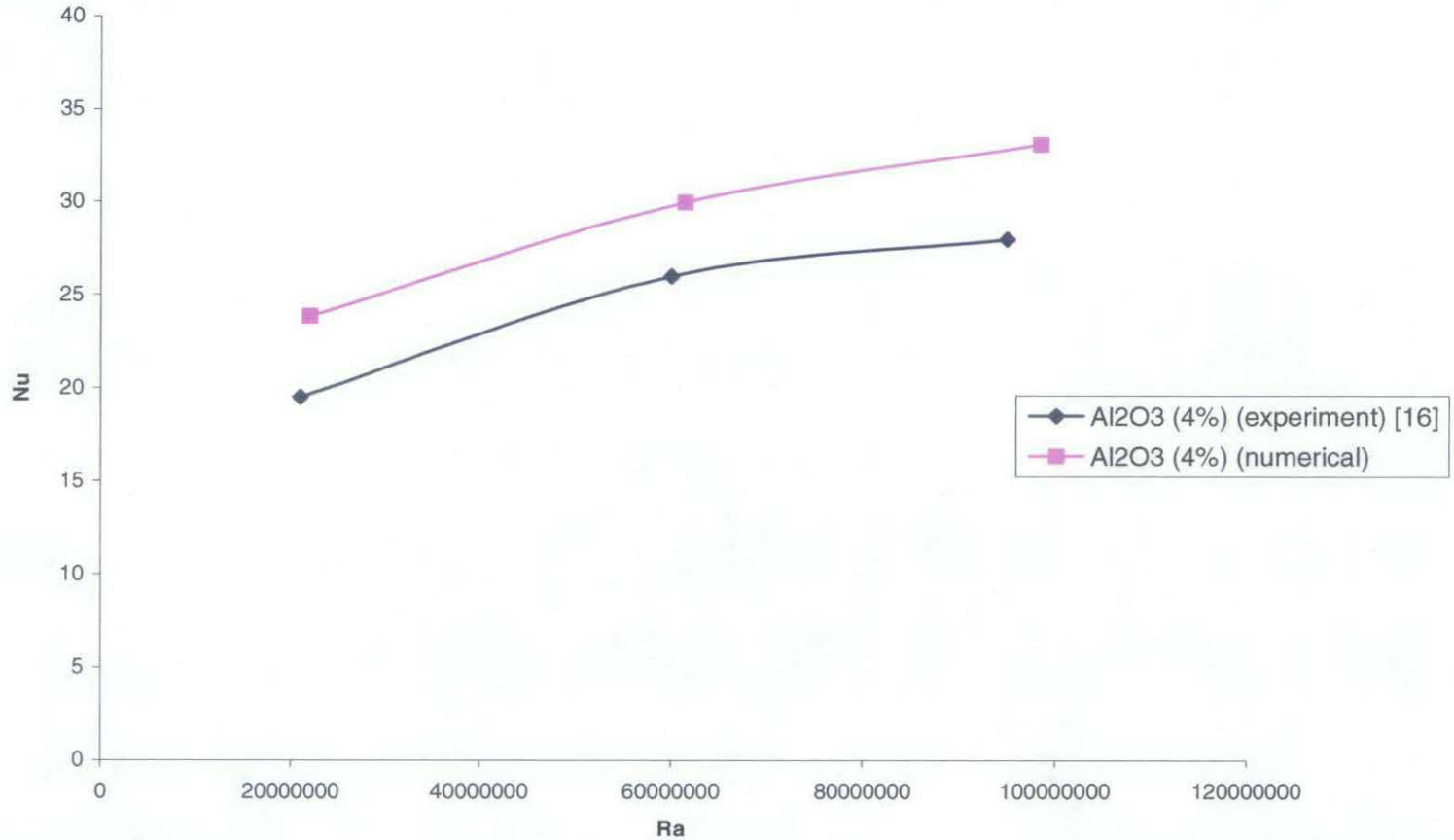

Fig 6-24: Graph of Nusselt No. vs Rayleigh No. for L/D=1.0 with Al_2O_3 Nanoparticles (ϕ=4%) in Water. Experimental Values of μ and k are Employed.

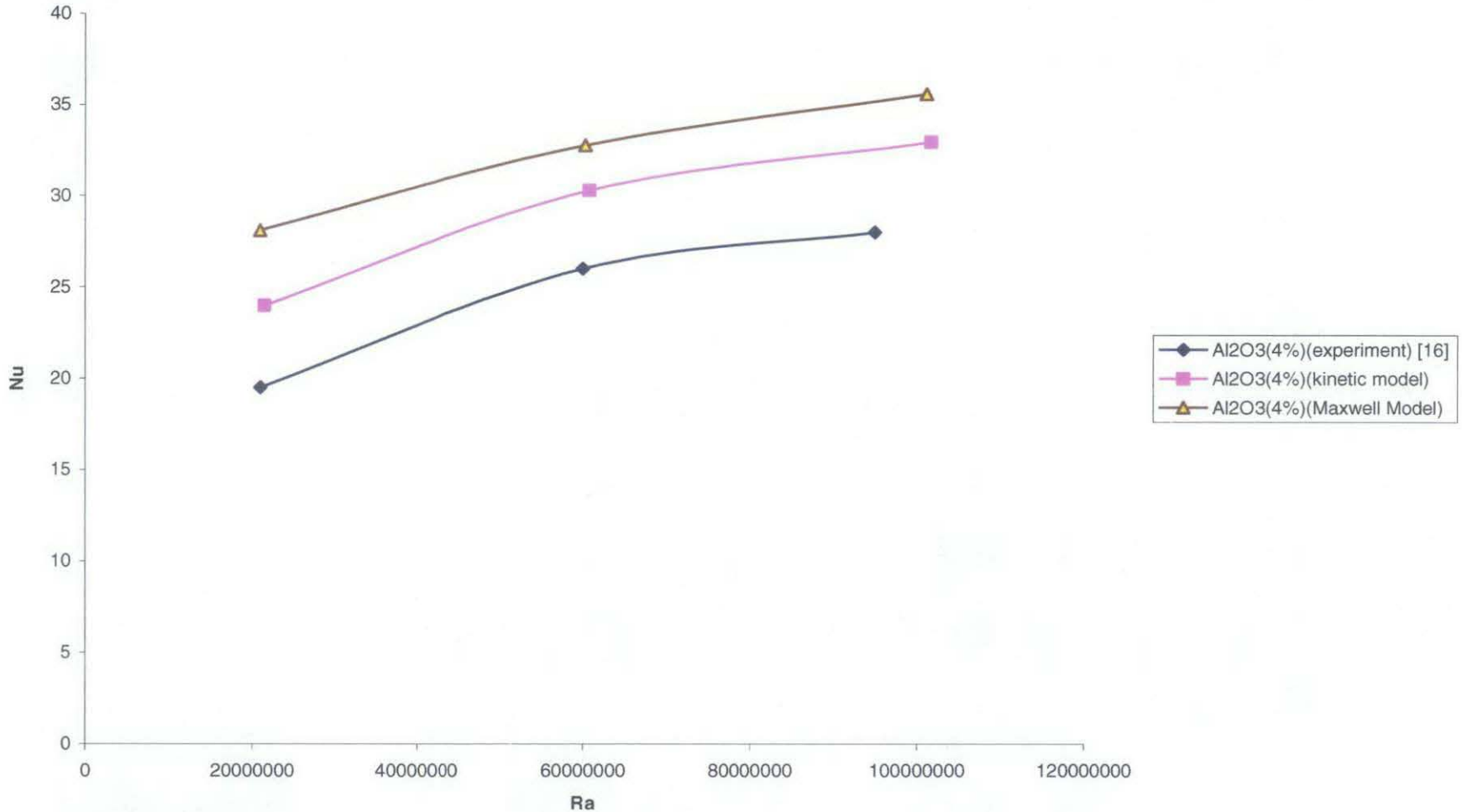

Fig 6-25: Graph of Nusselt No. vs Rayleigh No. for L/D=1.0 with Al_2O_3 Nanoparticles (ϕ=4%) in Water. Theoretical Models of Thermal Conductivity are Employed.

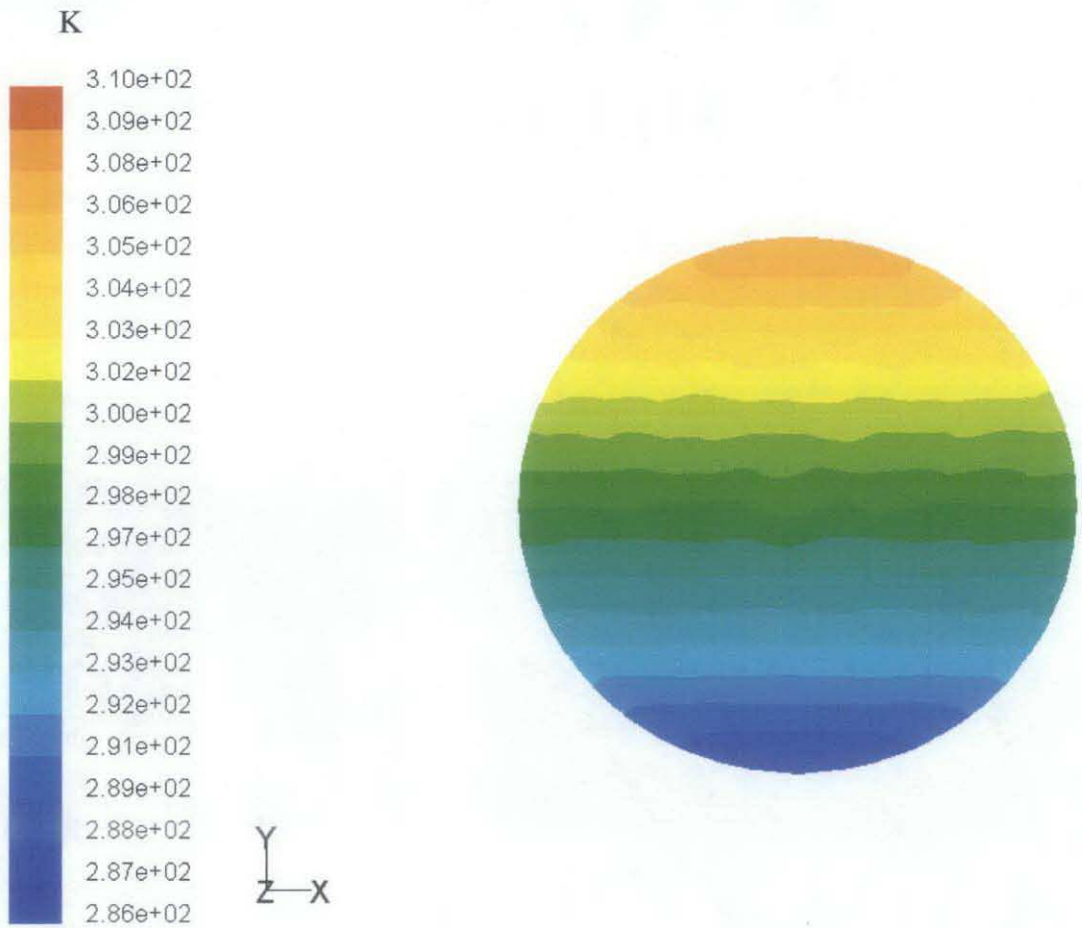

Fig. 6-26: Temperature Contours in x-y Plane at z=0.02m (the center of the cylinder), L/D=1.0, Al_2O_3 Nanoparticles (ϕ = 4%) in water , T_h=310K, T_c=298K

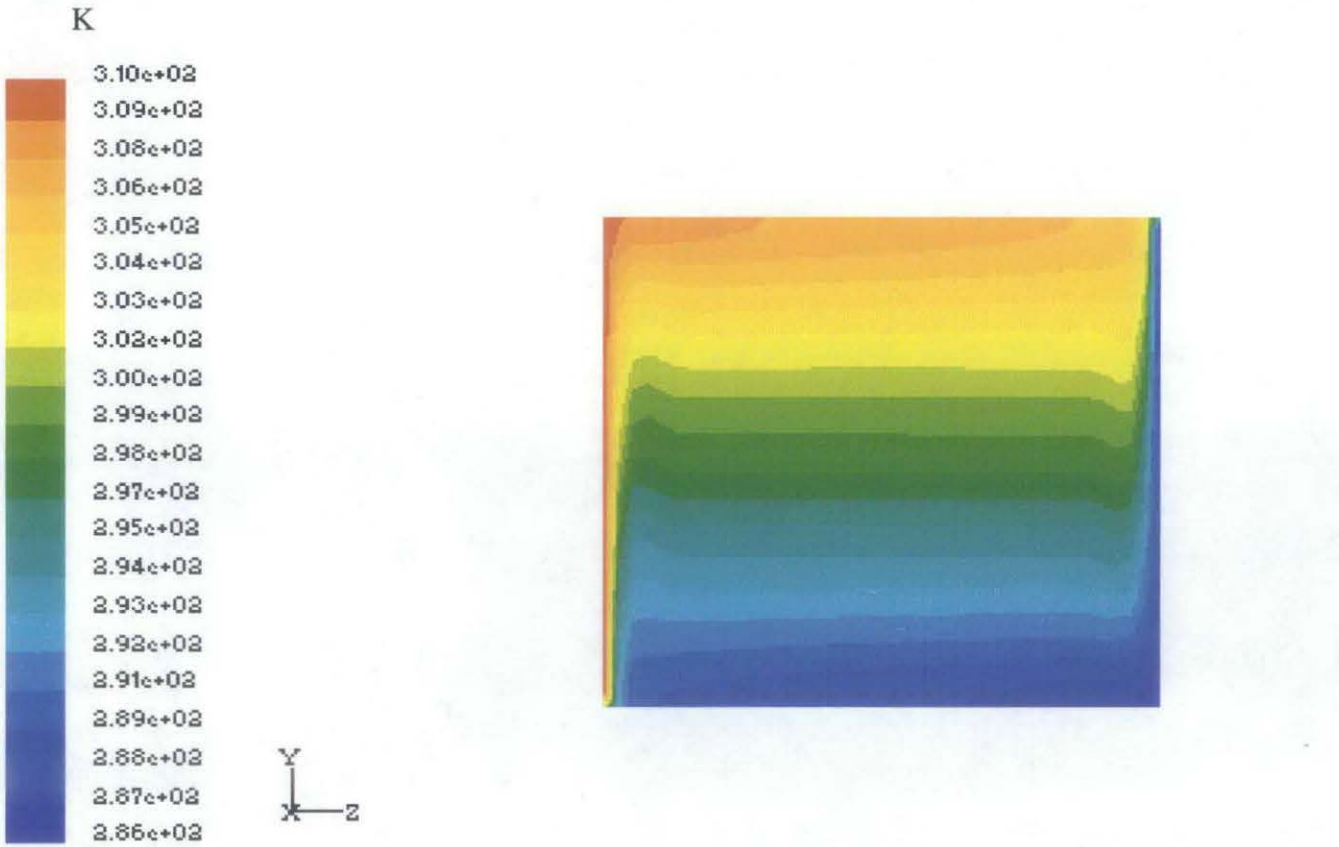

Fig. 6-27: Temperature Contours in y-z Plane at x=0 (the center of the cylinder), L/D=1.0, Al_2O_3 Nanoparticles (ϕ = 4%) in water , T_h=310K, T_c=298K

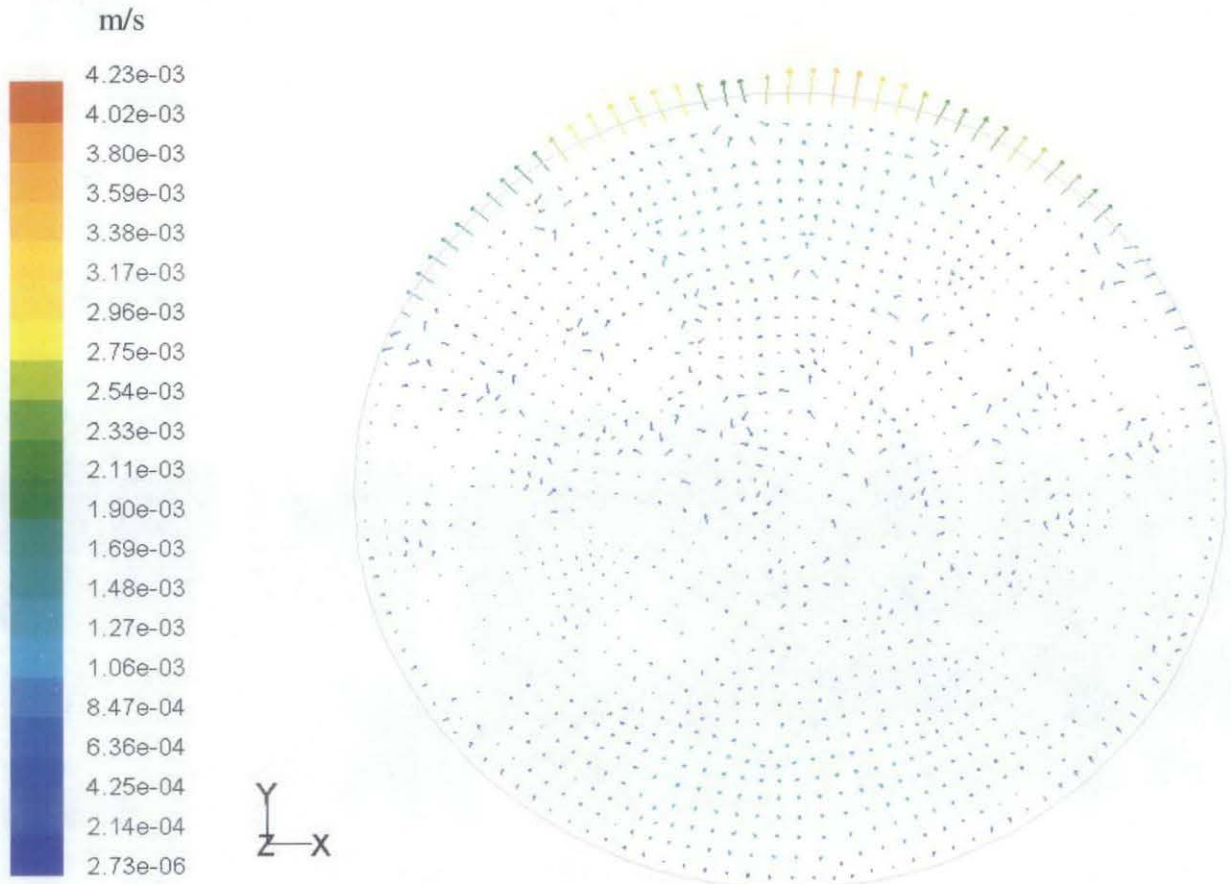

Fig. 6-28: Velocity Vectors in x-y Plane at z=0.02m (the center of the cylinder), L/D=1.0, Al_2O_3 Nanoparticles ($\phi = 4\%$) in water, T_h=310K, T_c=298K

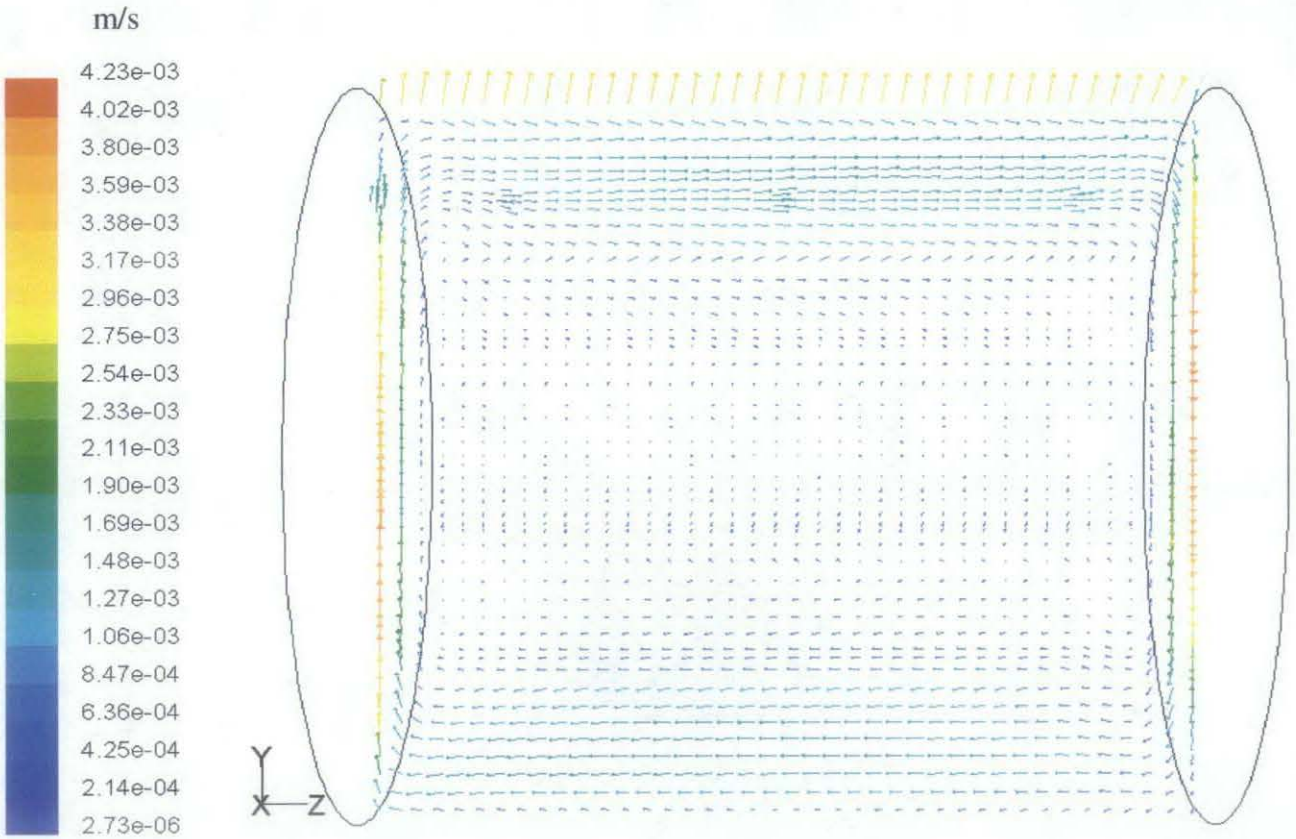

Fig. 6-29: Velocity Vectors in y-z Plane at x=0 (the center of the cylinder), L/D=1.0, Al_2O_3 Nanoparticles ($\phi = 4\%$) in water, T_h=310K, T_c=298K

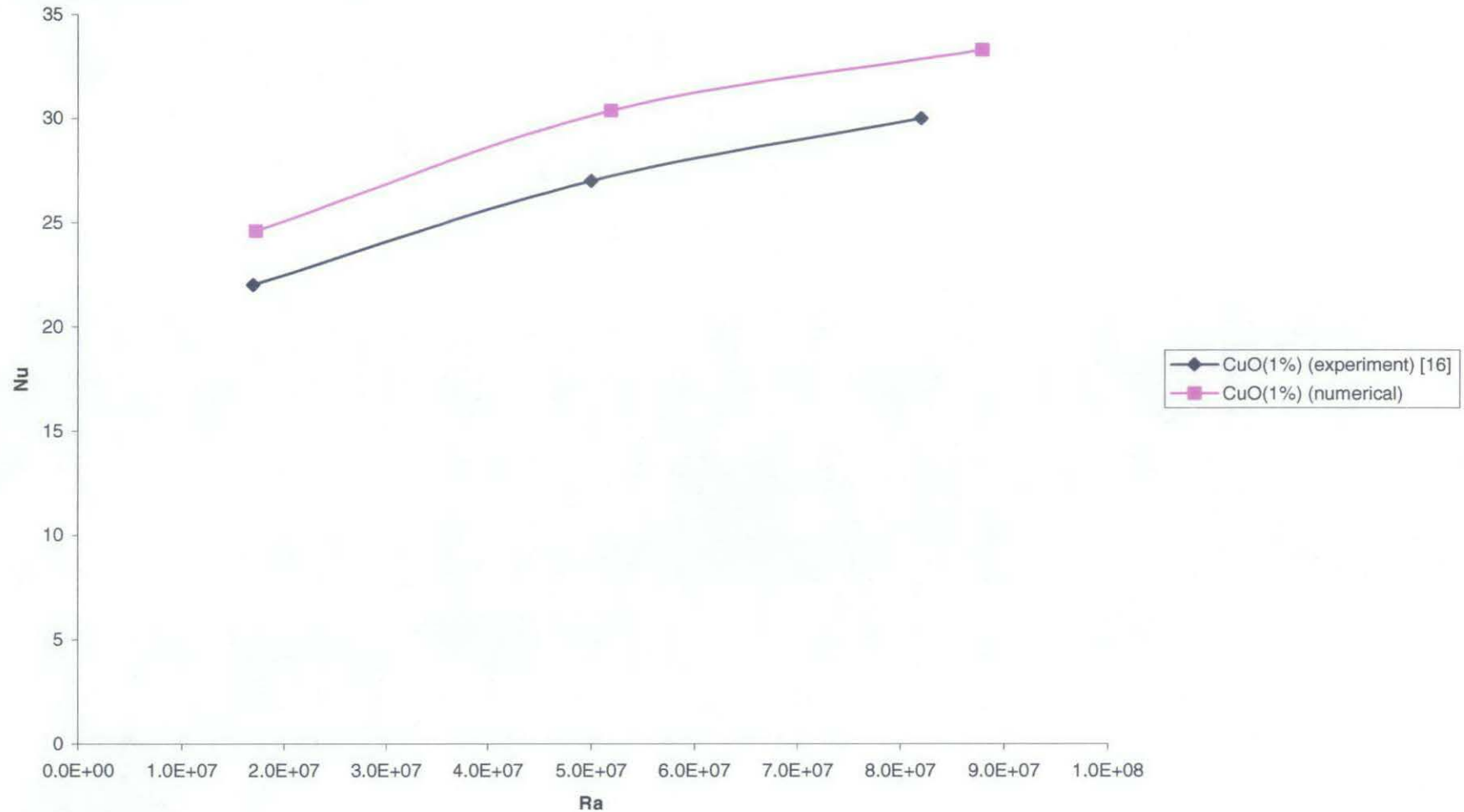

Fig 6-30: Graph of Nusselt No. vs Rayleigh No. for L/D=1.0 with CuO Nanoparticles (ϕ=1%) in Water. Experimental Values of μ and k are Employed.

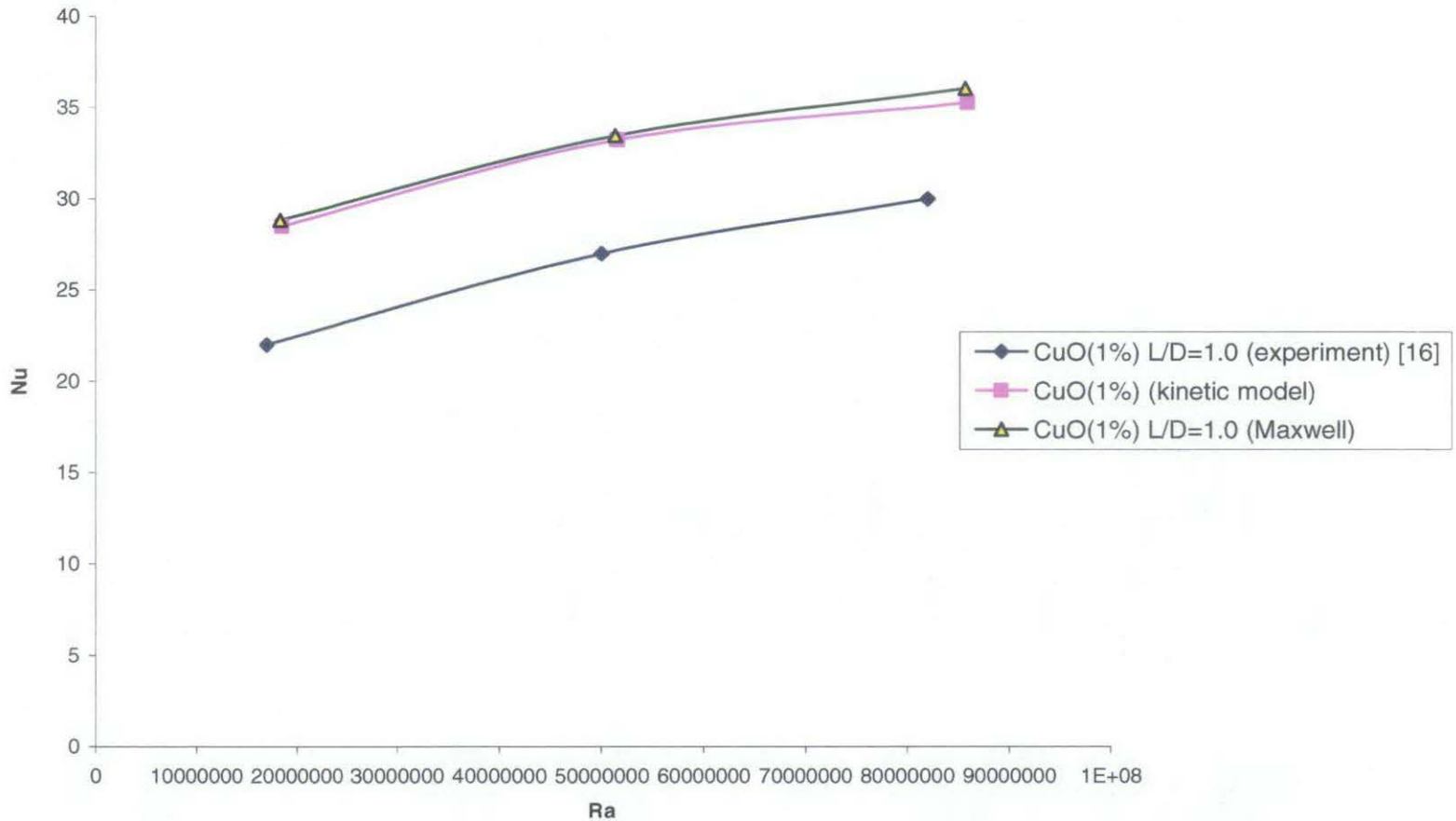

Fig 6-31: Graph of Nusselt No. vs Rayleigh No. for L/D=1.0 with CuO Nanoparticles (ϕ=1%) in Water. Theoretical Models of Thermal Conductivity are Employed.

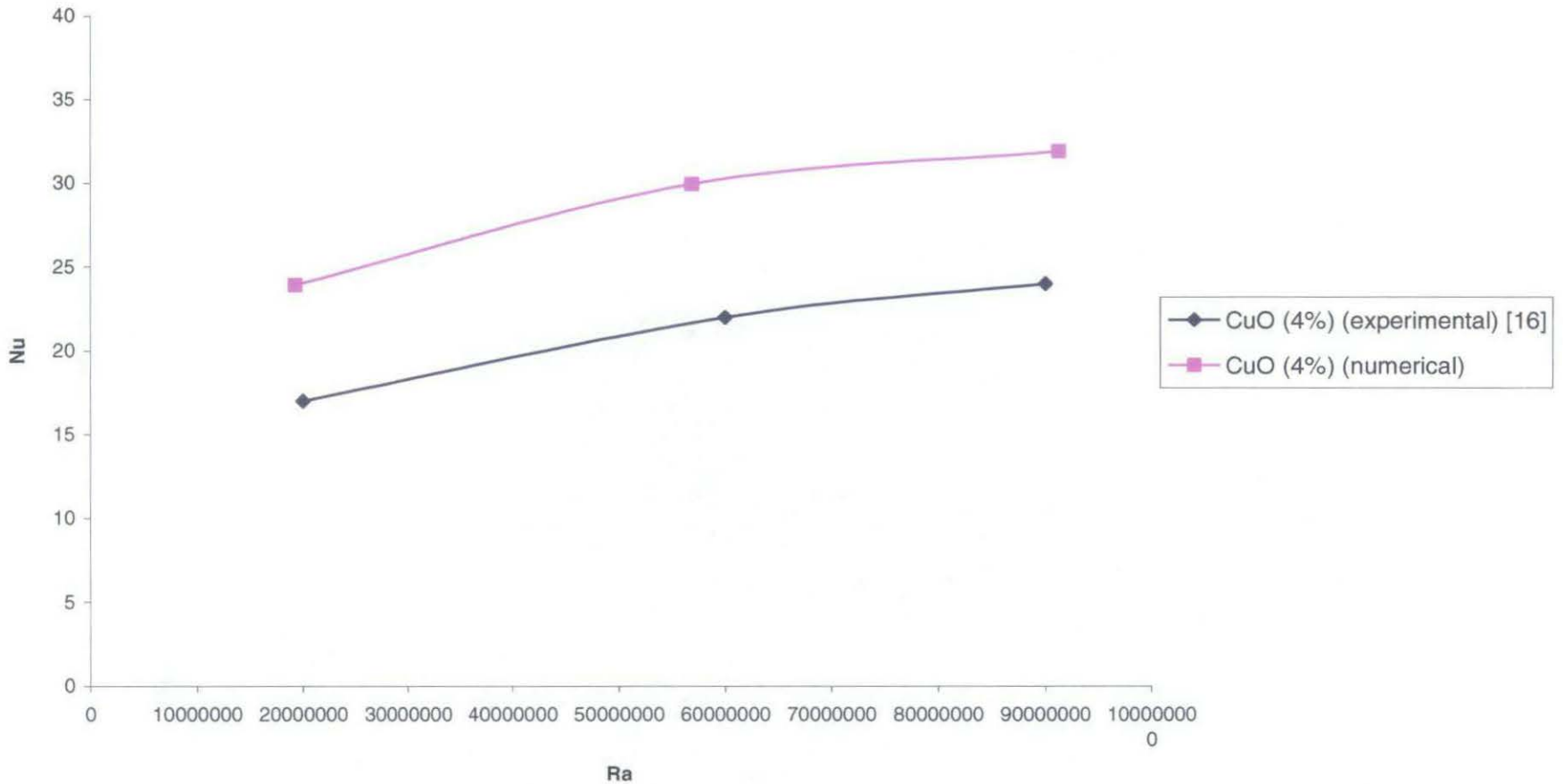

Fig 6-32: Graph of Nusselt No. vs Rayleigh No. for L/D=1.0 with CuO Nanoparticles (ϕ=4%) in Water. Experimental Values of μ and k are Employed.

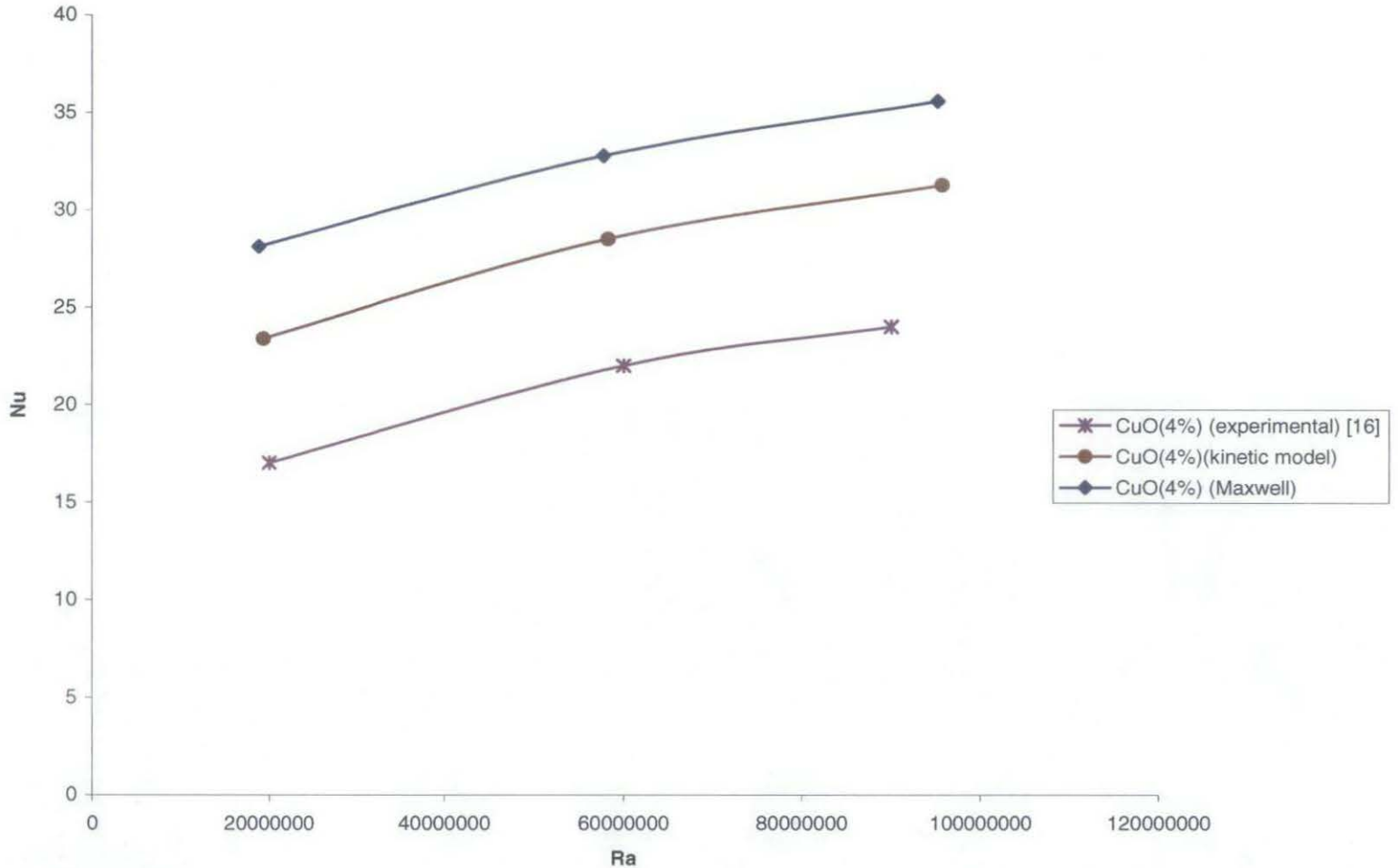

Fig 6-33: Graph of Nusselt No. vs Rayleigh No. for L/D=1.0 with CuO Nanoparticles (ϕ=4%) in Water. Theoretical Models of Thermal Conductivity are Employed.

Chapter 7: Conclusions

In this study, the heat transfer characteristics of nanofluids of Al_2O_3-water and CuO-water in natural convection flow in a horizontal cylinder with two end-walls at two different temperatures and an adiabatic curved wall are predicted by numerical solution of governing equations of fluid flow with properly defined material properties of nanofluids using the commercial CFD software FLUENT 6.0. Experimental and computational results for Nusselt number at various values of Rayleigh number show similar trend and are in fair agreement. The numerical solutions that utilize the experimental values of thermal conductivity and viscosity show closer agreement with the experimental data than the numerical solutions obtained with theoretical model of thermal conductivity, namely the Maxwell model and the kinetic model. Between the predictions of the two models, the results obtained with kinetic model are in better agreement with the experimental data. Kinetic model accounts for both the size and the volume fraction of nanoparticles in deriving the formula for thermal conductivity of the nanofluid while the Maxwell model accounts only for the volume fraction of the nanoparticles.

Computations show that at a given Rayleigh number, the Nusselt number decreases as the volume fraction of nanoparticles in the liquid increases; the same trend is observed in the experiment [16]. Thus it appears that there is degradation or deterioration in natural convection heat transfer in a nanofluid. This deterioration is dependent also on

the material density of the nanoparticles and the aspect ratio of the cylinder, in addition to its dependence on the volume fraction of the nanoparticles in the liquid. Both the computations and experimental data show that at a given Rayleigh number, Nusselt number decreases as the aspect ratio increases from L/D = 0.5 and 1.0 and it is lower for a nanofluid with CuO nanoparticles compared that for a nanofluid with Al_2O_3 nanoparticles (CuO has higher material density than Al_2O_3).

The deterioration in heat transfer in natural convevction flow of nanofluids is a result contrary to expectations. Although Nusselt number is inversely proportional to the thermal conductivity and the thermal conductivity of a nanofluid is higher than that of a pure liquid, it has been surmised that the heat transfer coefficient in a nanofluid should have a greater increase relative to the increase in thermal conductivity thereby resulting in an increased value of Nusselt number. This is indeed the case in forced convection heat transfer in a nanofluid [5]. Thus, this issue needs further investigation both computationally and experimentally. The authors of the experimental study [1] suggest several plausible physical causes for this deterioration in natural convection heat transfer in naofluids; however they do not fully explain this anomaly between natural and forced convection heat transfer in nanofluids.

Some of the plausible explanations are agglomeration and sedimentation of nanoparticles in the liquid as their concentration increases especially in low velocity natural convection flow compared to forced convection flow, and the larger negative influence of the slip between the nanoparticels and the liquid on heat transfer in low

velocity natural convection flow. The comparison of computations with experimental data also shows that there is a need for refinement of the theoretical models of fluid properties (μ , k, β, C_p) to improve the accuracy of the numerical predictions.

Chapter 8: Future Work

For future work, three critical issues have been identified to further improve the numerical simulation of natural convection heat transfer in nanofluids. One of the subjects that needs to be addressed is to find better models for the material properties of the nanofluids especially for higher volume-fraction of nanoparticles. Based on the results reported in this thesis, the difference between the numerical results and the experimental data is larger for 4% volume-fraction of nanoparticles than for 1% volume fraction of nanoparticles. Perhaps the currently available theoretical models for material properties of nanofluids are not adequate for higher concentration of nanoparticles. This issue begets further investigation. In particular, the relationship between thermal expansion coefficient β, considered to be constant in this study and the volume-fraction of nanoparticles needs to be explored and should be included in future computations for better predictions.

The numerical results presented in this thesis and in the experiement [16] show a degradation in heat transfer in natural convection flow of a nanofluid and this deterioration increases with increase in the volume-fraction of the nanoparticle. These results are contrary to the expectation that the heat transfer should increase due to increase in thermal conductivity. Therefore, simulations of forced convection heat transfer in nanofluids should be performed to determine what parameters contribute to increase in heat transfer due to the presence of nanoparticles. In forced convection, heat

transfer coefficient has been found to increase with increase in the volume-fraction of the nanoparticles [5].

Another area that needs to be investigated is the modeling of nanofluids as particle-liquid suspensions. In the current simulation, nanofluids are considered as a single phase fluid for reasons of simplicity. In particle-liquid suspensions, the interactive forces, heat flow and the buoyancy effect between the nanoparticles and the liquid particles must be considered, which will make the computations significantly more complex. Although there is significant body of literature on multi-phase particle-liquid suspensions with micro-sized particles, this area of research should be extended to the study of particle-liquid suspensions with nano-sized particles to determine in particular when the assumption of single phase fluid breaks down.

References

[1] Choi, U.S, *Enhancing Thermal Conductivity of Fluids with Nanoparticles*, in Developments and Applications of Non-Newtonian Flows, edited by D.A. Siginer and H.P.Wang, ASME, New York, FED-Vol. 231/MD-Vol. 66, 1995, pp.99-105.

[2] Choi, U.S., Zhang, Z. G., Yu, W, Lockwood, F.E., and Grulke, E.A., 2001, *Anomalous Thermal Conductivity Enhancement in Nanotube Suspensions*, Applied Physics Letters, Vol. 79, No.14, 2001, pp. 2252-2254.

[3] Crawford, M.E. and Kays, W.M., *Convective Heat and Mass Transfer*, 3rd ed., McGraw-Hill, New York, 1993.

[4] Das, K, Putra, N., Thiesen, P., and Roetzal, W., *Temperature Dependence of Thermal Conductivity of Nanofluids*, Journal of Heat Transfer, Vol. 125, 2003, pp 567-574.

[5] Eastman, J.A., Phillpot, S.R., Choi, U.S., and Keblinski, P., *Thermal Transport in Nanofluids*, Annual Review of Materials Research, Vol. 34, 2000, pp.219-246.

[6] Eastman, J.A., Choi, U.S., Li, S., Thompson, L.J., and Lee, S., *Enhanced Thermal Conductivity Through the Development of Nanofluids*, Material Research Society Proceedings, Vol 457, 1997, pp. 3-11.

[7] Eastman, J.A., Choi, U.S., Li, S., Yu, W., and Thompson, L.J., *Anomalously Increased Effective Thermal Conductivities of Ethylene Glycol-based Nanofluids Containing Copper Nanoparticles*, Applied Physics Letters, Vol. 78, No. 6, 2001, pp. 718-720.

[8] Farrashkhalvat, M, *Basic Structured Grid Generation*, Butterworth-Heinemann, Burlington, MA, 2003.

[9] Fluent 6.©: A CFD Software Package, Fluent Inc., Lebanon, NH, 2002.

[10] http://www.ac.wwu.edu/~vawter/PhysicsNet/Topics/Thermal/ThermExpan.html

[11] Kumar, D., Hemanth, H.E., Patel, V.R., Kumar, R., Sundarajan, T., Pradeep, T., and Das, S.K., *Model for Heat Conduction in Nanofluids*, Physics Review Letters, Vol. 93, No. 14., 2004.

[12] Lee, S., Choi, U.S., Li, S., and Eastman, J.A., *Measuring Thermal Conductivity of Fluids Containing Oxide Nanoparticles*, Journal of Heat Transfer, Vol. 121, 1999, pp. 280-289.

[13] Madireddi, S., *Computation of Three-dimensional Flow Field and Heat Transfer Inside an Open Refrigerated Display Case with Air Curtain*, M.S. Thesis, Washington University in St. Louis, MO, USA, 2004.

[14] Maxwell, J.C., *A Treatise on Electricity and Magnetism*, 2nd ed., Clarendom Press, Oxford University, U.K., 1881.

[15] Patel, H.E., Das, S.K., and Sundarajan, T., *Thermal Conductivities of Naked and Monolayer Protected Metal Nanoparticle Based Nanofluids: Manifestation of Anomalous Enhancement and Chemical Effects*, Applied Physics Letters, Vol. 83, No. 14, 2003, pp. 2931-2933.

[16] Putra, N., Roetzal, W., and Das, S.K., *Natural Convection of Nano-fluids*, Journal of Heat and Mass Transfer, Vol. 39, No. 8-9, 2003, pp. 775-784.

[17] Versteeg, H.K. and Malalasekera, W., *An Introduction to Computational Fluid Dynamics*, Longman Scientific & Technical, Essex, U.K, 1995.

[18] Wang, B., Zhou, L., Peng, X. and Zhang, X., *Enhancing the Effective Thermal Conductivity of Liquid with Dilute Suspensions of Nanoparticles*, 15th Symposium on Thermophysical Properties, 2003.

[19] Wang X., Xu, X. and Choi, U.S., *Thermal Conductivity of Nanoparticles-Fluid Mixture*, Journal of Thermophysical Heat Transfer, Vol. 13, 1999, pp. 474-480.

[20] White, Frank M., *Fluid Mechanics*, 4th ed., McGraw-Hill, New York, 1999.

[21] Xuan, Y. and Roetzal, W., *Conceptions for Heat Transfer Correlation of Nanofluids*, Int. Journal of Heat and Mass Transfer, Vol. 43, 2000, pp. 3701-3707.

[22] Xuan Y. & Li, Q., *Investigation on Convective Heat Transfer and Flow Features of Nanofluids*, Journal of Heat Transfer, Vol. 125, 2003, pp. 151-155.

Vita

Full Name : Mior Azman Meor Said

Born : 29 November 1978, Malaysia

Education : Bachelor of Mechanical Engineering, University of Tenaga Nasional, Malaysia, July 2001

May 2005